CHEMICAL KINETIC MODELING OF EMISSIONS FROM THE COMBUSTION OF HYDROCARBON FUELS IN A WELL-STIRRED REACTOR

Thesis

Submitted to

The School of Engineering of the

UNIVERSITY OF DAYTON

In Partial Fulfillment of the Requirements for

The Degree

Master of Science in Chemical Engineering

by

Gregory Michael Conrad

UNIVERSITY OF DAYTON

Dayton, Ohio

August 1998

CHEMICAL KINETIC MODELING OF EMISSIONS FROM THE COMBUSTION OF HYDROCARBON FUELS IN A WELL-STIRRED REACTOR

APPROVED BY:

Dilip R. Ballal, Ph. D.
Professor
Department of Mechanical and Aerospace Engineering
Committee Chairperson

Lourdes Q. Maurice, Ph. D., P.E.
Research Scientist
Air Force Research Laboratory
USAF
Research Advisor

Kevin J. Myers, D. Sc., P.E.
Professor
Department of Chemical and Materials Engineering
Academic Advisor

Ronald A. Servais, D. Sc., P.E.
Professor
Department of Chemical and Materials Engineering
Committee Member

Donald L. Moon, Ph. D.
Associate Dean
Graduate Engineering & Research
School of Engineering

Blake Cherrington, Ph. D., P.E.
Dean
School of Engineering

ABSTRACT

CHEMICAL KINETIC MODELING OF EMISSIONS FROM THE COMBUSTION OF HYDROCARBON FUELS IN A WELL-STIRRED REACTOR

Conrad, Gregory Michael
University of Dayton, 1998

Research Advisor: Lourdes Q. Maurice, Ph.D.
Academic Advisor: Kevin J. Myers, D. Sc.

Detailed kinetic modeling is applied to predict the emissions from the combustion of a variety of single component and complex hydrocarbon fuels at atmospheric pressure over the range of equivalence ratios ϕ = 0.43 - 0.88. The results are compared with experimentally determined emissions (CO_2, O_2, CO and NO_x) from a well-stirred reactor combusting methane, ethane, n-heptane, toluene, ethylbenzene, Jet A and an endothermic fuel simulant at the same conditions. The experimental data sets are useful for evaluating modeling tools. Computations are generally in reasonable qualitative agreement with experimental observation for all fuels. The temperature at which minimum CO emissions occur decreases with carbon number, and is accurately captured by the model. The quantitative agreement for CO emissions from Jet A is excellent. Predictions of CO for other fuels are within a factor of two or better, and improve with increasing temperature. Quantitative predictions of NO_x from Jet A, the endothermic simulant and the aromatics are in reasonably good agreement with measurements. Calculated NO_x emissions are

less accurate for the alkanes, but disagreement is within mechanistic uncertainties. Quantitative and qualitative predictions are also reasonable for both CO_2 and O_2.

A new detailed chemical kinetic model is created for the combustion of *n*-dodecane. Comparisons with experimental data show the model to reasonably predict the considered emissions.

A variety of experimental uncertainties are tested computationally to determine their effect on predictions. Temperature is the primary factor that affects NO_x emissions. However, detailed path analysis shows the need to consider the multi-component nature of the complex hydrocarbon fuels in order to predict emissions. Consideration of the effects of the sampling system on the measured emissions marginally improves predictions, while accounting for turbulent diffusion in the reactor results in significant underprediction of emissions.

Despite experimental and mechanistic uncertainties, emissions predictions are generally reasonable for a variety of fuels *without* relying on *ad hoc* adjustments to kinetic rate parameters. Thus, the applied detailed kinetic mechanism appears a sound basis for future simplifications to address the complex flowfields of practical systems.

ACKNOWLEDGMENTS

There are a great many people who have helped me along the way to this point in my life. I would like to thank Dr. Lourdes Maurice for her much needed assistance with the computer modeling and in writing this thesis. Thanks also go to Dr. Dilip Ballal for offering me this research opportunity and for serving on my committee. Thank you to Dr. Kevin Myers for the enjoyable, though usually frustrating, err challenging, classes and for being on my committee. Dr. Ronald Servais also deserves acknowledgment for being on my committee as well as teaching a wide variety of subjects.

Thank you to Dr. Tony Saliba for his guidance and discussions, even above and beyond academics. I would also like to thank my many co-workers at UDRI for their assistance and encouragement.

A special thank you to my parents and family for their love and support. And, most importantly, thanks to my bride-to-be, Allison. I don't think that I could have made it this far without her love and support.

I would also like to thank the Dayton Area Graduate Studies Institute for their financial assistance. This work was supported by the Propulsion Directorate, Air Force Research Laboratory, United States Air Force, Wright-Patterson Air Force Base, under contract numbers F33615-92-C-2207 and F33615-97-C-2719. Mr. Charles Frayne served as the technical monitor.

TABLE OF CONTENTS

LIST OF FIGURES

LIST OF TABLES

LIST OF SYMBOLS

a	=	constant terms in the JANAF polynomials
A	=	frequency factor
C_p	=	specific heat capacity at constant pressure
D	=	diffusivity
Da	=	Damköhler number
E_a	=	activation energy
h	=	mixture enthalpy
H	=	enthalpy
J	=	diffusive flux
k	=	reaction rate constant
K	=	equilibrium constant
m	=	mass flow rate
M	=	molecular weight
$\overline{M}$	=	mean molecular weight
n	=	mole number
n_{sp}	=	number of species
n_{reac}	=	number of reactions
P	=	reactor pressure

R	=	universal gas constant
R_k	=	net rate of formation of species k
S	=	entropy
T	=	temperature
V	=	reactor volume
V_c	=	correction velocity
x	=	mole fraction
y	=	cross-stream distance
Y	=	mass fraction

Greek Symbols

ϕ	=	equivalence ratio
Φ	=	molar concentration
ρ	=	fluid density
τ	=	nominal reactor residence time
Ξ	=	stoichiometric coefficient
ξ	=	concentration dependence

Subscripts

f	=	combustion or reactor
i	=	species i

in	=	inlet
j	=	reaction j
k	=	species k
n	=	temperature dependence exponent
reac	=	reactions
react	=	reactant
sp	=	species

Superscripts

f	=	forward reaction
r	=	reverse reaction
0	=	at standard conditions

CHAPTER I

INTRODUCTION

Combustion processes have been important to humankind since we first lived in caves. Early humans put fire to several uses including light, heat, and cooking their food (Weinberg, 1974). Today, the combustion of fossil fuels is the planet's primary energy source, providing more than 90-95% of the world's energy requirements (Griffiths and Barnard, 1995; Leung, 1995). Alternative energy sources, including nuclear, hydroelectric, solar, wind, and geothermal, provide us with some power, but at nowhere near the convenience, or the cost, of fossil fuel combustion. Unfortunately, the burning of fossil fuels produces undesirable emissions. We have become increasingly aware of the adverse environmental effects caused by such pollutants, especially oxides of nitrogen (NO_x), carbon monoxide (CO), and unburned hydrocarbons (UHC), resulting from combusting fossil fuels. This awareness has led to stringent restrictions on the emissions permissible from combustion processes (e.g. the Clean Air Act of 1990 and the recent Kyoto agreement). However, despite the threat to the environment, the demand for energy continues to grow in direct correlation to the world's population. Attempts at meeting the world's power requirements are being made by increasing the emphasis on burning crude and residual fuels in industrial gas turbine combustors that are

commissioned into service in developing countries. Moreover, the increased use of cheaper, low-volatility JP-8 fuel in aircraft engines, and the rising aromatic content of gasoline and diesel fuel for automotive use are also recent phenomena (Walker, 1992). As the world's requirements for energy sources increase, rising emissions require efforts to legislate air standards on a global scale (Selim, 1995).

Environmental restrictions, coupled with the reality of dwindling sources of fossil fuels, necessitate that we use our available fuels efficiently. However, emissions reduction is a challenging endeavor because it often conflicts with simultaneous performance improvements in mobile and stationary combustion systems. In order to reduce emissions to the levels required by recent legislation, one must understand the science of combustion processes. Yet, our knowledge of these processes has not kept pace with combustion technology. Technology has enabled us to use combustion as an energy source, in a variety of ways. However, the fundamental scientific processes that allow us to utilize it are not yet entirely understood. This has occurred over many years because "Nature has started us off with a combustion phenomenon which is so spontaneous that it could arise accidentally and works, in a fashion, without requiring any understanding of the mechanism (Weinberg, 1974)." Consequently, most significant developments in combustors and fuels have come from trial-and-error solutions, which involve extensive experimentation. However, the cost of experimental techniques that *may* lead to the development of combustors and fuels that meet both the desired performance and emissions requirements is rapidly rising. Fortunately, with the relatively recent advent of the inexpensive computer, techniques and tools have been devised that will allow us to study combustion processes through computer modeling.

Now, it is desired to develop computational tools for both combustor design and performance predictions using these new techniques and tools (Westbrook and Dryer, 1984).

Combustion is unique in that there are a wide variety of "types" of combustion: solid, liquid, vapor, low temperature, high temperature, laminar, turbulent, diffusion, and premixed, to name a few. Also, combustion processes occur at a medley of different temperatures, pressures, and compositions (Miller, 1996). Each "type" of combustion involves a diverse range of reactions between the species under consideration as well as disparate assumptions about how they react. There are also many different ways of examining the various combustion phenomena. Chemists, spectroscopists, physicists, and thermodynamicists can all find something different to study in even the simplest combusting system (Weinberg, 1974; Walker, 1992).

No matter what distinguishing characteristics a particular combustion event has, an analysis of it boils down to comparing the relative influences of the chemical reactions and the mass, momentum, and energy transport processes. These influences are determined by comparing the time scales of each of the processes. Whichever process is slower (has a longer time scale), controls the rate at which combustion occurs. A process that is controlled by the rate at which the species mix together (mixing time is slow compared to reaction time) could be investigated by examining a single global step. However, many important combustion processes, including pollution formation and destruction, are kinetically controlled. In these cases, the rates of the individual reactions control the process and so all of the individual steps need to be analyzed. In the case of combustors, such as high-speed aircraft engines, that have small residence times and a

range of operating conditions, consideration of the kinetics of the systems is even more important (Maurice, 1996; Levenspiel, 1996).

When a researcher works to develop a kinetic model of a combusting (reacting) system, the first step is to determine the appropriate chemical kinetic mechanism. A mechanism consists of the various elementary reactions that occur and the appropriate thermodynamic and transport data. For a combustion process, the mechanism is rather complicated because of the large number of elementary reactions (upwards of one thousand for complex hydrocarbon fuels) that can occur in a combustor. An elementary reaction is simply a reaction, which occurs on a molecular level, that is part of the overall, or global, reaction. Also, many of the reactions in a combusting system occur between highly reactive intermediate species, usually radicals, that are both generated and consumed during the combustion process. As the temperature of the reactor increases due to the heat release process, the number of possible reactions dramatically grows. At typical flame temperatures (~ 2000 K), reactions occur between almost all of the species present. Since most of these reactions occur on a molecular level between species that are not normally found outside a combustion reaction, chemical rate data on them is scarce at best (Walker, 1992).

In order to develop and analyze effective emissions reduction techniques through modeling, a thorough understanding of how pollutants are formed and destroyed is required. This understanding will allow an investigator to include the necessary reactions and reaction rates for the generation and consumption of pollutants in the mechanism that is being created. To produce a useful model for predicting emission concentrations one must include the appropriate reactions for a wide variety of fuels.

Because of the lack of chemical data for many intermediate species in a combustion system, early kinetic models had to assume that many reactions were either instantaneous or irrelevant. As discussed above, in some cases, particularly high temperature systems, these assumptions are valid because the chemical reactions occur much quicker than other processes in the system (such as species transport) (e.g. Jones and Whitelaw, 1984). However, such assumptions limit the predictive range of models. Fortunately, recent research has increased the amount of chemical rate data available as well as generated new kinetic modeling techniques. New spectroscopic techniques have increased our knowledge of intermediate concentrations (Walker, 1992). Knowledge of these concentrations, their decay, and the advanced data handling capabilities of computers has led to more information about elementary reaction rates. Kinetic modeling has also benefited from the development of theoretical chemical calculations of thermochemical data and reaction dynamics (Miller and Kee, 1990; Leung, 1995).

Despite the advances discussed above, the introduction of detailed chemical kinetic mechanisms, which take into account most of the mathematically possible elementary reactions that can occur at a significant rate, for complex hydrocarbon fuels into multi-dimensional fluid dynamics problems (such as an aircraft engine) is still not practical. Therefore, simplified, or reduced, kinetic mechanisms that have been thoroughly validated are needed to address specific issues arising in realistic combustor configurations (Westbrook and Dryer, 1984; Dryer, 1989). Simplified mechanisms consist of comparatively few reactions, and so may be possible to study in complex, realistic situations. These reduced mechanisms, however, must be firmly based on detailed mechanisms, and carefully validated against a wide range of experimental data.

Therefore, studying the emissions characteristics of a wide range of fuels over a variety of operating conditions both experimentally and computationally with a detailed kinetic mechanism is a crucial step toward elucidating the effects of fuel chemistry on overall engine emissions (Maurice, 1996).

Once a suitable model is developed, a combustion researcher's goal is to be able to accurately predict emissions for the combustion of fuels that are typically used in today's power plants. However, practical liquid hydrocarbon fuels are inherently difficult to study both experimentally and computationally. They comprise hundreds of components that vary as a function of crude oil feedstock, refining processes and storage techniques. For example, the composition of Jet A, shown in Figure 1, is incredibly complex. Each portion of the pie chart shown represents only a general type of compound. Because of the large number of components that make up such a practical liquid hydrocarbon fuel, data suitable for evaluating their emissions models are sparse, and such data are unavailable for endothermic fuels. Endothermic fuels are fuels that can be used to provide engine cooling before being injected into the combustion chamber. Currently, ambient air is used for engine cooling. But at higher speeds, and correspondingly higher engine temperatures, air no longer provides acceptable cooling. Development of fuels that could provide the necessary engine cooling would be a substantial improvement in aircraft design. As such, the study of endothermic fuels is of interest to aviation.

Notable progress in interpreting the mechanism of kerosene (Jet A) oxidation has been reported by Dagaut et al. (1994a), Guéret et al. (1990), and Vovelle et al. (1994). Also, Ranzi et al. (1994) proposed a comprehensive reaction mechanism for higher order

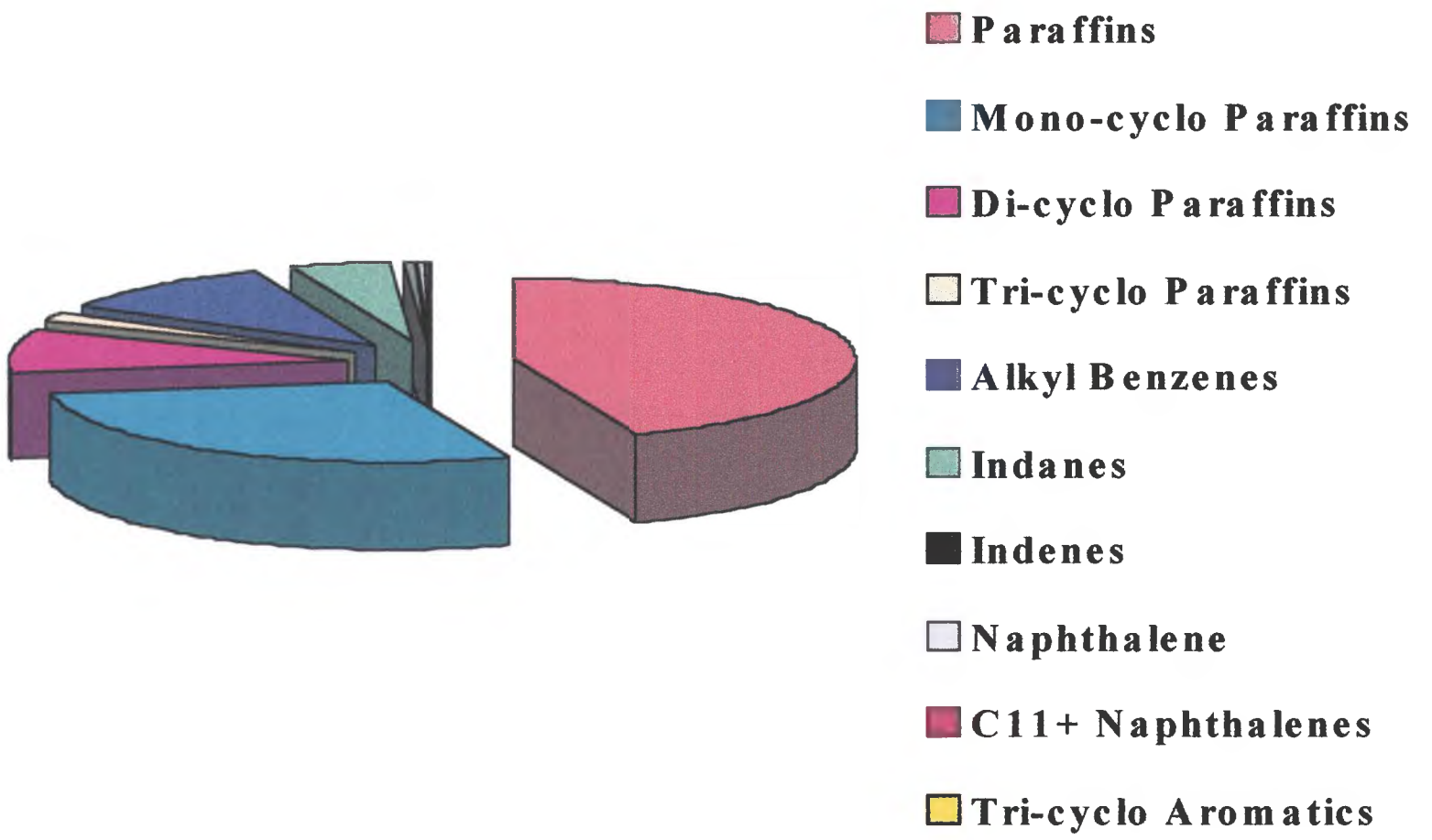

Figure 1. The composition of jet fuel.

hydrocarbon fuels, but considers benzene in only a semi-empirical manner. However, the need for further refinement of the aromatic models is recognized. The work of Lindstedt and Maurice (1997) and Maurice (1996) has provided a detailed chemical kinetic mechanism for higher order hydrocarbons including aromatic components. The model has also been shown to address the gas-phase chemistry of complex hydrocarbon fuels (Lindstedt and Maurice, 1997). By contrast, formation of NO_x in flames of high molecular weight hydrocarbons is difficult to model (Sturgess, 1997), and has been studied less extensively than the formation of emissions from lower order hydrocarbons such as methane (Williams and Pasternack, 1997).

The detailed chemical kinetic mechanism of Lindstedt and Maurice (1997) and Maurice (1996) has previously been compared to a variety of fuels, including alkanes up to *n*-decane, aromatics such as ethylbenzene and toluene, and fuel blends including Jet A (kerosene). Applicability of the model over relatively broad operating conditions (temperatures of 900 to 2000 K, equivalence ratios of 0.5 to 2.6, and residence times of about 2 to 240 ms) has been shown. The goal of the present thesis is to utilize the Lindstedt-Maurice mechanism to predict the concentrations of additional pollutant species, including NO_x, resulting from the combustion of a broad range of hydrocarbons at flame temperatures. The mechanism will also be extended to include reactions for the combustion of *n*-dodecane.

Experimental data is required for evaluation of the ability of the model to accurately predict the additional pollutants as well as its ability to predict emissions for *n*-dodecane. The choice of experimental device depends on how the combustor is going to be modeled. Some of the possible approaches to modeling gas turbine combustors

include an aerodynamic approach, modeling as a perfectly stirred reactor (PSR), or as a plug flow reactor (PFR). The aerodynamic approach typically models a combustor by a detailed simulation of the flow field and a few global combustion steps (e.g. Jones and Whitelaw, 1984). As discussed above, due to the kinetic control of most combustion processes, this method does not produce satisfactory results. A PSR is a zero dimensional theoretical reactor, so the combustion reactions are independent of aerodynamic effects. A PFR is a one-dimensional theoretical reactor. For modeling a combustor a series of PFRs (the tanks-in-series model) would be used. This approach requires knowledge of the flow pattern in the reactor and does not provide insight into the heat transfer characteristics of the combustor (Blust, 1998).

In this thesis, the modeled results will be compared with new experimental data obtained by Blust (1998) for pure hydrocarbons and hydrocarbon mixes, including Jet A and a cracked fuel simulant designed to represent an endothermic fuel. In the work of Blust (1998), the fuels are pre-vaporized, premixed with air, and reacted in a well-stirred reactor (WSR) in a self-sustained, lean combustion process. The WSR is a laboratory combustor that closely emulates perfectly stirred reactor theory, and thus provides a means to study emissions phenomena in a well-controlled laboratory configuration. The comparison between model predicted and additional experimental data will provide some of the validation of the model that is required before it can be used to predict emissions for systems for which experimental data cannot be obtained. The model can also be used to help elucidate some of the chemistry that is occurring in the WSR.

Further details of the model used in this research are shown in Chapter II. The second part of Chapter II shows how a mechanism is typically developed. Chapter III

discusses the well-stirred reactor and the experimental setup. The present contribution compares numerical predictions based upon the Lindstedt-Maurice mechanism with previously reported emissions data from the WSR (Blust, 1998). A variety of fuels are considered over a wide range of experimental conditions (Chapter IV). Reactions for the combustion of *n*-dodecane are also added to the kinetic mechanism. The predicted emissions from this new mechanism are also compared with experimental data. Since the WSR is (nearly) free of mixing effects, comparison of the kinetic model with emissions data provides a critical check of the model's predictive capabilities. Various uncertainties in the experimental results, including temperature sensitivity, probe effect, and turbulent diffusion are computationally investigated using the Lindstedt-Maurice mechanism. The effects of these uncertainties on predictions are examined in Chapter V. The final chapter, VI, presents the conclusions drawn from these experiments and predictions. It also suggests potential areas for further study.

CHAPTER II

CHEMICAL KINETIC MODELING

Introduction to Modeling

"Numerical modeling based on chemical kinetics has become a powerful technique for the analysis of many combustion phenomena (Leung, 1995)." Successful kinetic modeling requires several things. As discussed in Chapter I, the first thing needed is knowledge of the combustion reaction mechanism, including the various reactions and accurate reaction rate parameters for each reaction. One must also have applicable numerical methods that can solve the required highly nonlinear differential and algebraic equations and a computer program for easy use of said numerical methods (Miller and Kee, 1990).

Before a model can be considered useful for predicting emissions, it must be evaluated. The evaluation is accomplished by comparison with experimental measurements of major, intermediate, and free radical species concentrations at a variety of temperatures, reactor residence times, and equivalence ratios. Comparisons to various data sets obtained by different researchers using similar experimental conditions are also desirable. However, many kinetic mechanisms are compared with experimental data for only one combustion regime. Agreement in other regimes is sometimes obtained by

altering the kinetic rate parameters from experimental observations (Westbrook and Dryer, 1984, Dryer, 1989). Besides using data that is unrealistic, this method of constructing a mechanism is not very useful toward predicting emissions outside of a narrow range. One difficulty in creating an accurate model is that current mechanisms contain a rather large number of species and reactions each of which has its own thermodynamic and rate data. This means that a mechanism could easily produce results comparable to experimental data yet be constructed with arbitrary rate constants and thermodynamic data that are incredibly unrealistic. Also because of the large number of reactions, any errors or inaccuracies in the kinetic data that may not be evident under one set of conditions may have a substantial impact on the modeled results under different conditions. Thus, the desired mechanism is one that can accurately predict trends in emissions with different fuels, different stoichiometries (relative amounts of fuel and air), and in different combustion regimes (such as premixed and diffusion) without arbitrary changes to the mechanism (Skevis, 1996).

The most extensively developed kinetic model for the combustion of hydrocarbons applies to alkanes, e.g. Curran et al. (1996). The model dates more than 15 years, and considered hydrogen, carbon monoxide and methane as the primary fuels reacting at temperatures above 1200 K. The model has gradually evolved from the reactions of single carbon atom components to the present relevance to C_8 alkanes. The primary objective of this work was the understanding of gasoline combustion in spark ignition engines, e.g. Curran et al. (1996). Only recently has attention been paid to other classes of hydrocarbons or other organic compounds, such as the aromatics (Castaldi et al., 1996) and ethers (Curran et al., 1996). Warnatz (1984) also began the development

of comprehensive models at about the same time, and more recently the two sources have been drawn together (Chevalier et al., 1992). There have also been other, independent developments of comprehensive kinetic models which are applicable to alkane combustion (e.g. Dagaut et al., 1994b). Very important development of programs dedicated largely to the detailed understanding of diffusion and premixed flame chemistry has also been done. The work has placed particular emphasis on the chemical complexities that emerge in very fuel rich conditions, such as polycyclic aromatic hydrocarbons (PAH) and soot formation (Leung and Lindstedt, 1995; Lindstedt and Skevis, 1997), with extensions to the components of kerosene (Maurice, 1996; Lindstedt and Maurice, 1997).

Hence, the detailed kinetic mechanism used in the current research is based on the combustion kinetic models formulated by Lindstedt and coworkers (Maurice, 1996; Leung and Lindstedt, 1995; Lindstedt and Maurice, 1996; Lindstedt and Selim, 1994; Lindstedt et al., 1994; Lindstedt and Skevis, 1996; Lindstedt and Skevis, 1997). The ability of this mechanism to capture the high temperature combustion chemistry of the various hydrocarbons considered has been previously shown (Lindstedt and Maurice, 1997; Maurice, 1996; Leung and Lindstedt, 1995; Lindstedt and Maurice, 1996; Lindstedt and Selim, 1994; Lindstedt and Selim, 1994b; Lindstedt and Skevis, 1996; Lindstedt and Skevis, 1997).

As stated above, the kinetic rate data and thermochemical data on the species are important to the success of a mechanism. There are a number of existing databases from which thermodynamic and transport information is usually drawn, for example Burcat and McBride (1994). Computational packages also exist that may be used for the

estimation of thermochemical data. These include CHETAH (Seaton et al., 1974), THERM (Ritter, 1989), NIST DB 25 (Stein et al., 1994) and THERGAS (Muller et al., 1995). The major sources of kinetic rate data are the critically evaluated data sets published by the CEC group (Baulch, 1992, 1994) and NIST (Tsang, 1987, 1988, 1990, 1991). In addition, there are a number of data sheets that give data only at certain conditions. For example, Walker and Morley (1997) have data for hydrocarbon combustion at low temperatures (below 1200 K) and Warnatz (1984) has data at higher temperatures.

However, these sources of quantitative information do not cover the full range of reactions that are required for the combustion chemistry of higher hydrocarbons. Thus it is often necessary to estimate the appropriate kinetic parameters for many reactions. Confidence in the numbers may be gained by analogy to the (known) data for similar reactions within a particular class. Fortunately, the hierarchical nature of the mechanisms of hydrocarbon combustion (as discussed in the next section) permits quite extensive generalizations to be made. The pre-exponential factors of bimolecular reactions can be predicted relatively easily from Transition-State Theory (Benson, 1960). However, the accuracy of the temperature dependencies of the kinetic rate constants is problematic if wide temperature ranges have to be taken into account. Another difficulty arises because the pressure dependencies of the rate constants are arduous to quantify (e.g. Tsang et al., 1996). Unfortunately, this problem has not yet been widely recognized because verification of a model typically occurs at pressures other than those of a particular combustion application.

As discussed in the next section, the best way to create a mechanism is to combine together appropriate "sub-mechanisms," each of which contains reactions of a particular type. The mechanism used in the present research consists of several such sub-mechanisms. The starting hydrocarbon kinetic sub-mechanism features alkane molecules up to C_{10} and an aromatic model including mono-substituted and polycyclic aromatic hydrocarbon oxidation chemistry. The nitrogen sub-mechanism considers nitrogen oxides formation via (i) the thermal (Zel'dovich) channel, (ii) the prompt NO channel and (iii) intermediate N_2O. The mechanism also contains extensive nitrogen dioxide and nitrous oxide formation and destruction chemistry. The reactions that make up each of these NO_x mechanisms are discussed in Chapter IV. The complete detailed mechanism comprised 1132 elementary reactions and 176 chemical species. The rate constants for all elementary reactions and pertinent thermodynamic and transport data for the baseline have been reported elsewhere (Maurice, 1996; Selim, 1995).

After the kinetic mechanism, the next part of a kinetic model is the necessary equations and numerical methods used for solving these equations. The following mass, species conservation, and energy equations govern premixed reacting flows (Jones and Lindstedt, 1988a):

$$\frac{\mathrm{d}\rho}{\mathrm{d}t}+\frac{\mathrm{d}\rho v}{\mathrm{d}y}=0 \qquad \text{Equation 1}$$

$$\rho\frac{\partial Y_k}{\partial t}+\rho v\frac{\partial Y_k}{\partial t}=-\frac{\partial J_k}{\partial y}+R_k M_k \qquad \text{Equation 2}$$

$$\rho\frac{\partial h}{\partial t}+\rho v\frac{\partial h}{\partial y}=\frac{\partial}{\partial y}\left(\frac{\lambda}{C_p}\frac{\partial h}{\partial y}\right)+\frac{\partial}{\partial y}\left[\sum_{k=1}^{n_{sp}}h_k\left(-J_k-\frac{\lambda}{C_p}\frac{\partial Y_k}{\partial y}\right)\right] \qquad \text{Equation 3}$$

where

$$R_k = \sum_{j=1}^{n_{reac}} \Xi_{jk} \left[k_j^f \prod_{i=1}^{n_{sp}} \Phi_i^{\xi_{ji}^f} - k_j^r \prod_{i=1}^{n_{sp}} \Phi_i^{\xi_{ji}^r} \right] \qquad \text{Equation 4}$$

and

$$J_k = -\rho D_k \left(\frac{\partial Y_k}{\partial y} - Y_k \frac{1}{n} \frac{\partial n}{\partial y} \right) - \rho V_c Y_k \qquad \text{Equation 5}$$

As the current project is aimed at comparing modeled data to experimental data obtained from a well-stirred reactor, which is a laboratory device that attempts to simulate a perfectly stirred reactor, a number of assumptions can be made that simplify these equations. Perfectly stirred reactors are ideally zero-dimensional, adiabatic and isobaric. Reaction occurs at the homogeneous conditions of the reactor, which are also the exhaust conditions. Consequently, transport effects may be neglected for a spatially homogeneous reactor. For this situation the momentum equation does not have to be solved because the solution at a single point describes the entire reactor. So, the above species conservation and energy equations reduce to:

$$\rho \frac{dY_k}{dt} = R_k M_k \qquad \text{Equation 6}$$

and

$$\rho \frac{dh}{dt} = - \sum_{k=1}^{n_{sp}} h_k R_K M_K \qquad \text{Equation 7}$$

The equation of state:

$$P = \frac{\rho RT}{\overline{M}} \qquad \text{Equation 8}$$

where

$$\overline{M} = \sum_{k=1}^{n_{sp}} x_k M_k \qquad \text{Equation 9}$$

is also important.

A differential equation for each chemical species must be solved at each time step resulting in N equations. If the energy equation must also be solved, there would be N+1 equations for each time step (Westbrook and Dryer, 1984). Since the primary goal of this project was to compare modeled values to experimental results, the reactor temperature is specified in each case. Therefore, the energy equation was not solved. Rather the experimentally measured temperature was imposed upon the computations.

Stirred reactors are computed using a numerical model based upon the work of Jones and Lindstedt (1988a, 1988b). Their method involves solving the above equations using an implicit difference method with two-point backward time (t) differencing and with central differencing for the spatial (y) derivative. In order to solve the algebraic equations that this method generated, the source term was modified using the Newton linearization procedure to:

$$R'_k = \sum_{j=1}^{n_{reac}} \Xi_{jk} \left\{ k_j^f \prod_{i=1}^{n_{sp}} \Phi_i^{\xi_{jk}} - k_j^r \prod_{i=1}^{n_{sp}} \Phi_i^{\xi_{jk}} \right\} \qquad \text{Equation 10}$$

and

$$R_k^{v+1} = R_k^v + \sum_{i=1}^{n_{sp}} \frac{\partial R'_k}{\partial \phi_i} \frac{\partial \varepsilon_i}{\partial Y_i} \{ Y_i^{v+1} - Y_i^v \} \qquad \text{Equation 11}$$

The computational procedure involves specifying the measured temperature, the composition of the initial reaction zone, and the nominal residence time of the reactor. A suitable time step is specified and the conservation equations are solved until a steady state solution is achieved.

Creation of a Mechanism

The goal of a researcher who is creating a kinetic mechanism is to predict the behavior of systems for which experimental data does not exist. One way to do this is to create a generalized, or comprehensive, mechanism that would include all of the chemical species that could be present during a combustion reaction as well as all of the elementary reactions that could occur between them (Westbrook and Dryer, 1984). Fortunately, many of these mathematically possible reactions do not occur at all, or occur at an insignificant rate. Therefore, many "possible" reactions can be eliminated (Leung, 1995). As the goal of this research (e.g. Lindstedt and coworkers) is to construct a mechanism for determining the emissions from the combustion of aviation fuels, the mechanism can be further simplified by including only reactions that occur at higher temperatures (in this case, greater than about 1000 K).

A mechanism includes those elementary reactions that have been determined to be important and their associated rate data as well as the thermochemical and transport data for the species involved in those reactions. One way to create a mechanism is to start with the reactions of the largest molecule in the system, consider the reactions it undergoes, and then the reactions the products from those reactions undergo, and so on. Fortunately, a "natural hierarchy" exists in the reactions. This allows mechanisms to be "built" sequentially, starting with reactions for the simplest species and then adding reactions for other species, as they are necessary. To use this method to create a mechanism for a more complex fuel, one must simply include the reactions of the complex molecule and its breakdown to the species that have been previously included in the mechanism (Westbrook and Dryer, 1984).

If a researcher wishes to start a mechanism from scratch, he or she would start to create a mechanism using the reactions for the combustion of hydrogen. Then methane reactions would be added, then other alkanes, and then aromatics in order of increasing complexity (e.g. Westbrook and Dryer, 1984). This process simplifies the creation of the mechanism because the simpler reactions are an important part of the combustion of more complex molecules.

As part of this thesis, a mechanism for *n*-dodecane was constructed. This involved only the adding of certain reactions to the formerly existing *n*-decane mechanism (Maurice, 1996). The reactions for *n*-dodecane added to this mechanism are shown in the Appendix. These include thermal decomposition via C-C bond rupture, H atom abstraction via H, OH, O, HO_2, and CH_3 radical attack, reaction with O_2, and isomerization reactions. The rates of these reactions are expressed in the form:

$$k = AT^n e^{-E_a/RT} \qquad \text{Equation 12}$$

The frequency factor (A) for each reaction was calculated from the corresponding reaction for *n*-decane according to the equation:

$$A_{dodecane} = A_{decane}\sqrt{M_{decane}/M_{dodecane}} \qquad \text{Equation 13}$$

The temperature dependence exponent (n) for each reaction was ascertained directly by comparison with the corresponding *n*-decane reaction. The activation energy for each reaction was determined from the heat of formation for the different species in the reaction. The heats of formation are from Lias et al. (1994), as found in Stein (1994).

As mentioned previously, a computer program is required to solve the various differential equations and generate the predicted emissions. The program used in the current research requires three input files. A file called chmlam.dat contains the

elementary reactions and their rate parameters. A second file called janlam.dat contains the thermodynamic data for each species considered. The janlam.dat file also includes the number of species, the desired equivalence ratio (ϕ), and the desired residence time (τ). The thermodynamic data are needed for the calculation of the heat released (if the reactor temperature were not specified) as well as the equilibrium constants of each reaction. The equilibrium constants are calculated according to:

$$\ln(K) = \frac{\Delta H}{RT} + \frac{\Delta S}{R} \qquad \text{Equation 14}$$

The thermodynamic data is stored in JANAF (Joint Army Navy Air Force) type polynomials as:

$$\frac{Cp}{R} = a_1 + a_2 T + a_3 T^2 + a_4 T^3 + a_5 T^4 \qquad \text{Equation 15}$$

$$\frac{H}{RT} = a_1 + \frac{a_2 T}{2} + \frac{a_3 T^2}{3} + \frac{a_4 T^3}{4} + \frac{a_5 T^4}{5} + \frac{a_6}{T} \qquad \text{Equation 16}$$

and

$$\frac{S}{R} = a_1 \ln(T) + a_2 T + \frac{a_3 T^2}{2} + \frac{a_4 T^3}{3} + \frac{a_5 T^4}{2} + a_7 \qquad \text{Equation 17}$$

The data for each species is represented by fourteen coefficients corresponding to temperature ranges below 1000 K (second set) and above 1000 K (first set). The third input file is called rstart.dat. This file contains an initial "guess" of the solution to facilitate convergence by providing the program with an appropriate starting point. For this project, the rstart.dat file was also used to specify the desired reactor temperature.

The program's output file is called result.stir. It echoes back the input reaction rates and thermodynamic data. Then it lists the concentration of each species for each

time step. This file is easily imported into a spreadsheet (Microsoft Excel was used for this research) to be analyzed and plotted.

CHAPTER III

EXPERIMENTAL DATA USED FOR VERIFICATION

Verification of kinetic mechanisms requires comparison with experimental data for different fuels, over a wide range of operating conditions. As discussed in Chapter I, a well-stirred reactor (WSR) was chosen for this thesis because it emulates a perfectly stirred reactor. The experimental data used in this thesis was obtained in a 250-mL toroidal WSR, as designed by Nenniger et al. (1984) and modified by Zelina and Ballal (1994). The reactor is constructed of alumina cement, and features a jet ring with 32 stainless steel, 1 mm I.D. jets to inject the fuel/air mixture at high subsonic velocity (Ma = 0.42 - 0.85). An illustration of the reactor setup is shown in Figure 2. The WSR was operated at one atmosphere pressure. Nominal reactor residence time, τ, is computed via the following formula:

$$\tau = \frac{PV}{\frac{R}{M} T_f m_{react}} \qquad \text{Equation 18}$$

For the current project, data from the WSR was obtained over the range of equivalence ratios (ϕ) between 0.43 - 0.88 and a loading parameter (Longwell and Weiss, 1955) (LP) of approximately 1 g-mol/sec·L·atm$^{1.75}$. Also, the reactor was operated at residence times (τ) between approximately 5 and 8 milliseconds, and reactor temperatures (T_f) between 1350 - 2000 K.

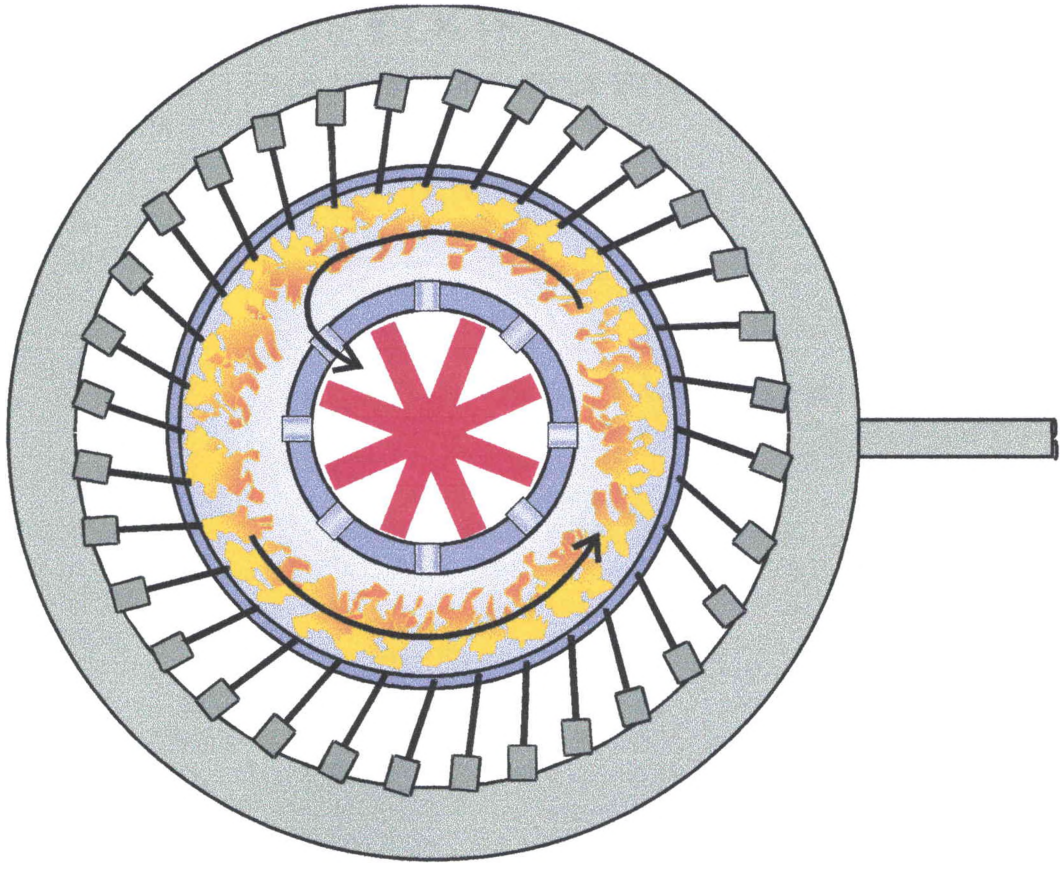

Figure 2. The toroidal well-stirred reactor.

Blust (1998) measured efflux composition via Horiba Emissions Analyzers comprising the following units: Model MPA-510 oxygen analyzer (0 - 50%), Model VIA-510 CO analyzer (0 - 20%) and CO_2 analyzer (0 - 100%), and Model CLA-510 SS NO and NO_x analyzer (0 - 2000 ppmV). The units were calibrated with gases of the following concentrations: NO = 92 ppmV, NO_2 = 1.6 ppmV, CO = 0.4%, O_2 = 4.03 or 5.02% and CO_2 = 11.06%. Emissions readings were delivered on a dry basis, with water scrubbed from the sample gas to a maximum dew point of 5 °C. The units required a total of 4 sLpm gas sample, with a pressure within $\pm$10 cm of water of ambient.

A gas sample was drawn from the WSR by a water-cooled stainless steel probe as described by Blust et al. (1997a), and pumped into each unit through a heated sampling line to be analyzed for the various product species. The stainless steel probe used features a small inside diameter, which resulted in a pressure drop when hot sample is drawn from the reactor. The subsequent vacuum necessitated connecting a single speed corrosion resistant pump rated 12 sLpm to the sampling line.

Combustion temperature (T_f) was measured by insertion of a Type B thermocouple (platinum-6% rhodium, platinum-30% rhodium) into the toroidal volume. This thermocouple was coated with alumina ceramic for protection from the reactor environment, since platinum-rhodium alloys are subject to high-temperature contamination that can make them brittle. Temperature measurements were corrected for heat loss by radiation and conduction, and heat gain by convection and catalysis via the procedures outlined by Blust et al. (1997b).

A vaporizer was used to pre-vaporize liquid fuels, mix the vaporized fuel with air, and subsequently supply the combustible mixture to the WSR. The vaporizer design comprised a 3 kW Hotwatt air heater, pressurized fuel tank, vaporization chamber, various flow-meters, nozzle air line, safety devices, and a fuel atomization nozzle. Combustion air was metered through a rotameter and passed through a heater. The air temperature was measured by a Type K (chromel-alumel) thermocouple. Combustion air was heated to a temperature sufficient to vaporize the hydrocarbons, but below the fuel's autoignition temperature. Heated air was subsequently injected into the vaporization chamber perpendicular to the hydrocarbon mist stream. This established a recirculation zone in the vaporizer to provide additional time for fuel vaporization. Residence time in

the vaporizer was greater than 1.2 seconds, which is significantly greater than the vaporization time predicted for pure hydrocarbons (e.g. *n*-heptane 0.36 sec (Ballal and Lefebvre, 1979)). Additionally, this residence time provides insufficient time for thermal decomposition of hydrocarbons in the vaporizer (Stoffel and Reh, 1995). Liquid fuels were preheated prior to atomization via a copper block heater clamped on the fuel delivery tube to ensure complete vaporization.

Gaseous fuel flow was monitored to within $\pm$2% of reading using a Gilmont rotameter. Air flow was regulated to within $\pm$2% of full scale using a Brooks rotameter. The combined error produced an uncertainty of $\pm$3.5% in ϕ during the combustion of methane in air. Nozzle air was monitored to within $\pm$2% of reading using a Gilmont rotameter. Liquid hydrocarbons were controlled to within $\pm$0.3 g/min by the liquid fuel delivery system. The combined error produced an uncertainty of $\pm$3.5% in ϕ during combustion of liquid fuels in air. The T_f measurements are accurate to approximately $\pm$50 K. The Horiba emissions analyzers feature a quoted accuracy within 1% of full scale. This represents an error of 2 ppmV NO_x, 50 ppmV CO, 0.25% O_2 and 0.5% CO_2. Residence time was typically controllable to within $\pm$0.6 msec, and CO and NO_x measurements are repeatable within $\pm$100 ppmV and $\pm$1.5 ppmV respectively. A schematic of the test facility and instrumentation is shown in Figure 3.

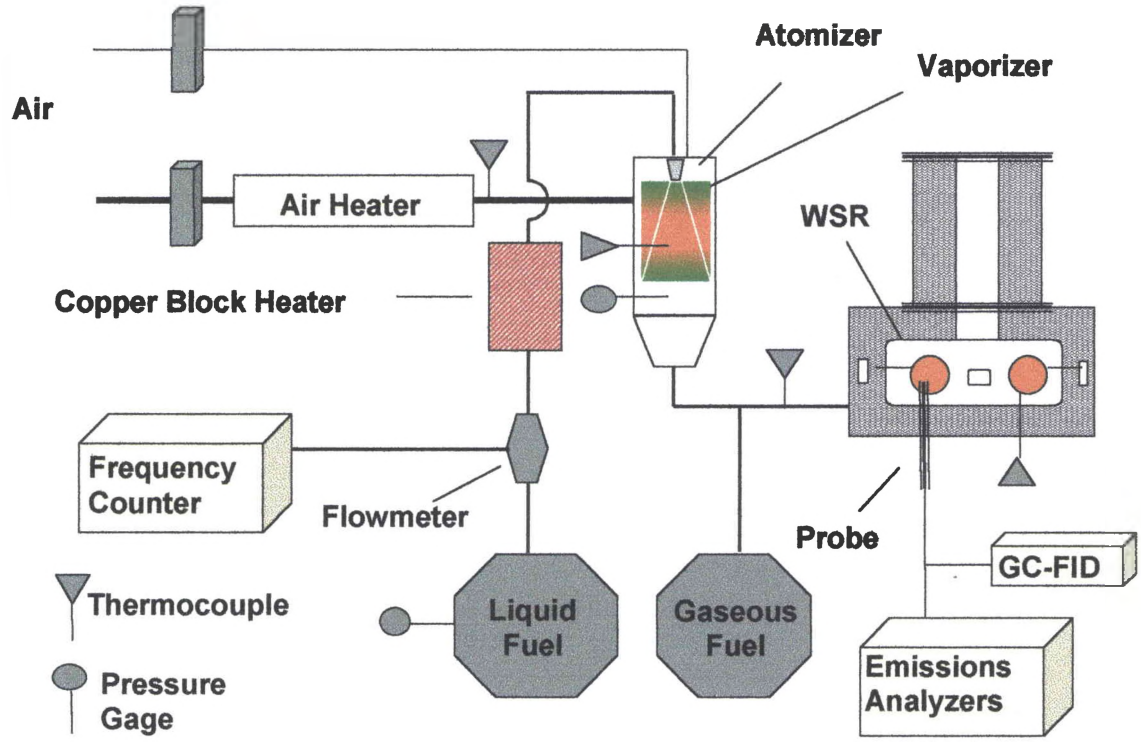

Figure 3. Well-stirred reactor test facility and instrumentation.

Hydrocarbons studied in the WSR include: methane, ethane, *n*-heptane, toluene, ethylbenzene, Jet A, and a gaseous mix comprising 13% methane, 22% ethane, 52% ethylene and 13% toluene by volume. The endothermic cracking of normal paraffins has been investigated experimentally by Sobel and Spadaccini (1997). The product efflux consisted primarily of low molecular weight alkenes and alkanes (ethylene, propene, propane, ethane and methane) and hydrogen. Hence, the gaseous mix is a simulant of a cracked endothermic fuel. Gaseous fuels were commercially pure grade and pure hydrocarbon liquids were spectroscopic grade (99+ %). Jet A comprised 22% aromatics by volume. A complete test matrix is shown in Table 1.

Table 1. Well-stirred reactor test matrix

Fuel	Carbon Number	C/H ratio	τ (msec)	ϕ_{min}	ϕ_{max}	$T_{f,min}$ (K)	$T_{f,max}$ (K)
CH_4	1	0.2500	7.30	0.55	0.88	1507	1967
			6.32	0.59	0.83	1517	1918
C_2H_6	2	0.3333	7.26	0.48	0.84	1407	1996
C_7H_{16}	7	0.4375	7.19	0.53	0.84	1517	1975
			5.49	0.54	0.81	1595	1974
C_7H_8	7	0.8750	7.32	0.46	0.79	1499	1946
			5.35	0.50	0.78	1552	1936
C_8H_{10}	8	0.8000	7.43	0.48	0.76	1478	1958
$C_{12}H_{26}$	12	0.4615	7.39	0.46	0.80	1357	1979
			5.48	0.46	0.79	1329	1983
Endothermic Simulant (Average $C_{2.52}H_{4.96}$) *13% CH_4 22% C_2H_6 52% C_2H_4 13% C_7H_8	~2.52	~0.5081	6.75	0.49	0.77	1530	2007
Jet A (Average $C_{10}H_{19}$)	~10	~0.5263	7.54	0.43	0.74	1342	1949

* By Volume

CHAPTER IV

RESULTS AND COMPARISONS

Introduction

During the course of the present research, modeling studies were completed for each of the fuels discussed in Chapter III. In this chapter computations are compared with the experimental data obtained by Blust (1998) described in Chapter III. Emissions of O_2 and CO_2 are examined briefly, while a more in depth look is taken at CO and NO_x. Since most of the fuels investigated are "pure" alkanes or aromatics, modeling them is fairly straightforward. However, a detailed computational consideration of all the individual components of complex, practical fuels (such as Jet A) is prohibitive (Lindstedt and Maurice, 1997; Maurice, 1996). Previous Jet A modeling studies (Lindstedt and Maurice, 1997) show that global combustion characteristics, as well as many key intermediate hydrocarbons, are captured by a surrogate fuel model comprising alkane and aromatic molecules. Therefore, due to the analogies previously observed between *n*-decane and Jet A combustion (Vovelle et al., 1994; Lindstedt and Maurice, 1997; Douté et al., 1995), the latter is presently represented by a surrogate model comprising 78% *n*-decane and 22% ethylbenzene by volume.

All measurements and computations are reported on a dry basis with standard air.

The equivalence ratios that correspond to the reactor temperatures in the various figures throughout this chapter are shown in Table 2. Equivalence ratio (ϕ) is the ratio of the measured fuel to air ratio divided by the stoichiometric fuel to air ratio. Thus, a ϕ of 1.0 indicates the stoichiometric condition. As ϕ approaches 1.0, the reactor temperature increases as more fuel is available to react with the available oxygen.

Table 2. Corresponding reactor temperatures and equivalence ratios.

Methane		Ethane		n-Heptane		n-Heptane, $\tau \sim 5.3$ msec		n-Dodecane	
T(K)	ϕ	T(K)	ϕ	T(K)	ϕ	T(K)	ϕ	T(K)	ϕ
1507	0.549	1403	0.487	1517	0.528	1595	0.538	1357	0.460
1596	0.599	1523	0.529	1638	0.601	1699	0.614	1412	0.490
1696	0.658	1597	0.566	1707	0.652	1787	0.679	1498	0.520
1754	0.705	1658	0.609	1779	0.701	1868	0.724	1561	0.540
1842	0.767	1743	0.655	1842	0.749	1923	0.761	1626	0.570
1893	0.811	1826	0.703	1922	0.804	1974	0.808	1685	0.610
1967	0.879	1898	0.758	1975	0.837			1725	0.630
		1950	0.767					1793	0.670
		1996	0.839					1862	0.720
								1912	0.760
								1958	0.790

Ethylbenzene		Toluene		Toluene, $\tau \sim 5.3$ msec		Jet A		Cracked Fuel Simulant	
T(K)	ϕ	T(K)	ϕ	T(K)	ϕ	T(K)	ϕ	T(K)	ϕ
1478	0.481	1439	0.464	1552	0.497	1411	0.444	1558	0.508
1532	0.501	1548	0.506	1650	0.555	1480	0.464	1652	0.562
1589	0.528	1643	0.556	1717	0.598	1596	0.519	1728	0.602
1633	0.553	1713	0.598	1785	0.651	1657	0.551	1801	0.642
1669	0.577	1787	0.651	1851	0.706	1696	0.573	1888	0.690
1722	0.608	1847	0.712	1904	0.751	1762	0.613	1953	0.737
1752	0.626	1886	0.752	1936	0.780	1836	0.660	2007	0.767
1796	0.655	1946	0.785			1899	0.703		
1830	0.674					1949	0.737		
1876	0.708								
1906	0.726								
1958	0.764								

Computations and measurements were made for a residence time (τ) of approximately 7.3 msec. For *n*-heptane and toluene, τ is approximately 5.3 msec data were also obtained. As shown throughout this chapter, comparisons of experimental data and computations generally show reasonable agreement for major species. Typically, agreement between the model and computations is within a factor of two or better, and qualitative agreement is very good.

Carbon Dioxide

Carbon dioxide emissions computed for all of the fuels considered are plotted versus reactor temperature, T_f, in Figure 4. For lean combustion, emissions of CO_2 should increase with equivalence ratio (ϕ). As can be seen in Figure 4, this is accurately predicted by the detailed kinetic mechanism. It is also observed that these predicted emissions are not strongly affected by fuel type.

Predicted CO_2 emissions are compared to the experimental emissions by fuel type. Alkanes (methane, ethane and *n*-heptane) are shown in Figure 5, aromatics (toluene and ethylbenzene) in Figure 6, and fuel blends (Jet A and the cracked fuel simulant) in Figure 7. Unfortunately, the CO_2 analyzer was not functioning properly when Blust (1998) was collecting data for toluene. Thus, there is only one experimental point for toluene at a τ of 7.3 msec, and none for a τ of 5.3 msec in Figure 6. In all three cases (except toluene), both qualitative and quantitative agreement between the predicted and

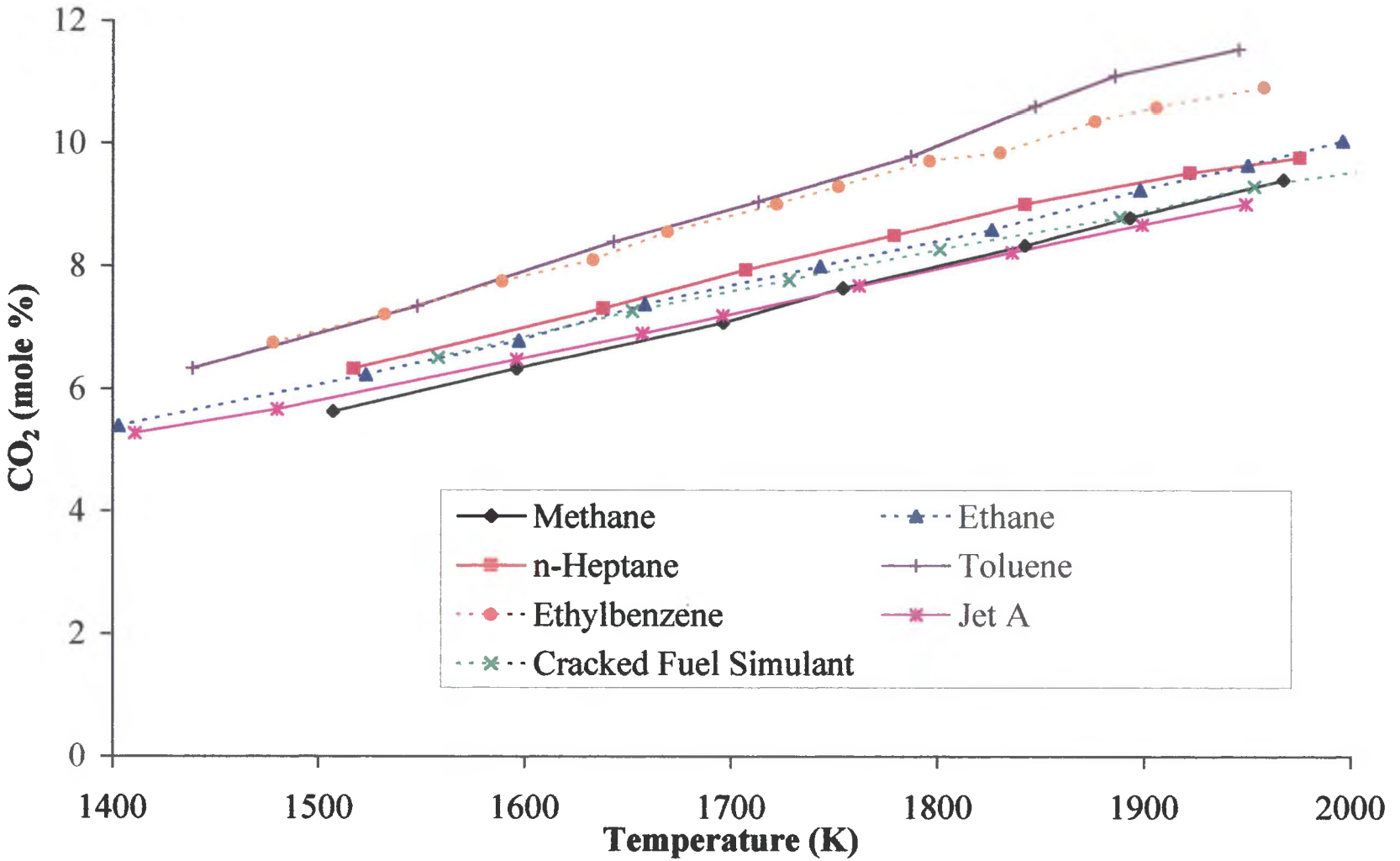

Figure 4. Computed CO_2 emissions versus reactor temperature.

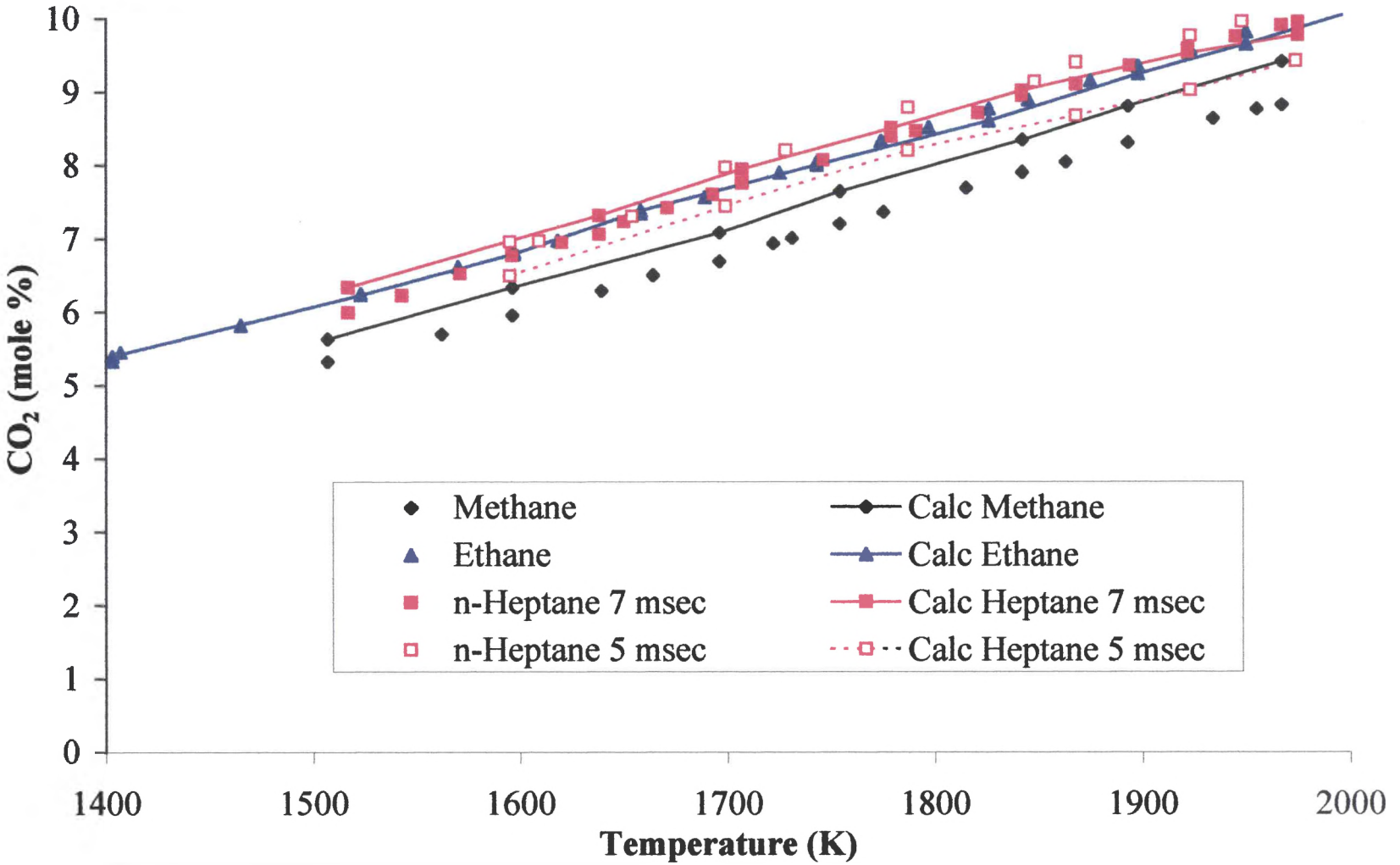

Figure 5. Computed and measured CO_2 emissions for alkanes versus reactor temperature.

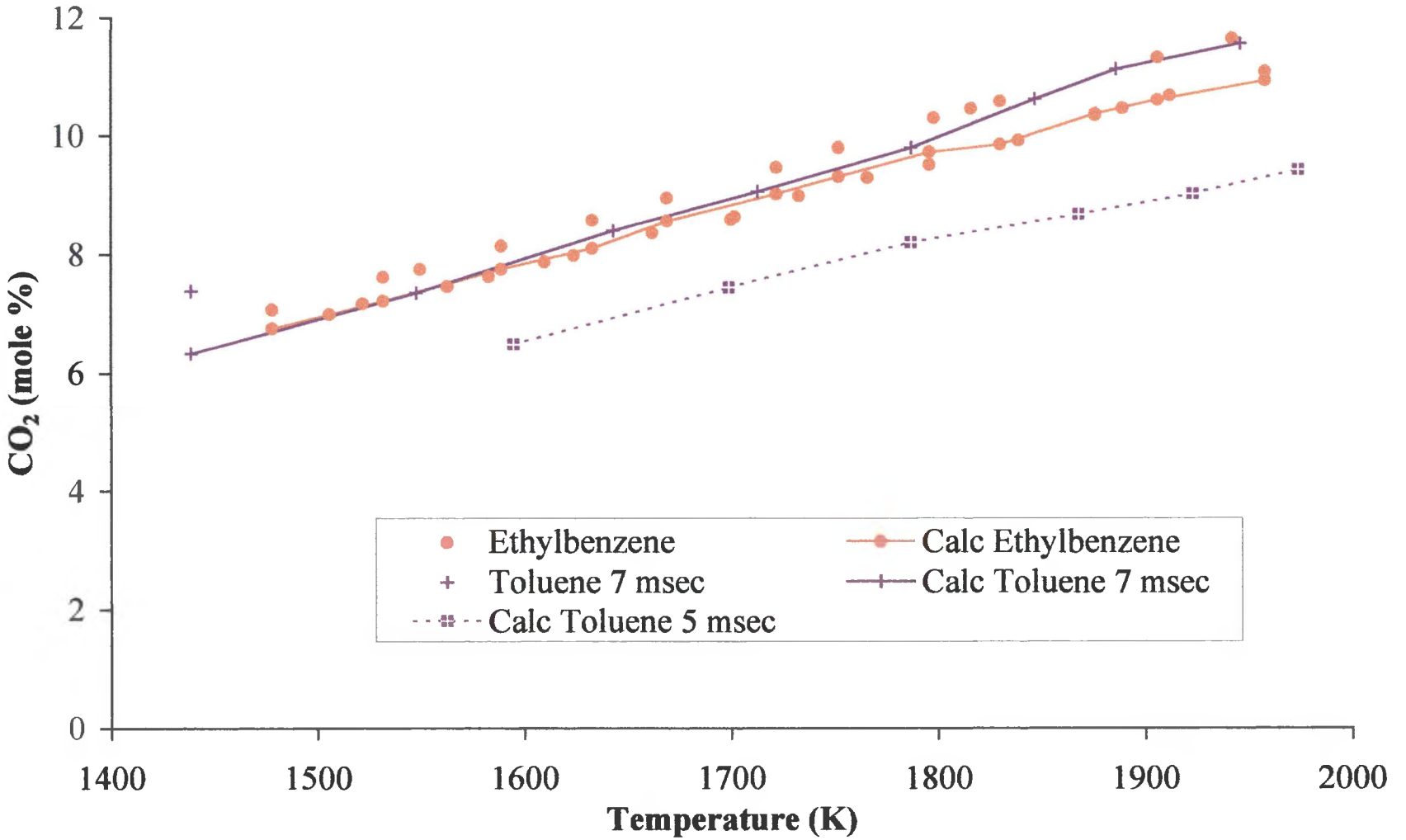

Figure 6. Computed and measured CO_2 emissions for aromatics versus reactor temperature.

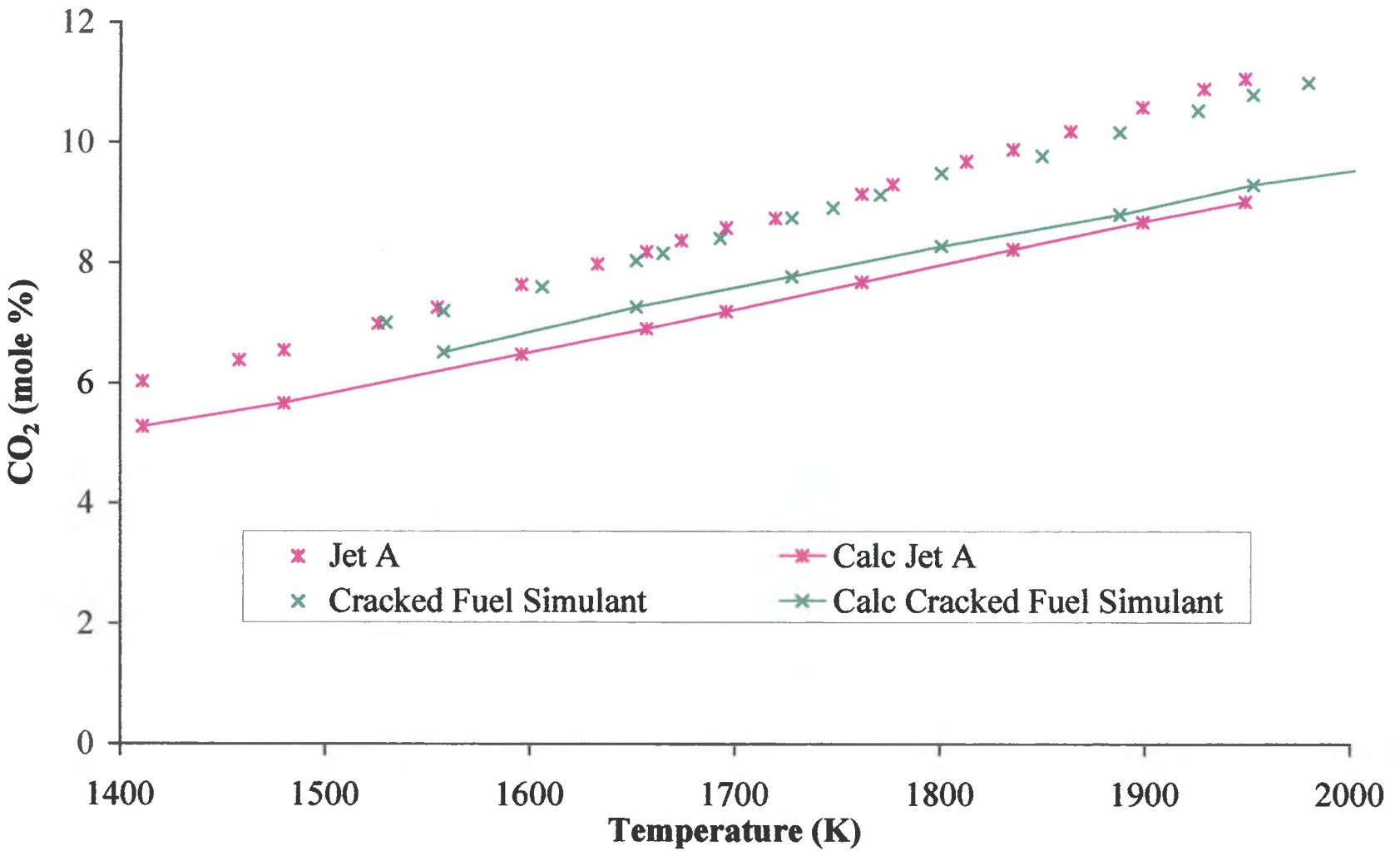

Figure 7. Computed and measured CO_2 emissions for hydrocarbon mixes versus reactor temperature.

measured values is observed. Within each fuel type, CO_2 emissions are observed to increase slightly with increasing molecular weight.

Oxygen

Oxygen emissions computed for all of the fuels are plotted versus reactor temperature, T_f, in Figure 8. Emissions of O_2 should drop to near zero as ϕ approaches 1.0 (the stoichiometric condition). As can be seen in Figure 8, this is accurately predicted by the detailed kinetic mechanism. It is also observed that these predicted emissions are not strongly affected by fuel type.

Predicted O_2 emissions are compared to the experimental emissions by fuel type. Alkanes (methane, ethane and *n*-heptane) are shown in Figure 9, aromatics (toluene and ethylbenzene) in Figure 10, and fuel blends (Jet A and the cracked fuel simulant) in Figure 11. Data for *n*-heptane at a τ of 7 msec is not shown because of trouble with the oxygen analyzer during the experiment. In all three cases (except for *n*-heptane), both qualitative and quantitative agreement between the predicted and measured values is observed. Within each fuel type, O_2 emissions are observed to increase slightly with increasing molecular weight.

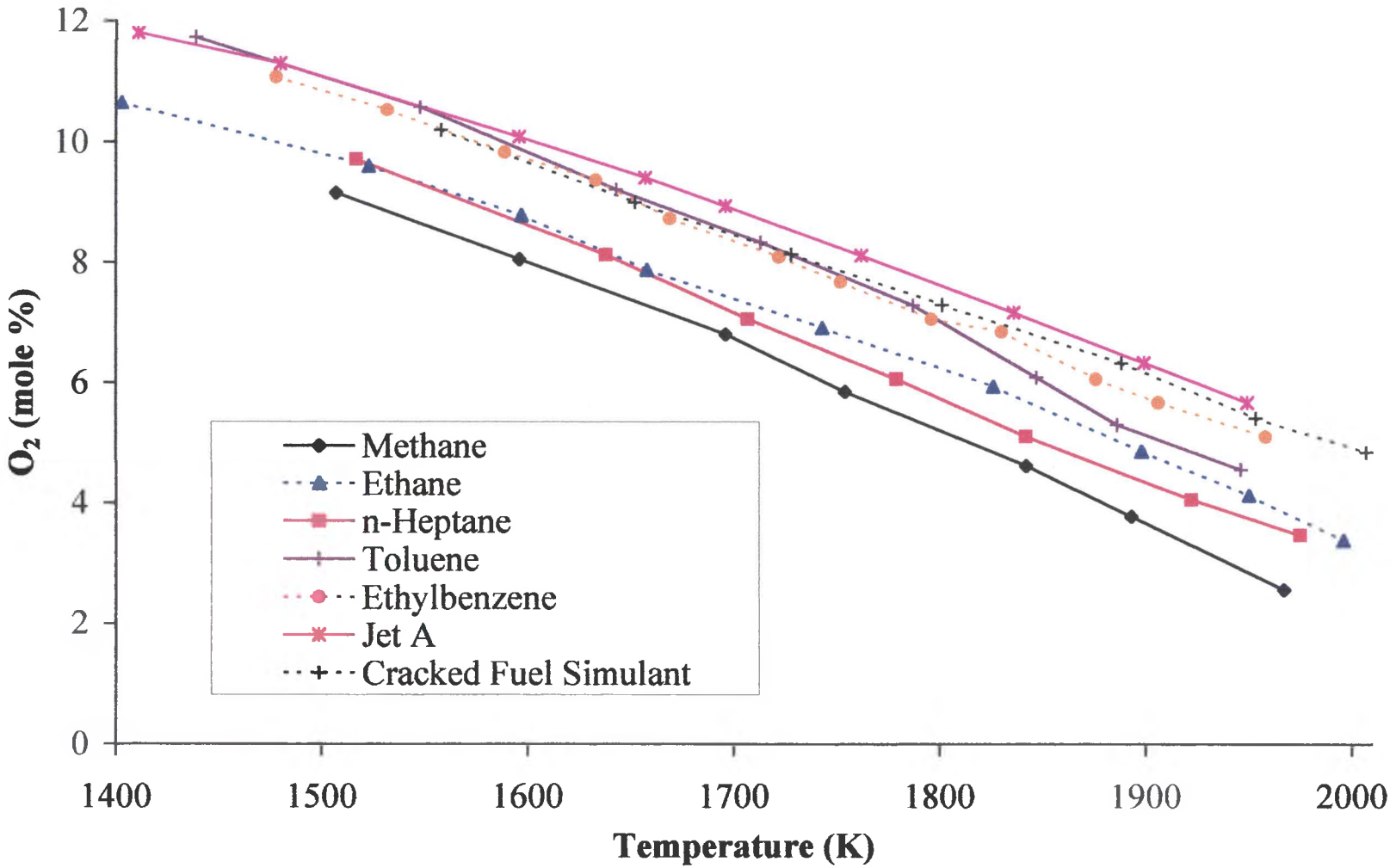

Figure 8. Computed O_2 emissions versus reactor temperature.

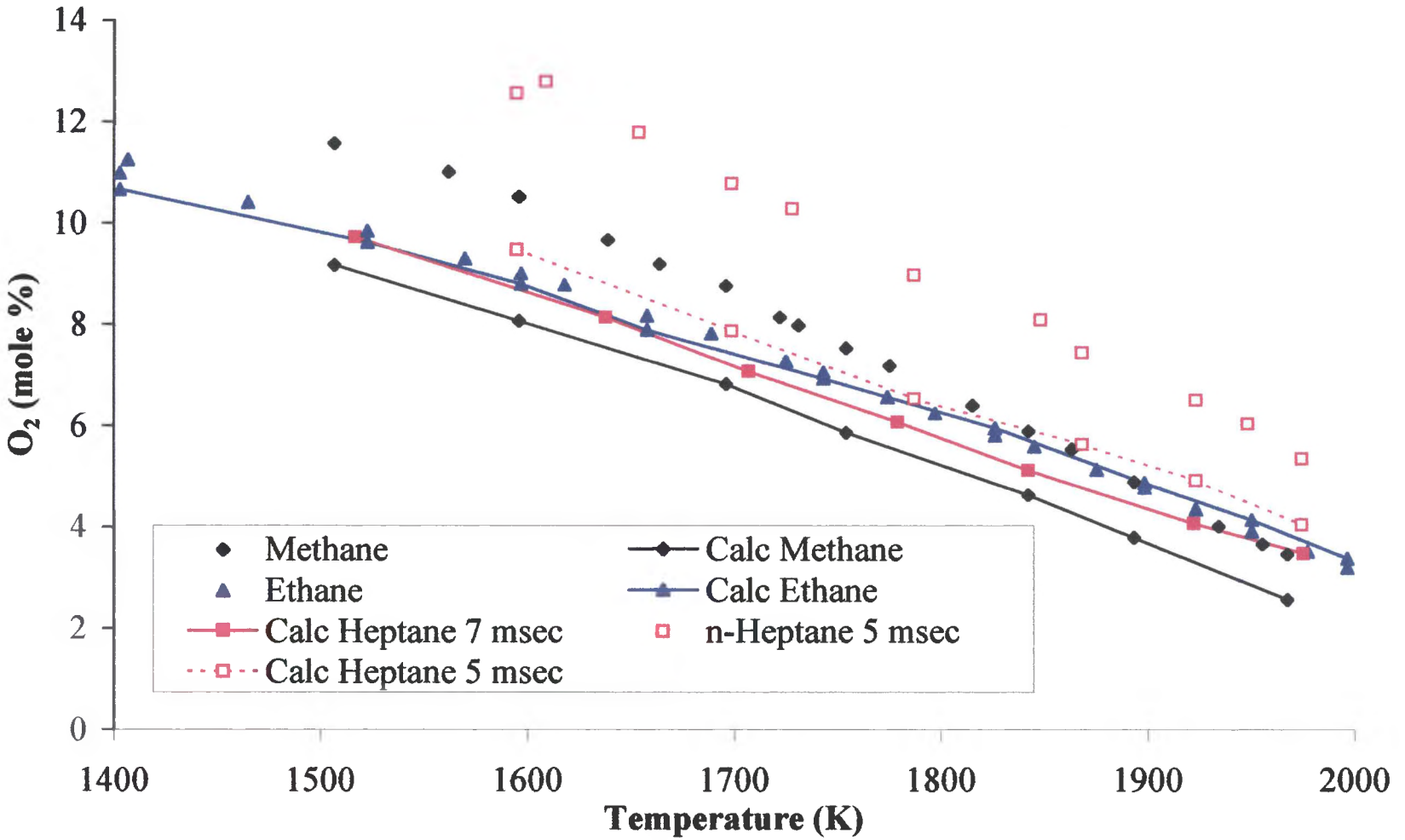

Figure 9. Computed and measured O_2 emissions for alkanes versus reactor temperature.

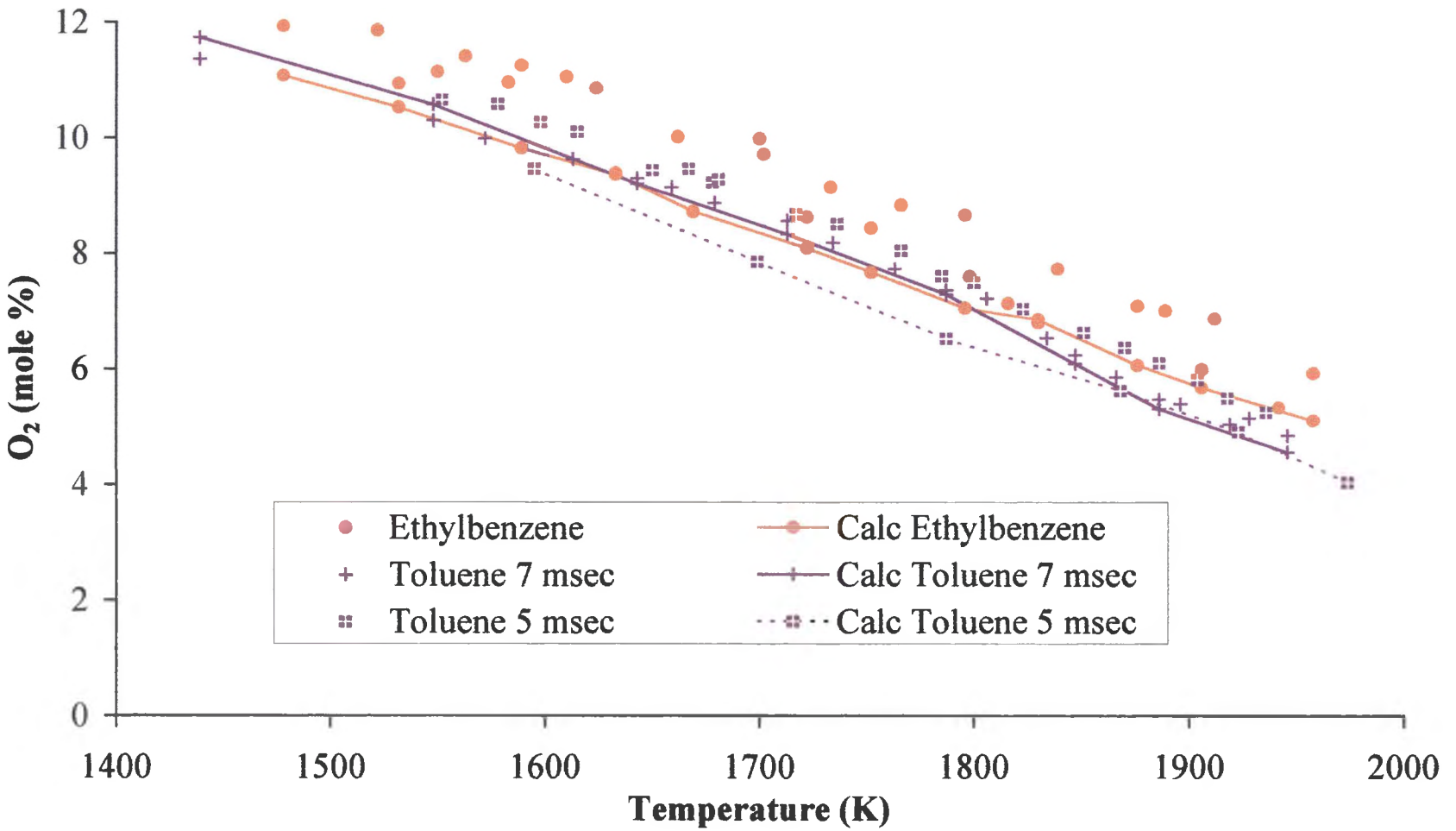

Figure 10. Computed and measured O_2 emissions for aromatics versus reactor temperature.

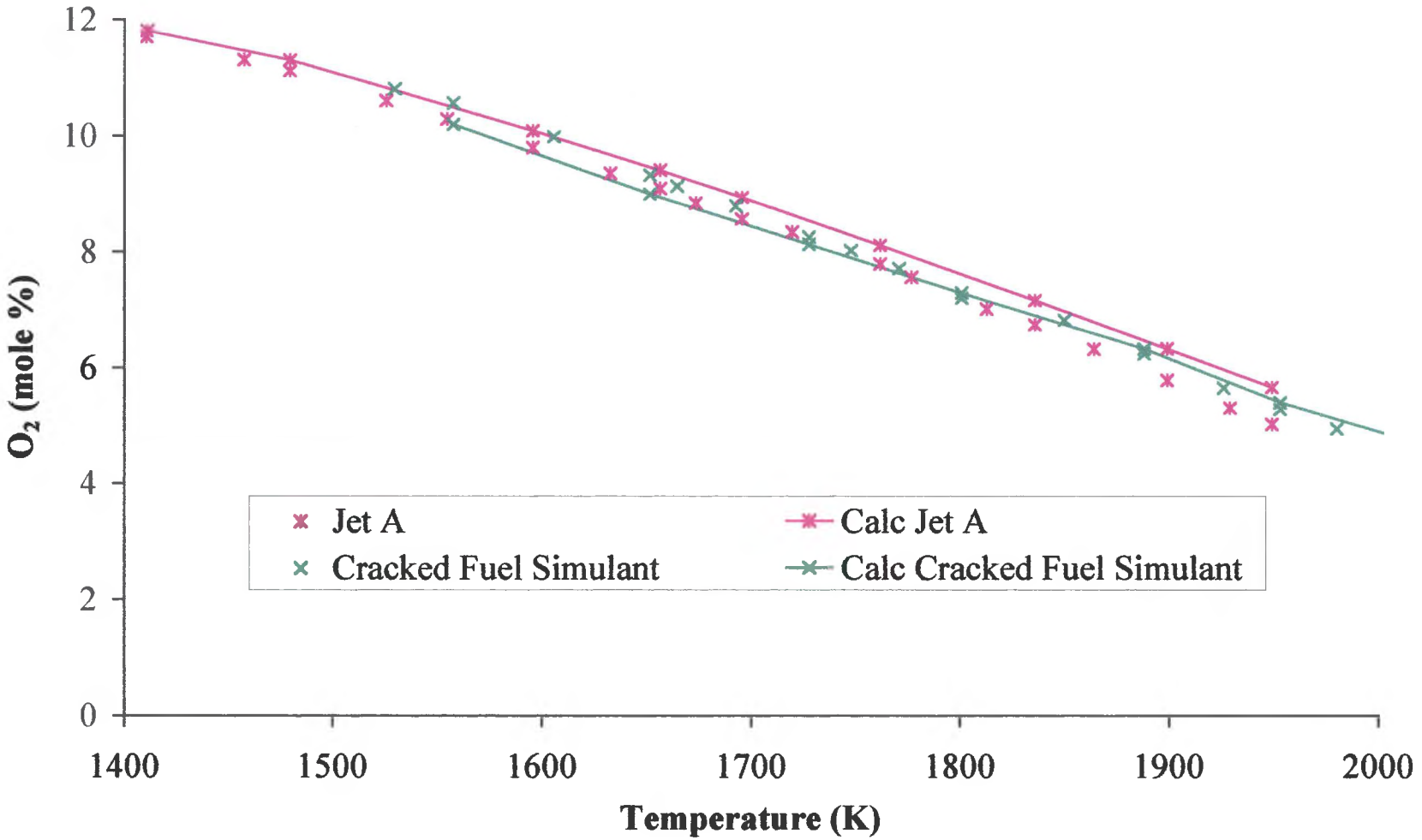

Figure 11. Computed and measured O_2 emissions for hydrocarbon mixes versus reactor temperature.

Carbon Monoxide

The predicted emissions of carbon monoxide as a function of T_f are shown in Figure 12. Carbon monoxide produced in the combustion of hydrocarbons over a range of temperatures exhibits a U-shaped trend, with clearly defined points of minimum CO concentration. This occurs because at low temperatures (ϕ less than about 0.5) the oxidation of CO to CO_2 is slow and at high temperatures (ϕ greater than about 0.9) CO burns quickly to an equilibrium condition (Lefebvre, 1983). The corresponding equilibrium CO concentration profile for methane, computed using the Gordon and McBride model (1976), is also shown in Figure 12.

Predicted CO emissions are then compared to the experimental emissions by fuel type. Alkanes (methane, ethane and *n*-heptane) are shown in Figure 13, aromatics (toluene and ethylbenzene) in Figure 14, and fuel blends (Jet A and the cracked fuel simulant) in Figure 15. The quantitative agreement achieved for CO emissions generally improves with increasing temperature. Carbon monoxide emissions are predicted within 10% for Jet A. The worst agreement for CO emissions is observed for the cracked fuel simulant, arguably a very complex experimental case because of the difficulties in mixing both vaporized liquid fuels and gaseous fuels in the reactor in the right proportions. However, as with other fuels, the agreement substantially improves with increasing temperature.

In all three cases, the temperature at which the CO concentrations reach a minimum, T_{min}, decreases as a function of carbon number, in direct agreement with experimental observation. Inlet temperature is corrected to a standard temperature of 296 K for the T_{min} calculations. As seen in Figure 12, super-equilibrium CO values are

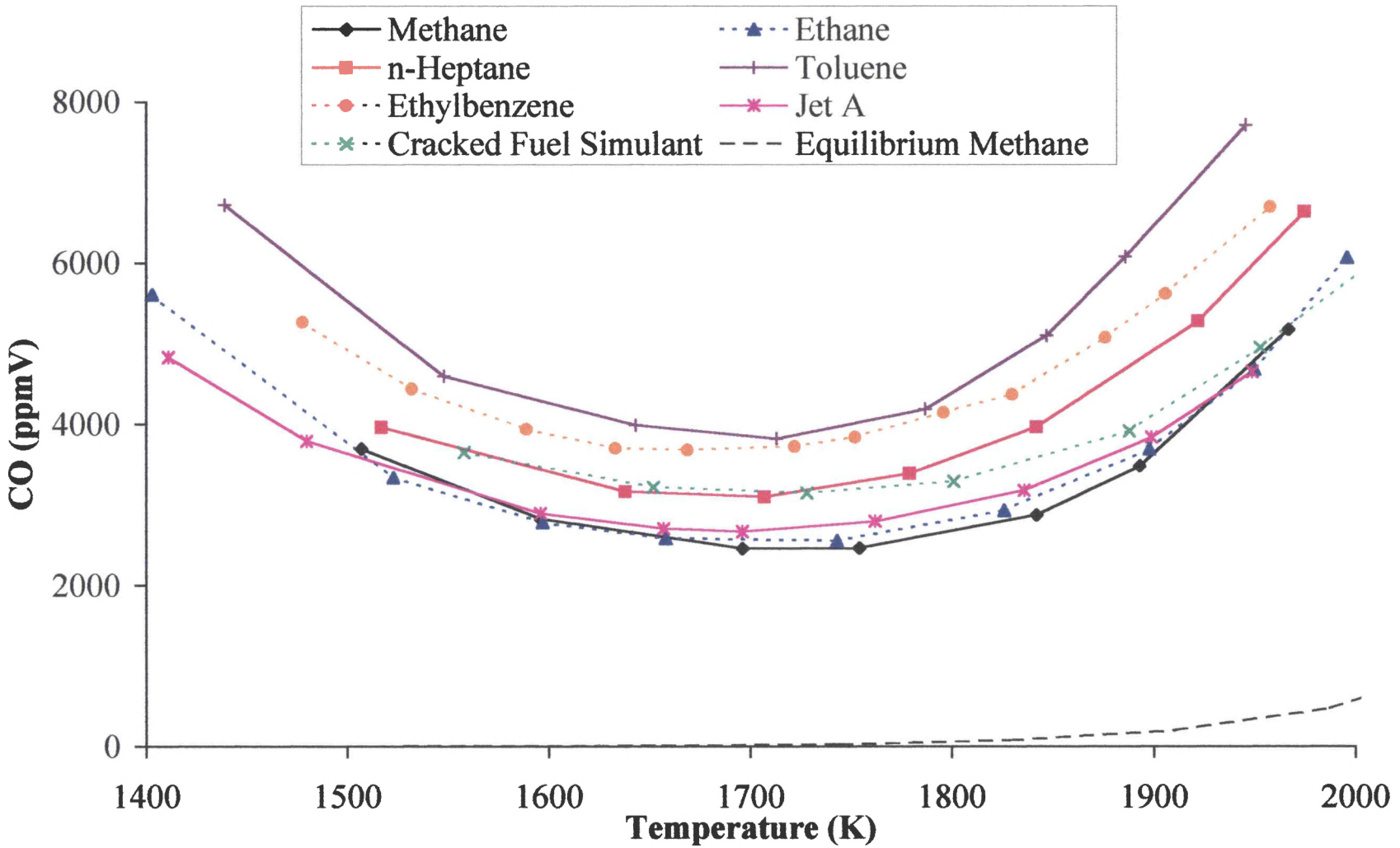

Figure 12. Computed CO emissions versus reactor temperature.

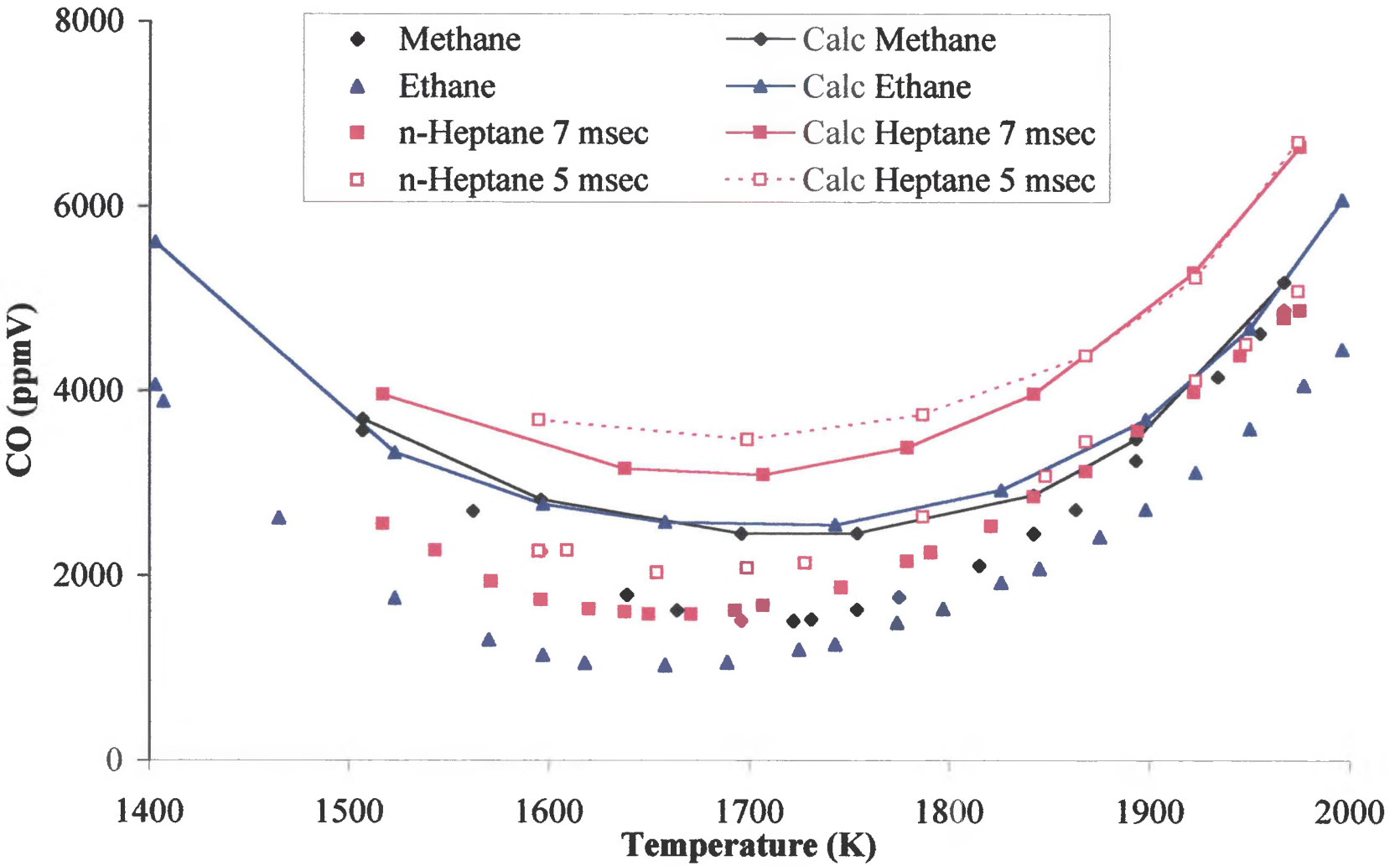

Figure 13. Computed and measured CO emissions for alkanes versus reactor temperature.

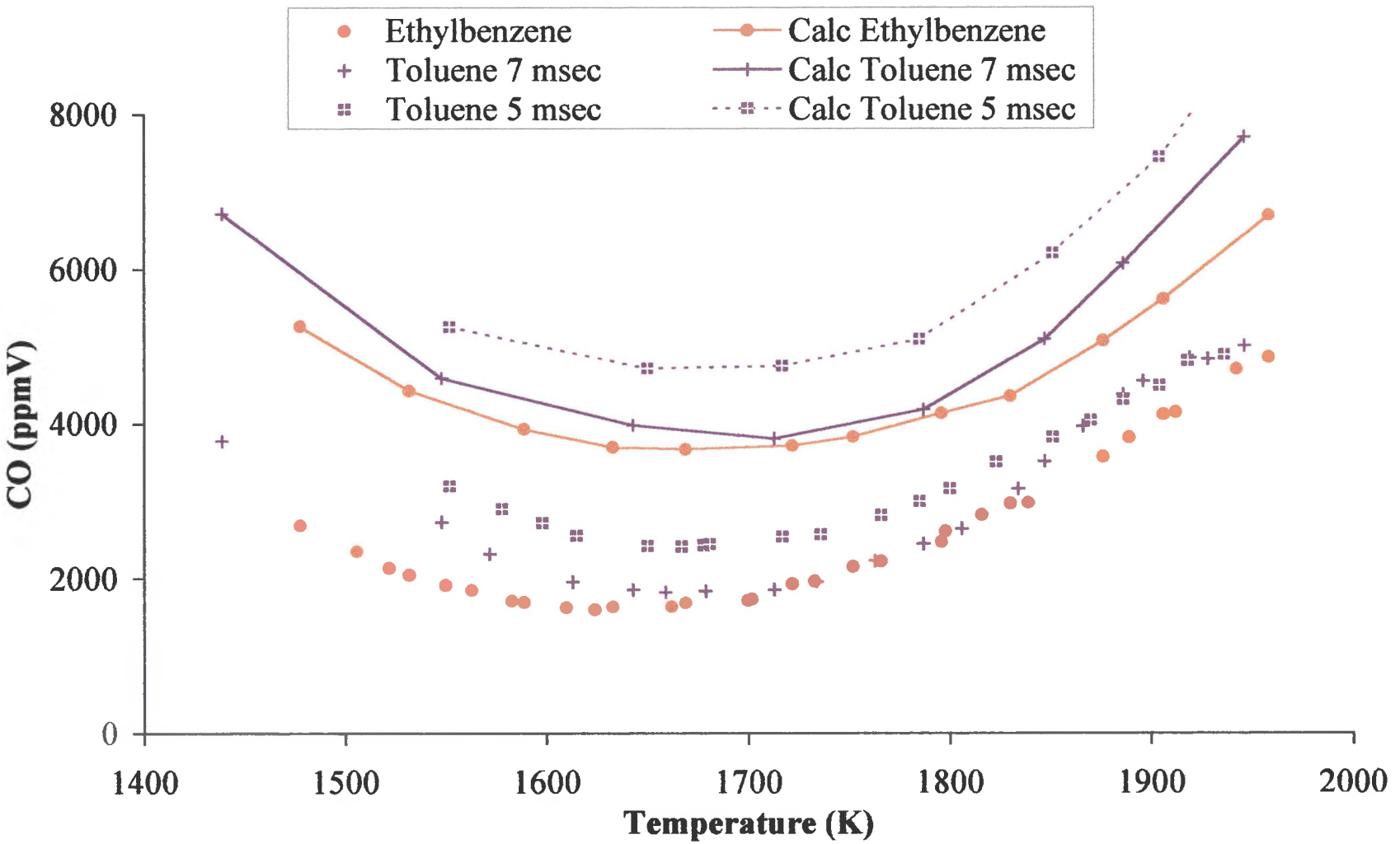

Figure 14. Computed and measured CO emissions for aromatics versus reactor temperature.

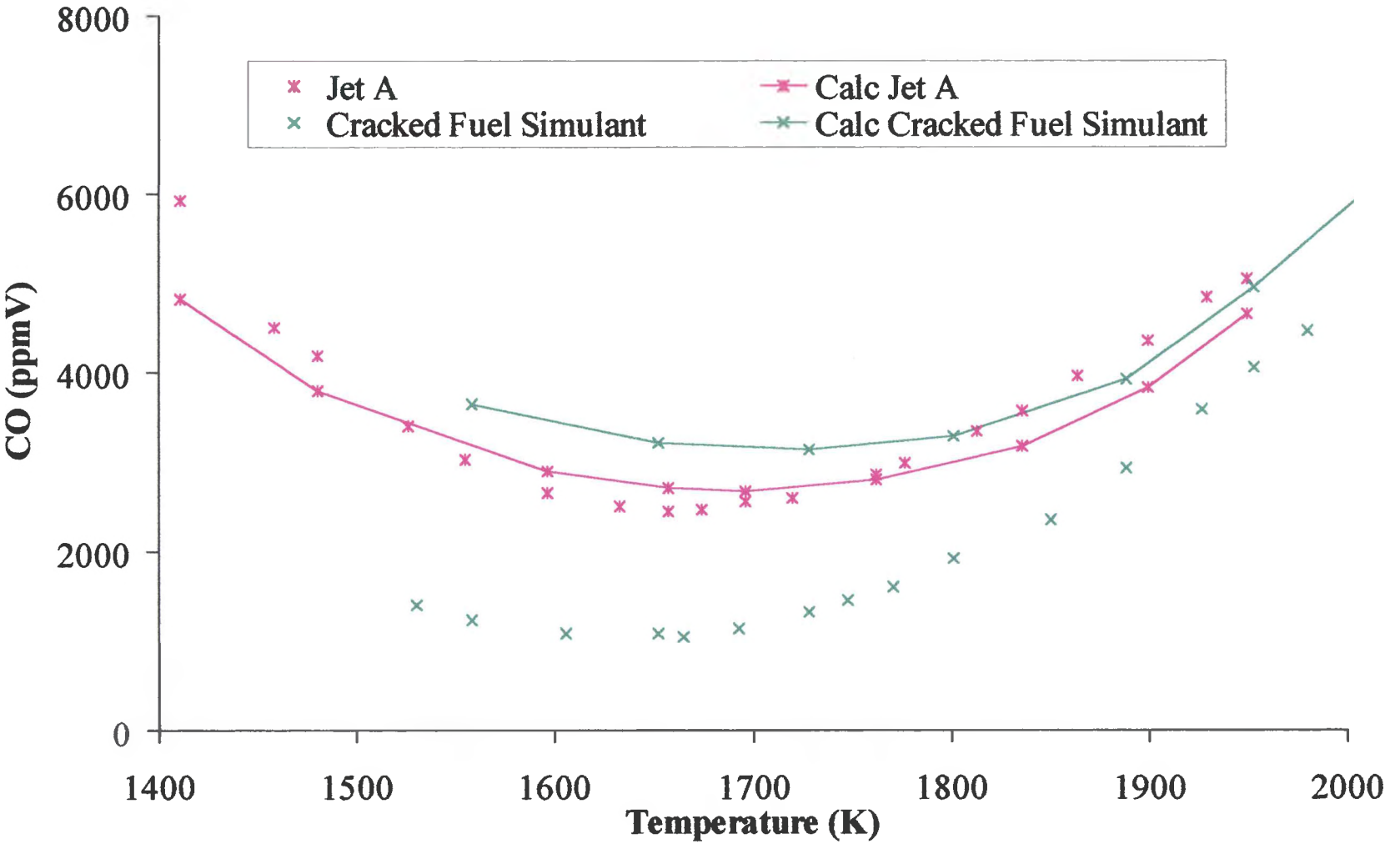

Figure 15. Computed and measured CO emissions for hydrocarbon mixes versus reactor temperature.

predicted since the residence time is significantly lower than that required to achieve equilibrium. It is also observed that within each fuel type, CO emissions are generally greater for fuels with greater carbon number. Finally, as shown in Figures 13 and 14 the model accurately reproduces the effect of reactor residence time on emissions. Increasing τ decreases the amount of both calculated and measured CO.

Oxides of Nitrogen

The predicted emissions of oxides of nitrogen are shown in Figure 16 as a function of T_f. In contrast to CO concentrations, computations of NO_x emissions are not strongly affected by fuel type. A notable exception is methane, which exhibits greater NO_x formation at T_f less than 1900 K.

NO_x emissions from the combustion of alkanes (methane, ethane and *n*-heptane) are shown in Figure 17, aromatics (toluene and ethylbenzene) in Figure 18, and fuel mixes (Jet A and the cracked fuel simulant) in Figure 19. Emissions of NO_x are very well predicted for Jet A and the cracked fuel simulant (Figure 19). Predictions for aromatic fuels (Figure 18) are also very reasonable. However, it is noted that predictions become less accurate as temperature increases. Computed NO_x emissions are generally less accurate for alkanes, where the model over-predicts NO_x even at lower temperatures. Moreover, in contrast to numerical predictions (Figure 16), experimental observations indicate that methane generates less NO_x than the other fuels investigated. The observed discrepancies may be due in part to the inherent difficulties of modeling the methyl radical chemistry (Lindstedt and Skevis, 1997), and hence the relative effects of the

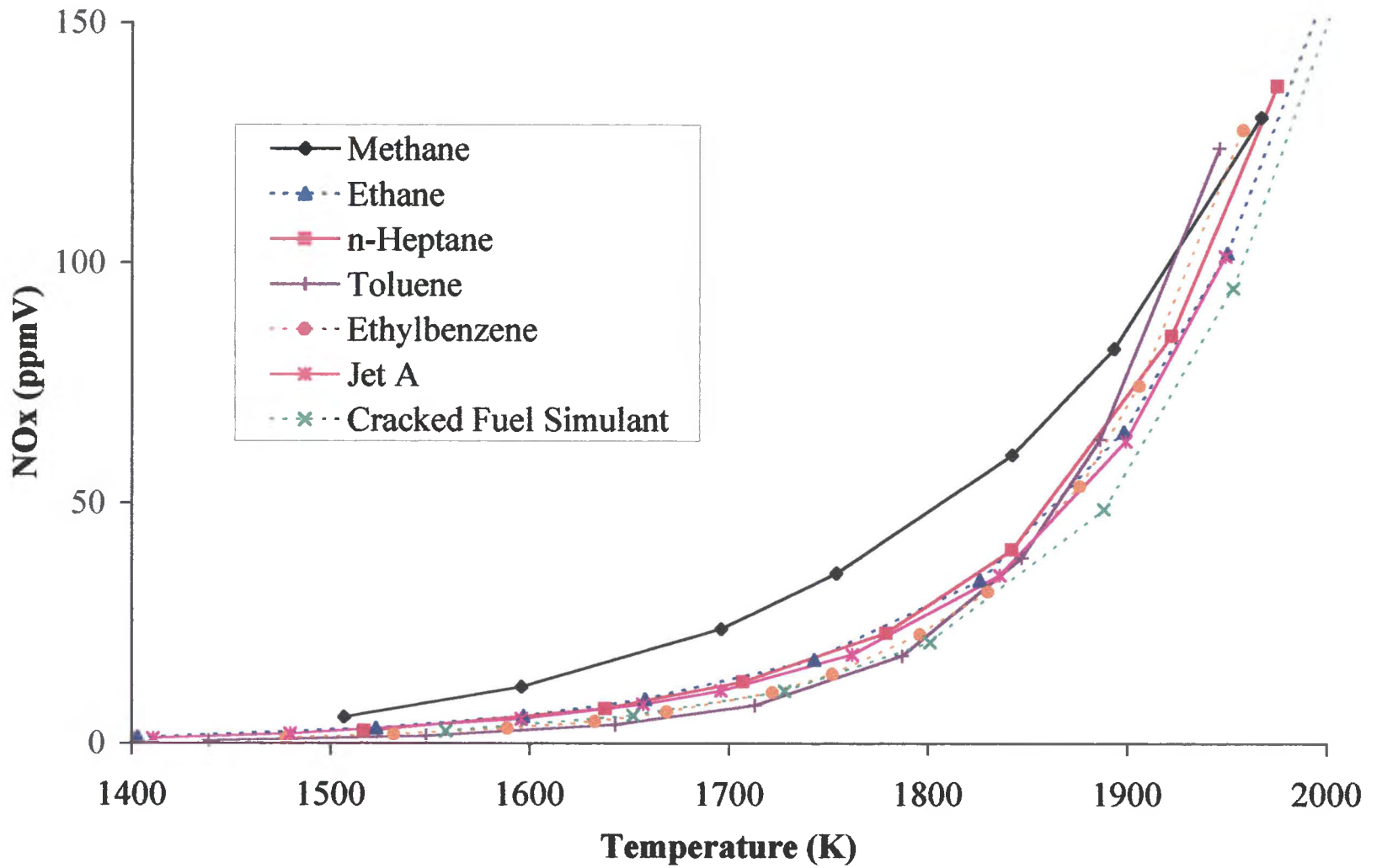

Figure 16. Computed NO_x emissions versus reactor temperature.

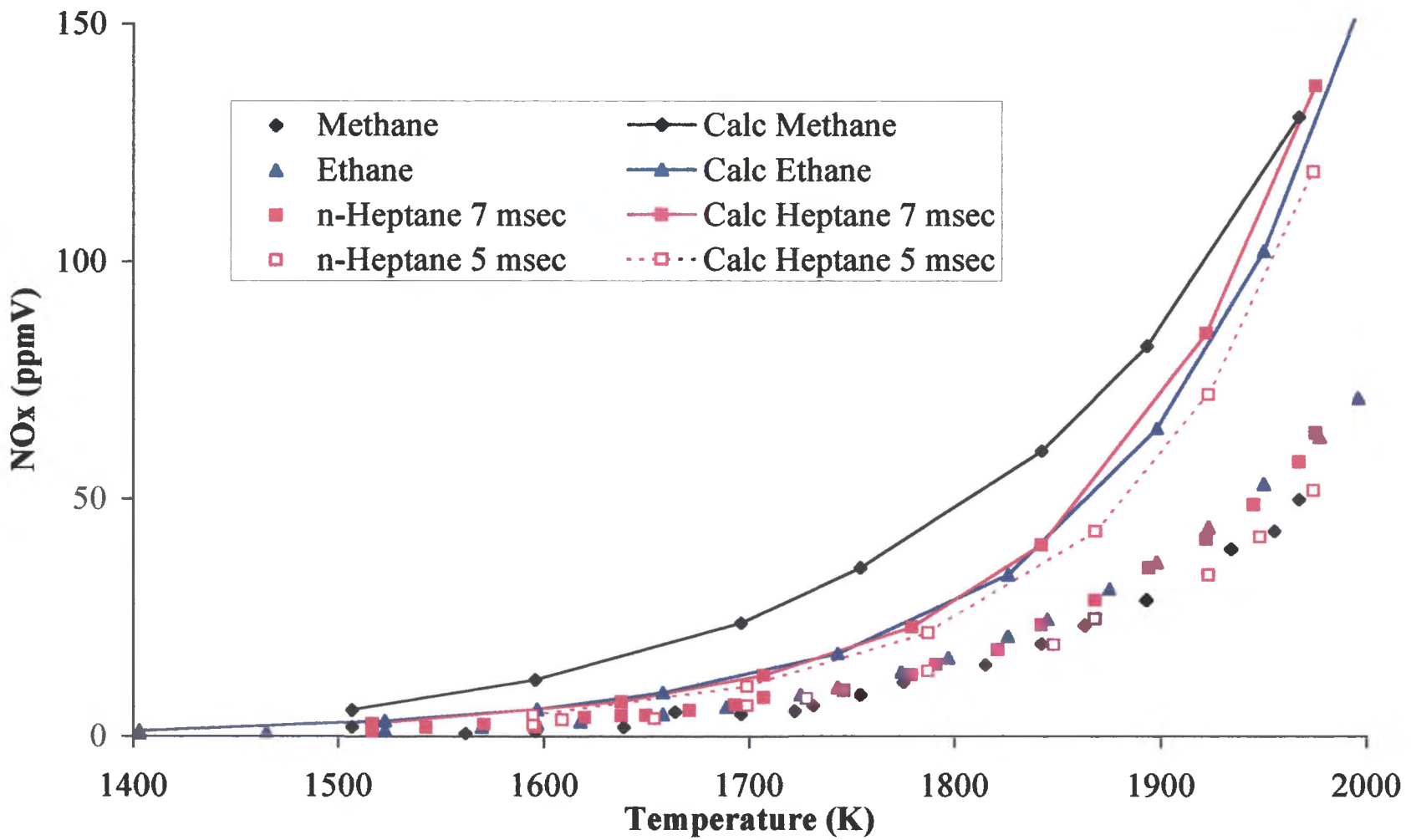

Figure 17. Computed and measured NO_x emissions for alkanes versus reactor temperature.

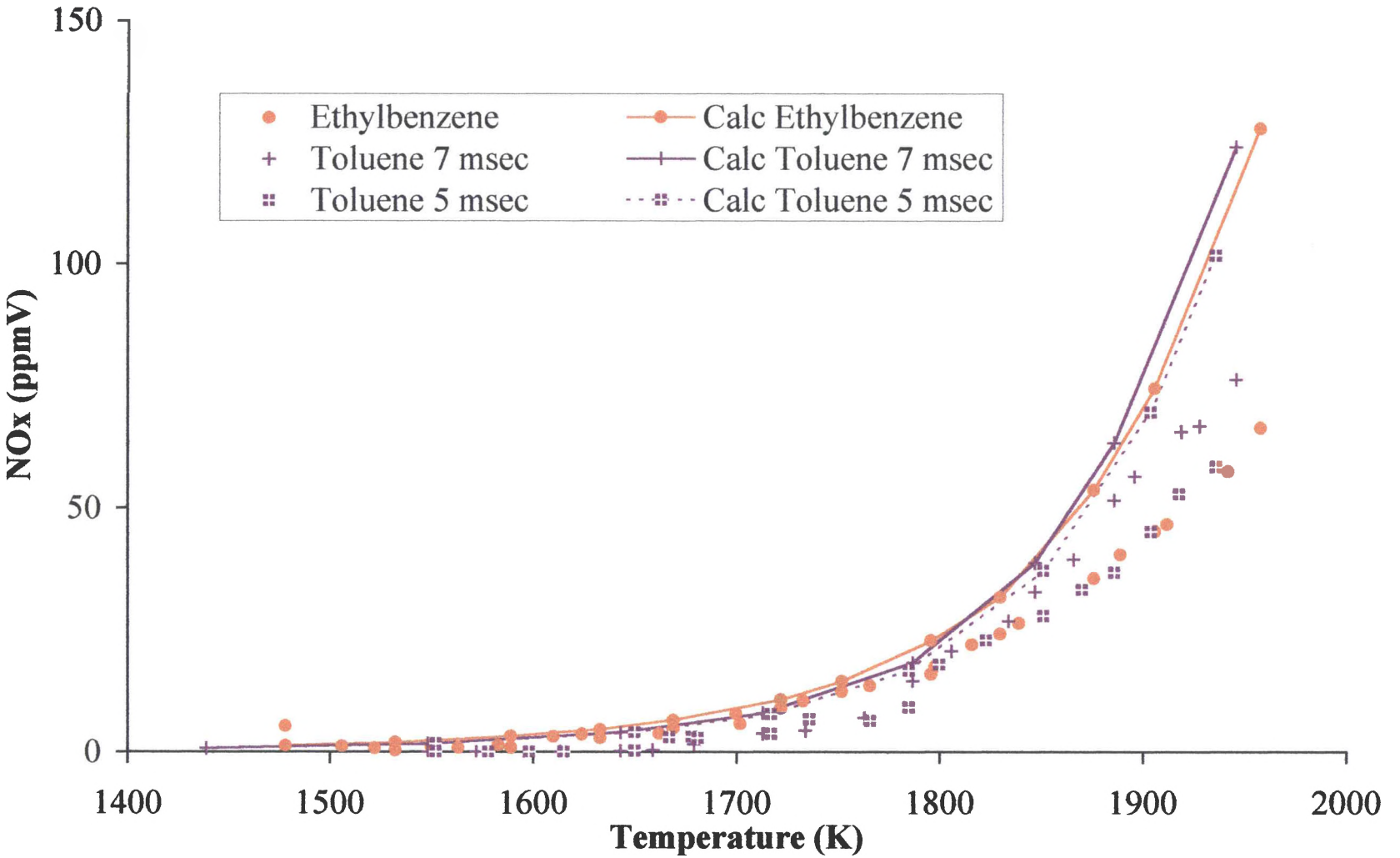

Figure 18. Computed and measured NO_x emissions for aromatics versus reactor temperature.

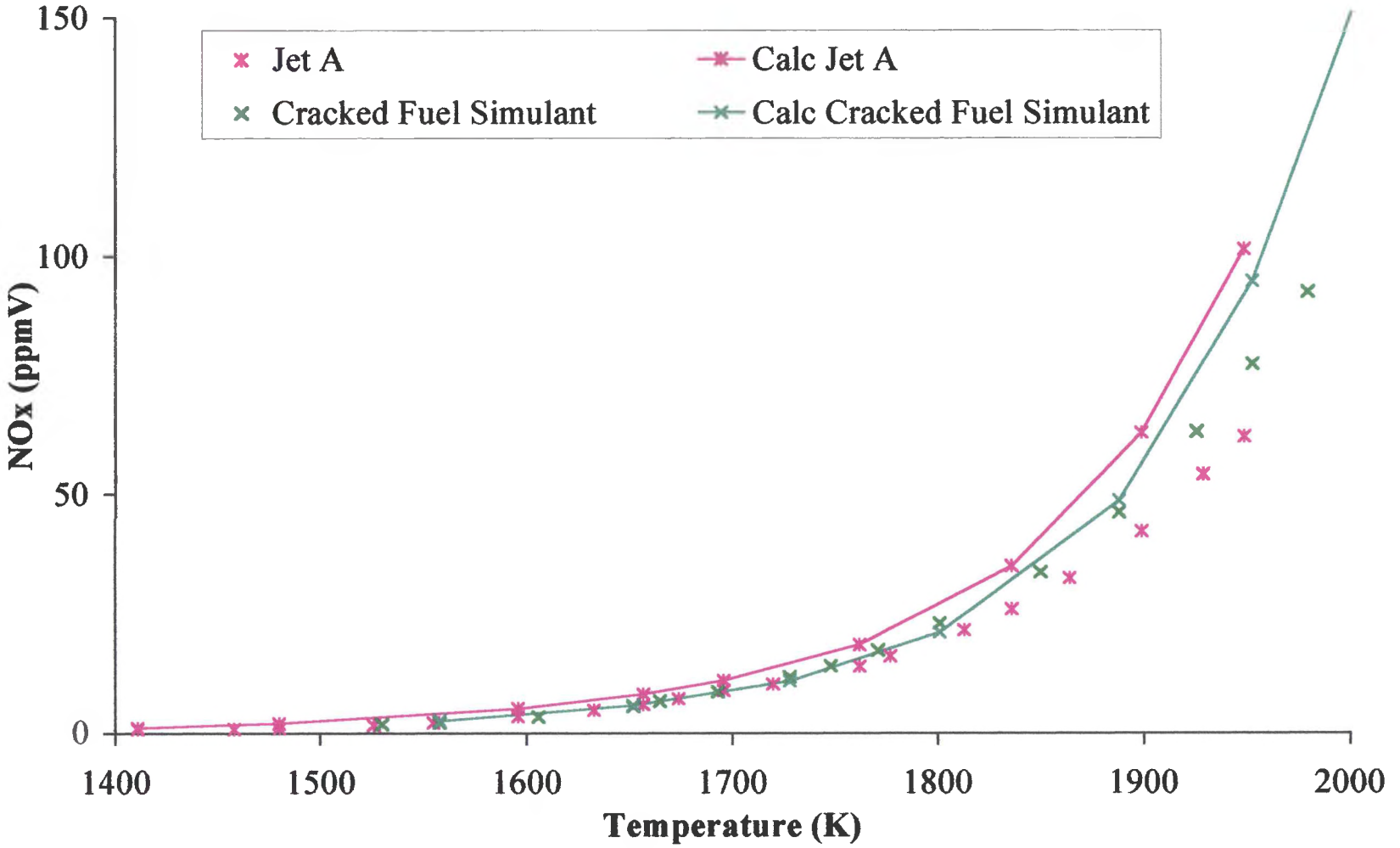

Figure 19. Computed and measured NO_x emissions for hydrocarbon mixes versus reactor temperature.

prompt NO formation channel and the reburn mechanism (in which NO is destroyed by reaction with hydrocarbon fragments, see Equations 27 through 31 below) on emissions. Finally, as shown in Figures 17 and 18, the model accurately reproduces the effect of reactor residence time on emissions. Increasing τ increases the calculated and measured NO_x.

In direct agreement with experimental observations, computations show that aromatics feature somewhat lower NO_x emissions than alkanes at T_f less than 1850 K. This occurs because the formation of CH_x molecules is slower for aromatics at lower temperatures than that observed for alkanes since overall fuel consumption is significantly faster for the latter. Hence, the contribution from the prompt NO_x formation channel is somewhat reduced for the aromatics at T_f less than 1850 K. Also in direct agreement with measurements, calculated NO_x from aromatics is higher than that from alkanes for T_f greater than 1850 K. At these conditions, the efflux of the branched aromatics comprises greater (~20-30%) amounts of CH_x molecules than observed for the alkanes at equivalent temperatures. Consequently, the net rates of the NO_x formation reactions are generally faster for the aromatics at T_f greater than 1850 K.

The reaction paths of NO_x are analyzed in order to assess mechanistic differences between the fuels. The primary paths of NO_x formation and destruction are generally similar. Variations in relative contributions caused by differences in the radical pools are modest. However, observed differences in net rates as a function of fuel type clearly show the need to consider the multi-component nature of complex hydrocarbon fuels for predicting emissions.

The primary (~80%) NO_x species observed for all fuels is NO. The principal path of NO formation at lower equivalence ratios is the prompt channel, which is initiated by CH attack on molecular nitrogen yielding hydrogen cyanide (HCN).

$$N_2 + CH \longleftrightarrow HCN + N \qquad \text{Equation 19}$$

Subsequently, hydrogen cyanide is primarily converted to NO via the series of intermediate steps outlined by Selim (1995). As equivalence ratio (hence T_f) increases, the contribution of the Zel'dovich channel is more apparent, and NO_x formation increases exponentially.

$$N_2 + O \longleftrightarrow NO + N \qquad \text{Equation 20}$$

$$N + O_2 \longleftrightarrow NO + O \qquad \text{Equation 21}$$

$$N + OH \longleftrightarrow NO + H \qquad \text{Equation 22}$$

Nitrogen dioxide, which accounts for ~20% of NO_x emissions, is rapidly converted to NO via H and O atom attack.

$$NO_2 + H \longleftrightarrow NO + OH \qquad \text{Equation 23}$$

$$NO_2 + O \longleftrightarrow NO + O_2 \qquad \text{Equation 24}$$

The concentrations of N_2O predicted in the efflux of all the fuels are an order of magnitude lower than NO emissions. Nitrous oxide is principally converted to molecular nitrogen, and the N_2O intermediate channel is a secondary contributor to NO formation via H and O atom attack for all fuels.

$$N_2O + H \longleftrightarrow NO + NH \qquad \text{Equation 25}$$

$$N_2O + O \longleftrightarrow 2NO \qquad \text{Equation 26}$$

Removal of NO occurs via reactions with hydrocarbon fragments.

$$NO + CH \longleftrightarrow HCN + O \qquad \text{Equation 27}$$

$$NO + {}^1CH_2 \longleftrightarrow HCN + OH \qquad \text{Equation 28}$$

$$NO + CHO \longleftrightarrow HNO + CO \qquad \text{Equation 29}$$

$$NO + C \longleftrightarrow N + CO \qquad \text{Equation 30}$$

$$NO + C \longleftrightarrow CN + O \qquad \text{Equation 31}$$

The relative contribution of each path is generally unaffected by fuel type. However, the radical concentrations vary significantly at equivalent T_f amongst the fuels considered. Consequently, the net removal rates vary as a function of fuel type.

n-Dodecane

As discussed in Chapters I and II, a new detailed kinetic mechanism was created as part of this thesis. This mechanism expanded the *n*-decane mechanism of Lindstedt and Maurice to include reactions for *n*-dodecane. Thus, the computed and measured emissions from the combustion of *n*-dodecane are presented separately. This will make comparisons between them easier as well as highlight the predictive ability of the new mechanism.

The predicted and measured emissions from the combustion of *n*-dodecane are shown in Figures 20 (CO_2), 21 (O_2), 22 (CO), and 23 (NO_x) as a function of T_f. Residence times of 7.3 msec and 5.3 msec are shown. It is observed that the new detailed mechanism accurately predicts these emissions from the combustion of *n*-dodecane.

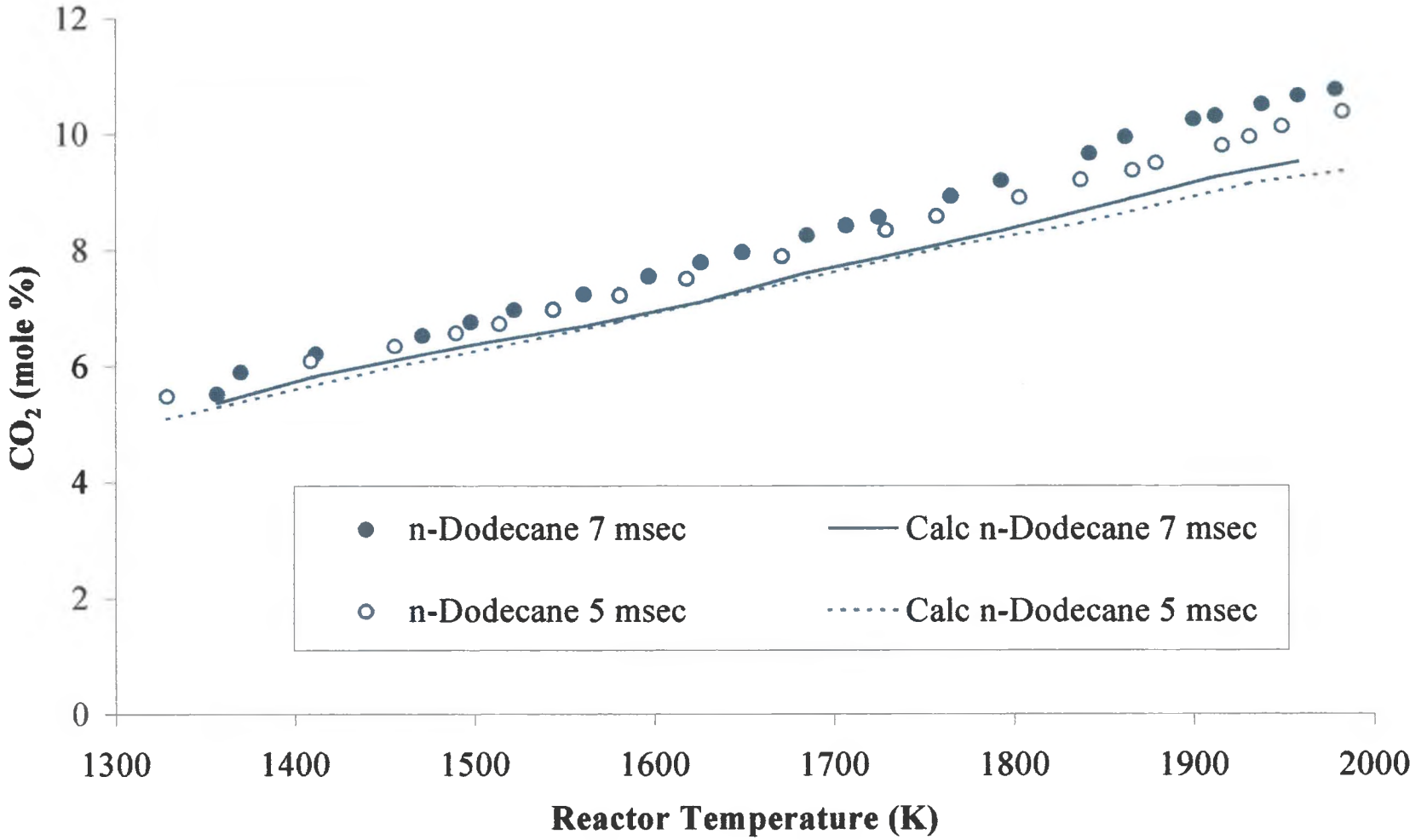

Figure 20. Computed and measured CO_2 emissions for *n*-dodecane versus reactor temperature.

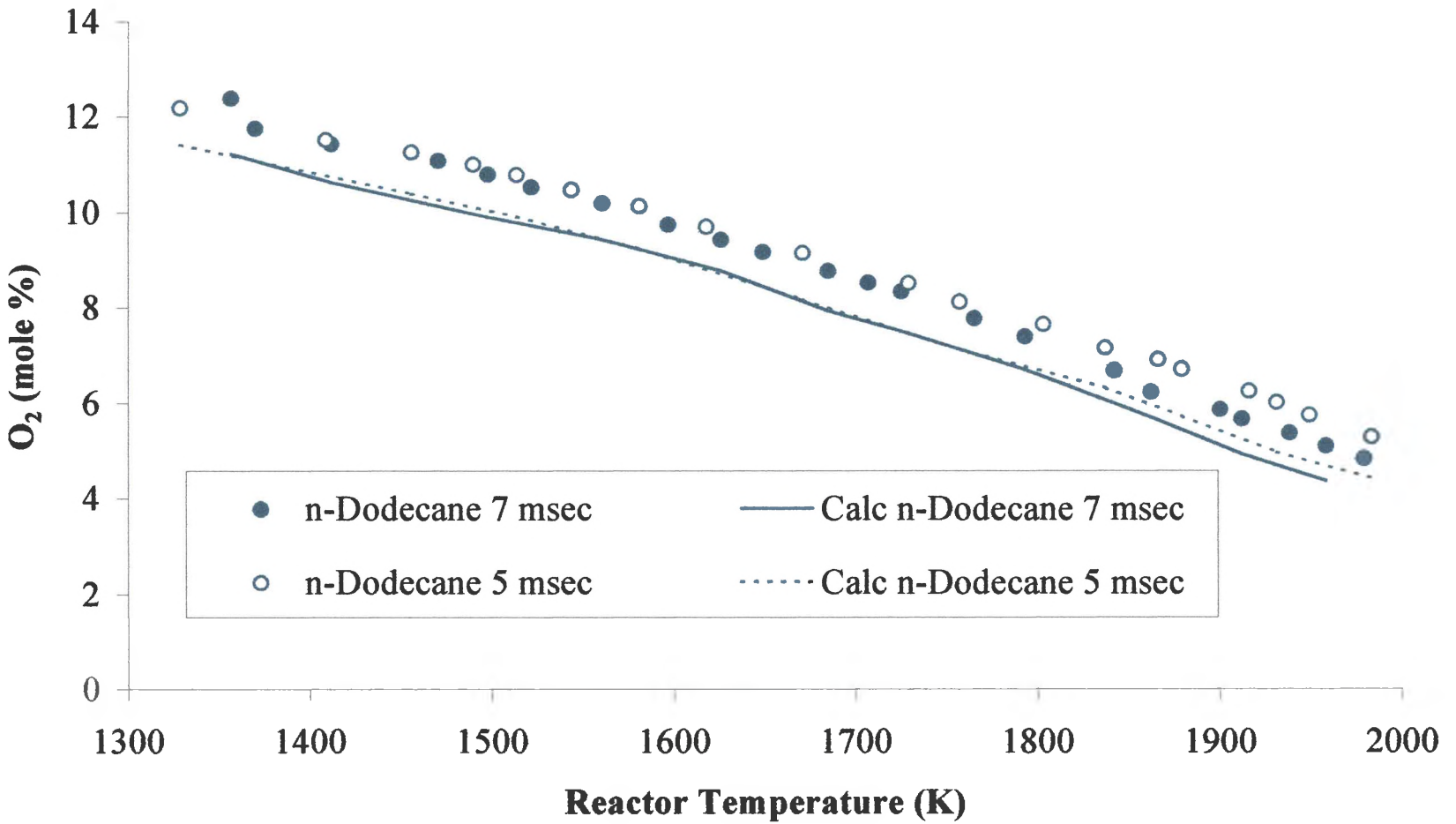

Figure 21. Computed and measured O_2 emissions for *n*-dodecane versus reactor temperature.

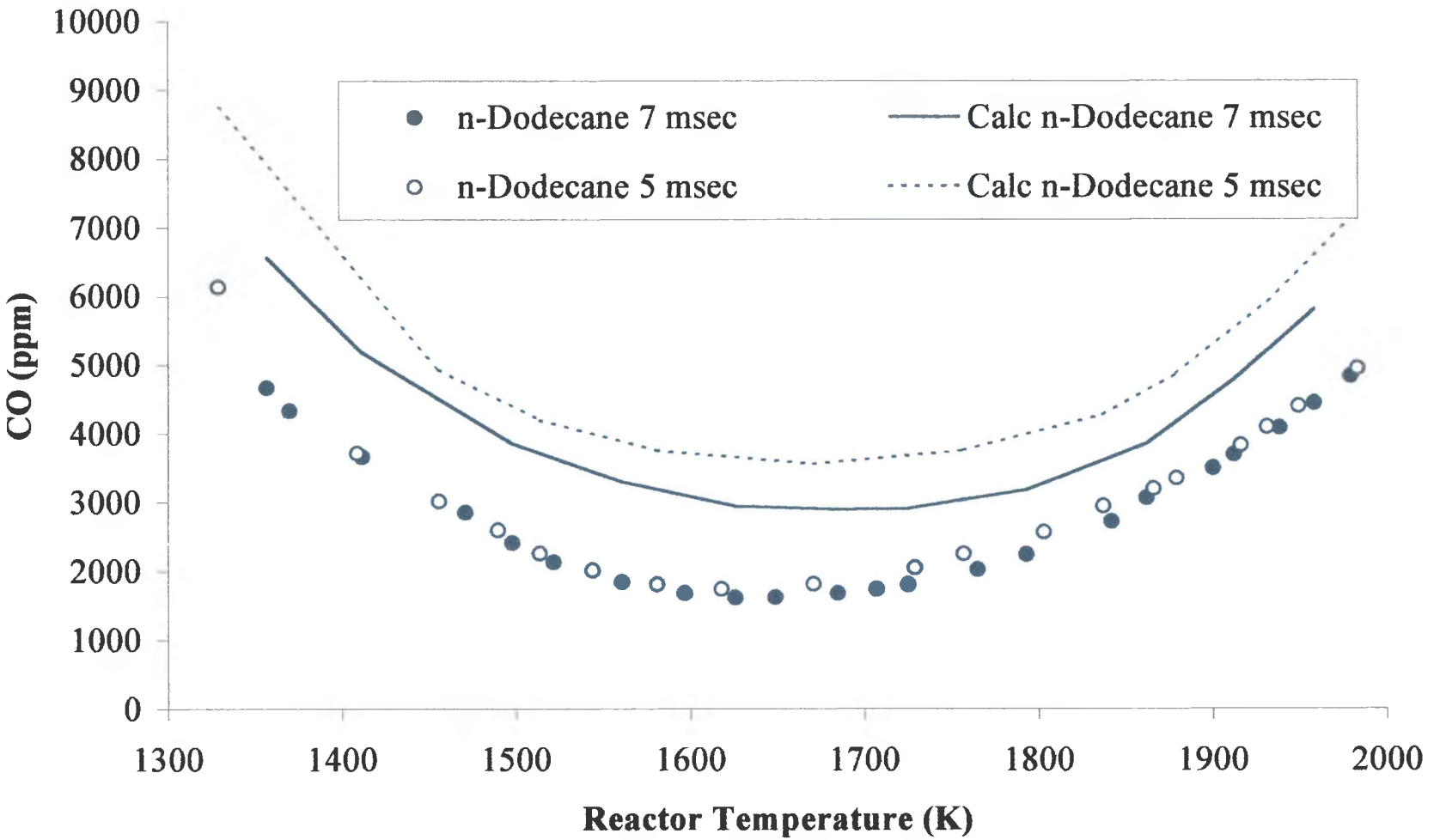

Figure 22. Computed and measured CO emissions for *n*-dodecane versus reactor temperature.

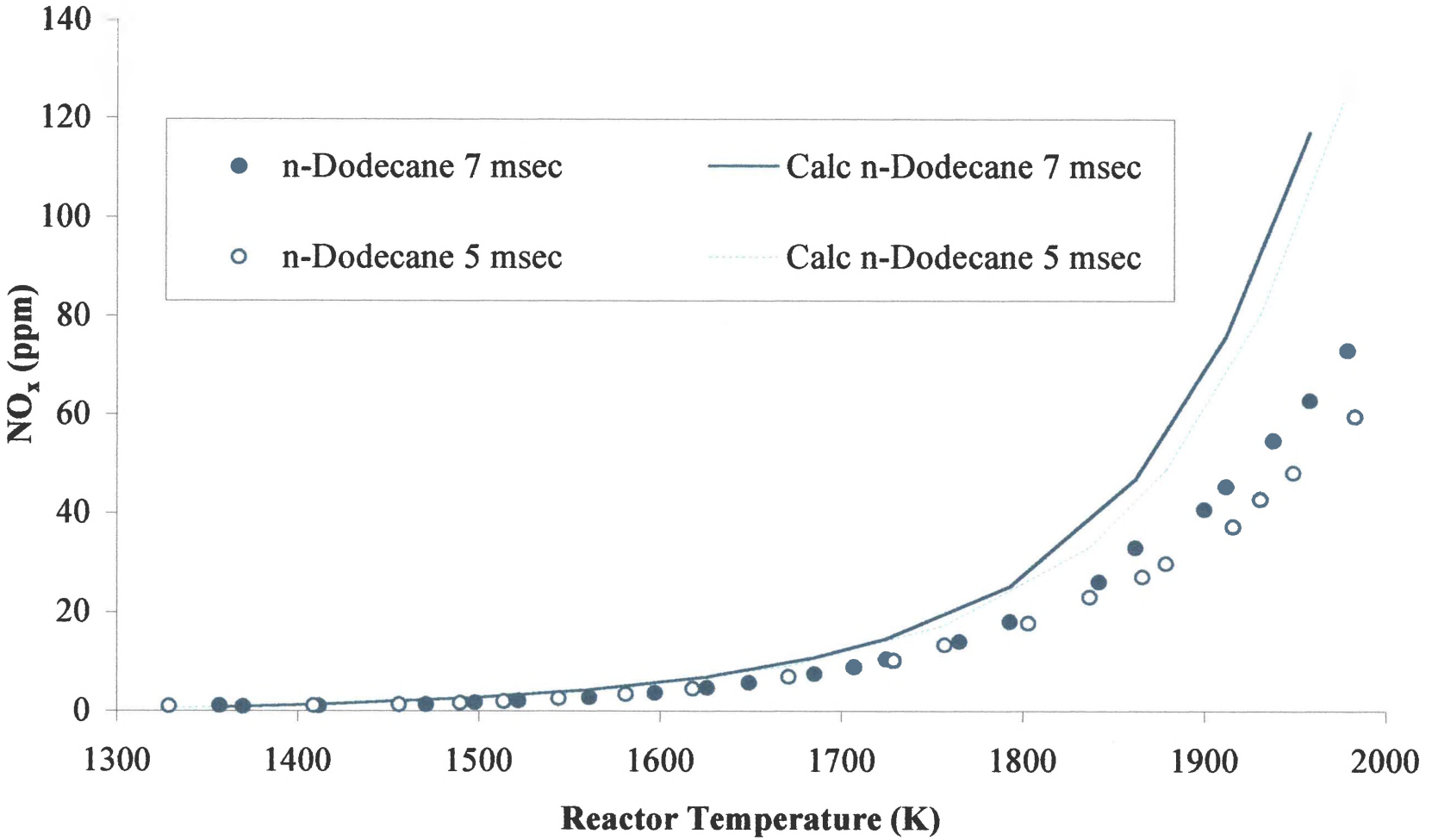

Figure 23. Computed and measured NO_x emissions for *n*-dodecane versus reactor temperature.

Both qualitative and quantitative agreement is very good. These emissions follow the same trends discussed above: CO_2 emissions reach a peak at high temperature, O_2 emissions approach zero at ϕ near 1.0, CO concentration reaches a minimum, and NO_x emissions increase exponentially. In general, the effect of changing the residence time is also accurately predicted, although this effect is minor.

An Application of the Detailed Chemical Kinetic Mechanism

As discussed above the principal path of NO formation at low equivalence ratio (ϕ) is the prompt NO channel. Because the reactions that comprise the prompt NO channel happen rapidly, there was concern that the reactor might not be well-stirred with respect to those reactions. So, during the course of this research, a modeling study was done to compare the chemical time of the various NO_x reactions with the mixing time of the well-stirred reactor. This is one example of how the model can help us determine something that the laboratory reactor cannot.

For reacting systems, characteristic times can be compared by calculation of the Damköhler number (Da). This is the ratio of the characteristic mixing time to the characteristic time for chemical reaction. If Da is large then chemistry is fast relative to mixing. For small Da, chemistry is slow and well-stirred situations can occur. However, many different Damköhler numbers can be defined for a given turbulent flow. Thus, conclusions cannot readily be drawn from the numerical value of a certain Da (Libby and Williams, 1980). Bray (1980) suggests that a fast chemistry regime exists when Da is much greater than unity. In this regime, turbulent mixing rather than chemical kinetics

would control the combustion. Analysis becomes more difficult when there are many reactions (i.e. a combusting system) because the various reactions will behave with different chemical times (Libby and Williams, 1980). Chemical time scales are usually defined by an exponential dependence upon reactor temperature. For instance, Mellor and Ferguson (1980) define the chemical time scale (in milliseconds) for NO formation in a vehicular gas turbine combustor as:

$$\tau_{NO} = 10^{-12} \exp(66{,}969/T_{\phi=1}) \qquad \text{Equation 32}$$

A modeling study was undertaken to computationally determine NO_x concentration as a function of residence time. In this study, the model was run with methane at four different reactor temperatures and equivalence ratios (see Table 3). Initially, the residence time, τ, was set at 20 μsec. It was then increased in the increments shown in Table 4 until a typical residence time was reached.

Table 3. Reactor temperatures and equivalence ratios for NO_x study.

T_f (K)	ϕ
1596	0.60
1747	0.70
1863	0.79
1967	0.88

Table 4. NO_x study residence time increments.

τ range (μsec)	τ increment (μsec)
20 - 400	20
400 - 1000	50
1000 - 2000	100
2000 - 7400	200

The resulting plots from this study are shown in Figures 24 to 26. NO_x formation by the prompt NO channel is represented by the initial portion of the curves. The remaining portions of the curves indicated NO_x formation by both thermal (Zel'dovich) and intermediate N_2O channels. Notice that the amount of time for which the prompt NO channel is predominant is about 120 μsec for a T_f of 1596 K, about 60 μsec for a T_f of 1747 K, about 40 μsec for a T_f of 1863 K, and about 30 μsec for a T_f of 1967 K.

Blust (1998) calculated a mixing time of approximately 19 μsec for methane combustion in the WSR at typical combustion conditions. Using the time required for completion of the prompt NO channel reactions as the chemical time of that process, this yields Damköhler numbers less than unity for all of the reactor temperatures examined. As temperature is increased, however, Da approaches unity. These results indicate that the reactor is arguably *not* well-stirred with respect to prompt NO formation, especially at lower reactor temperatures.

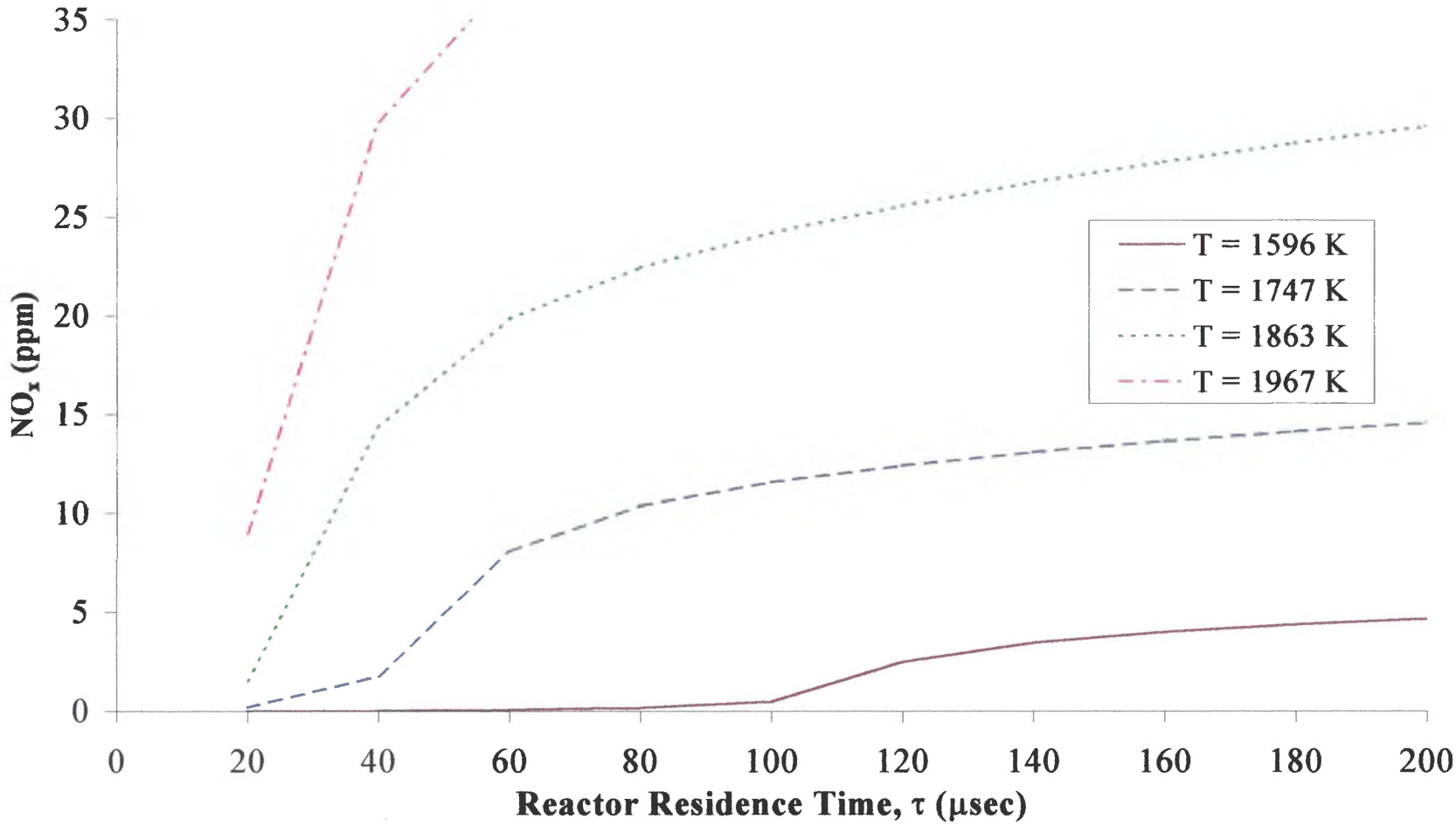

Figure 24. Computed NO_x emissions for methane versus reactor temperature for τ from 0 to 200 μsec.

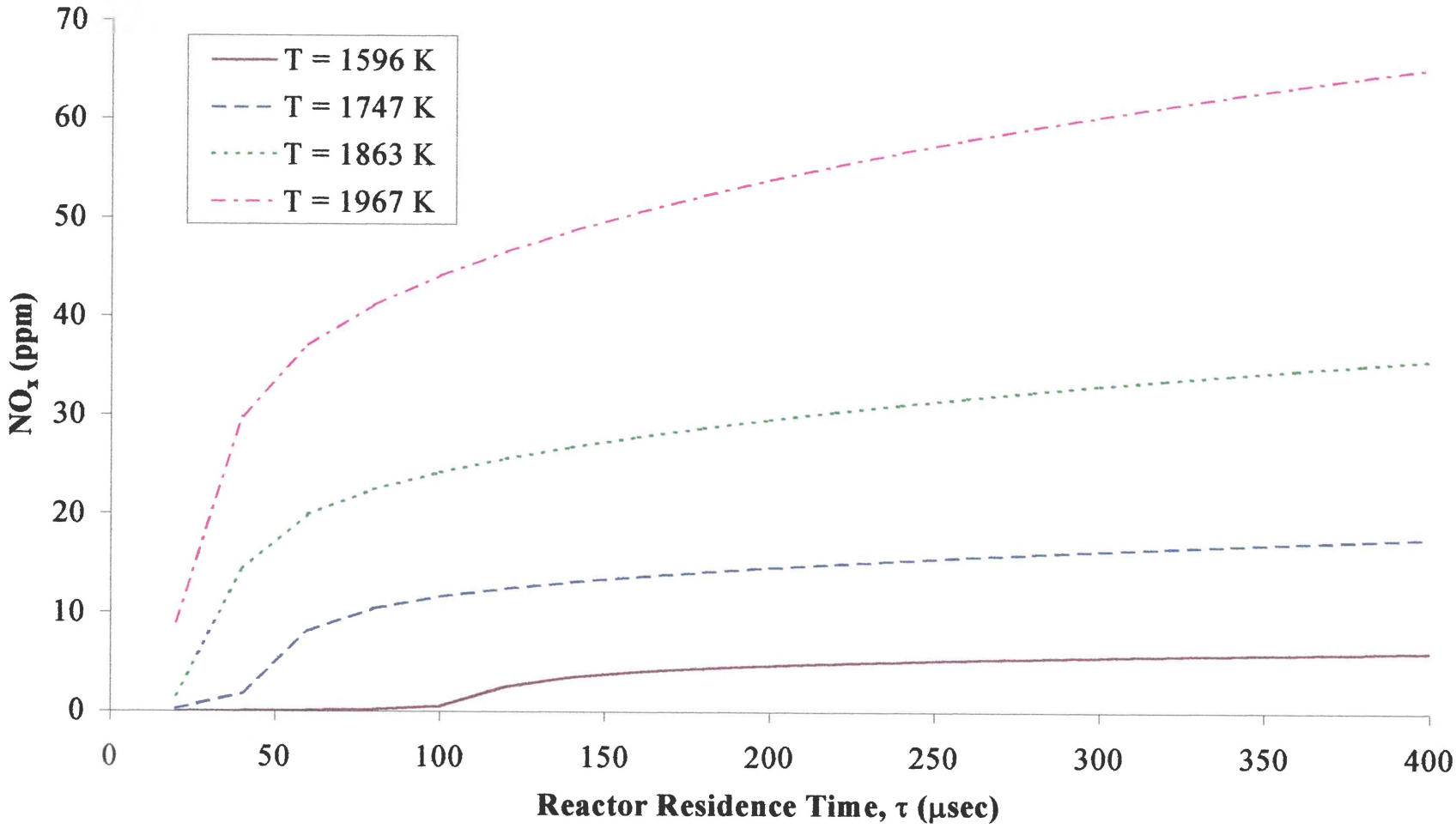

Figure 25. **Computed NO_x emissions for methane versus reactor temperature for τ from 0 to 400 μsec.**

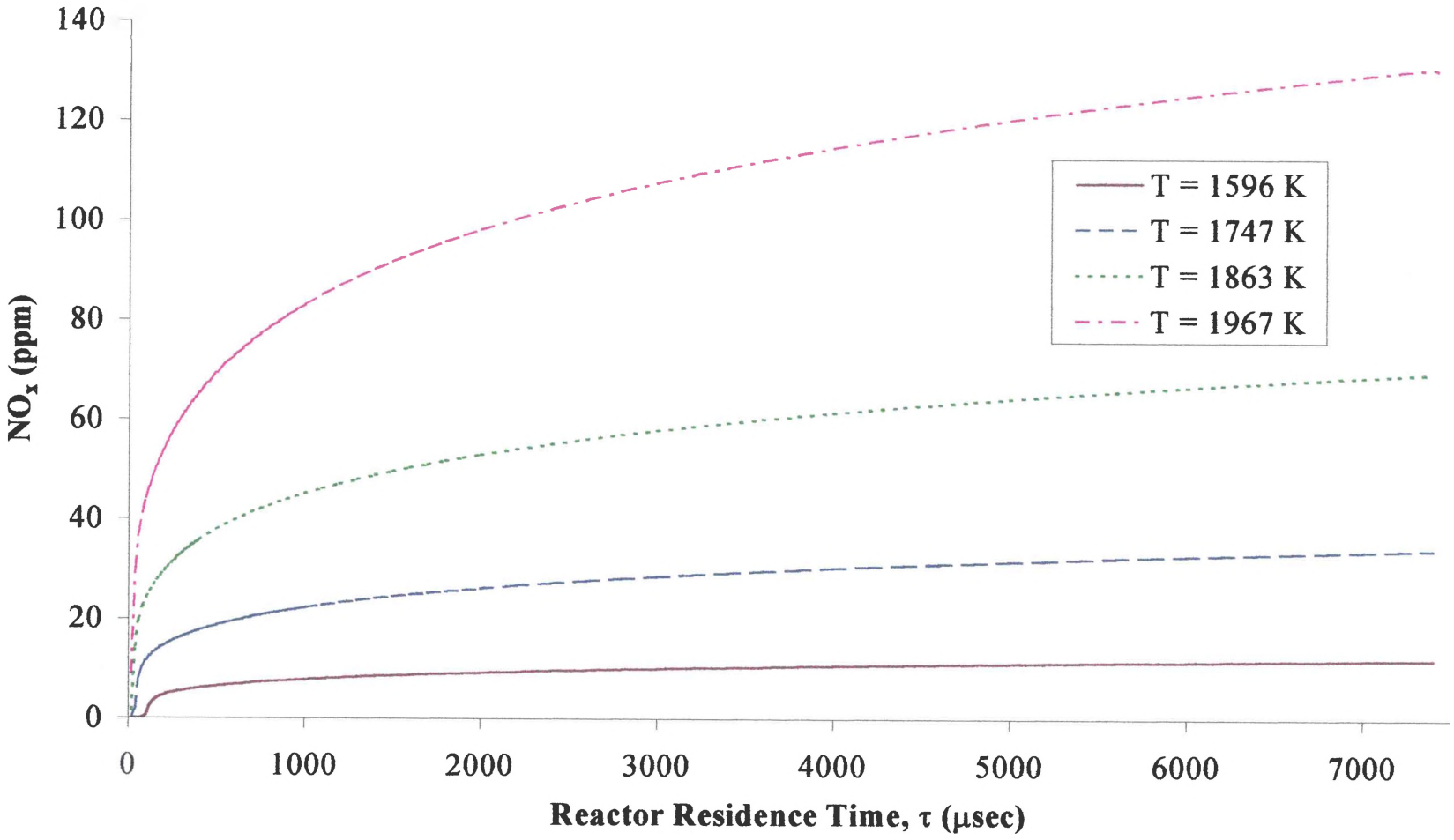

Figure 26. Computed NO_x emissions for methane versus reactor temperature for τ from 0 to 7.4 msec.

CHAPTER V

EVALUATION OF EXPERIMENTAL UNCERTAINTIES

As discussed above, various levels of disagreement occur between computations and experimental data. The sensitivity of NO_x formation to the kinetic rate parameters has been previously investigated (Selim, 1995). Therefore, the present analysis focuses on the sensitivity of computations to experimental uncertainties. The ability of the model to depict the effects of residence time has been shown in Chapter IV, therefore only the effects of temperature, probe effect, and turbulent diffusion (mixing) are further addressed.

Temperature Uncertainty

The sensitivity of calculated CO and NO_x emissions to uncertainties in measured T_f are shown Figures 27 through 30. Experimental T_f values are accurate within $\pm$50 K (Blust, 1998). Hence, the temperatures imposed on the calculated emissions profiles for methane at a τ of approximately 6 msec are varied $\pm$50 K, while ϕ remains constant, in order to assess the sensitivity of the predictions to the experimental uncertainty in the reactor temperature. For completeness, predictions are shown as a function of both ϕ and T_f. For reference, the measured emissions are also included.

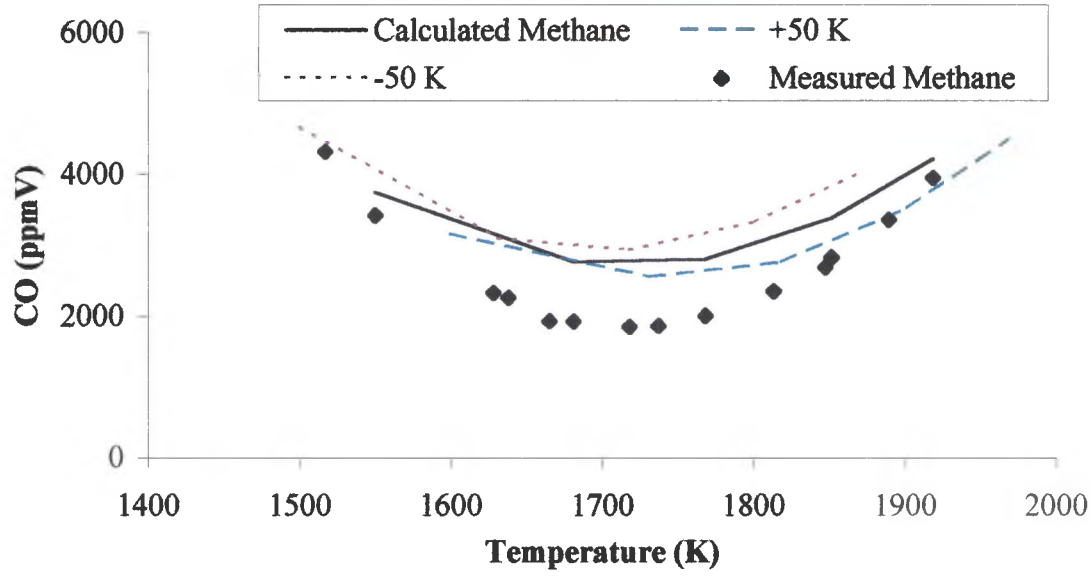

Figure 27. **Computed and measured CO emissions for methane at $\tau \sim 6.3$ msec versus T_f. The temperature is varied ± 50 K at each computed point to illustrate the sensitivity of emissions to temperature uncertainty.**

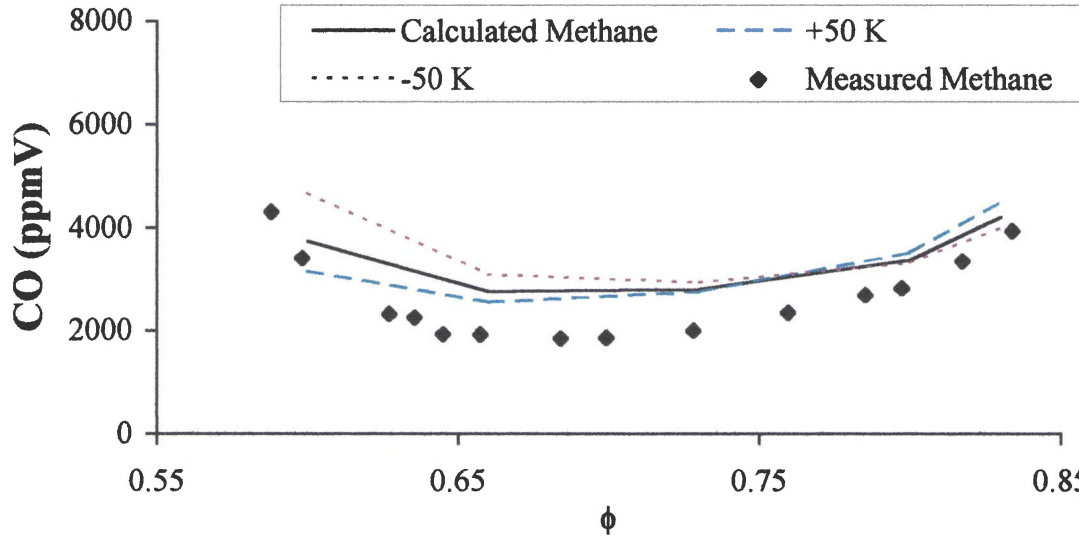

Figure 28. **Computed and measured CO emissions for methane at $\tau \sim 6.3$ msec versus ϕ. The temperature is varied ± 50 K at each computed point to illustrate the sensitivity of emissions to temperature uncertainty.**

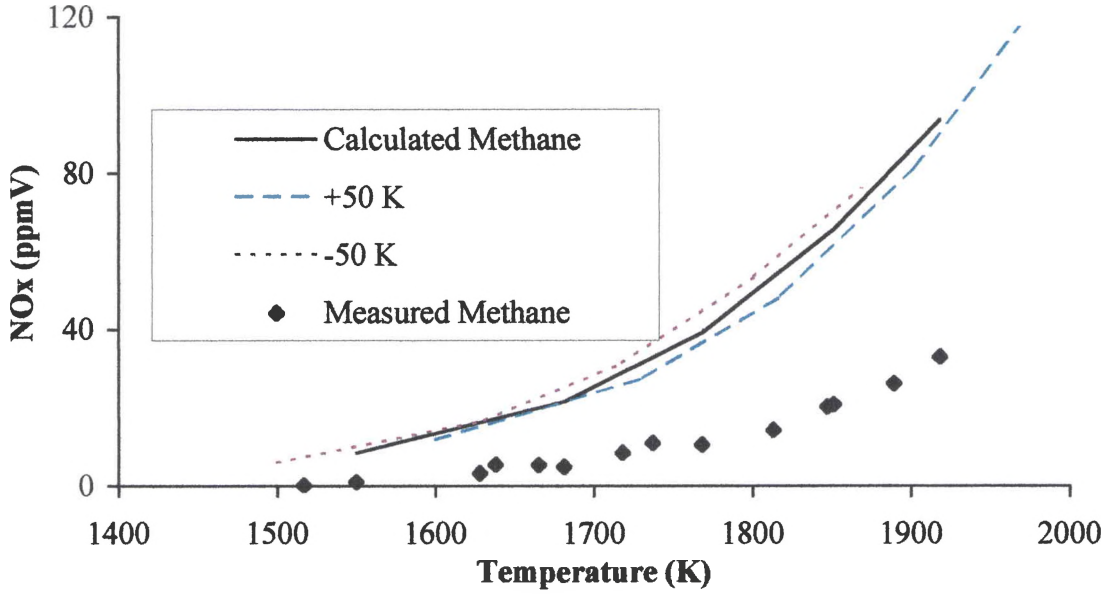

Figure 29. **Computed and measured NO_x emissions for methane at $\tau \sim 6.3$ msec versus T_f. The temperature is varied ± 50 K at each computed point to illustrate the sensitivity of emissions to temperature uncertainty.**

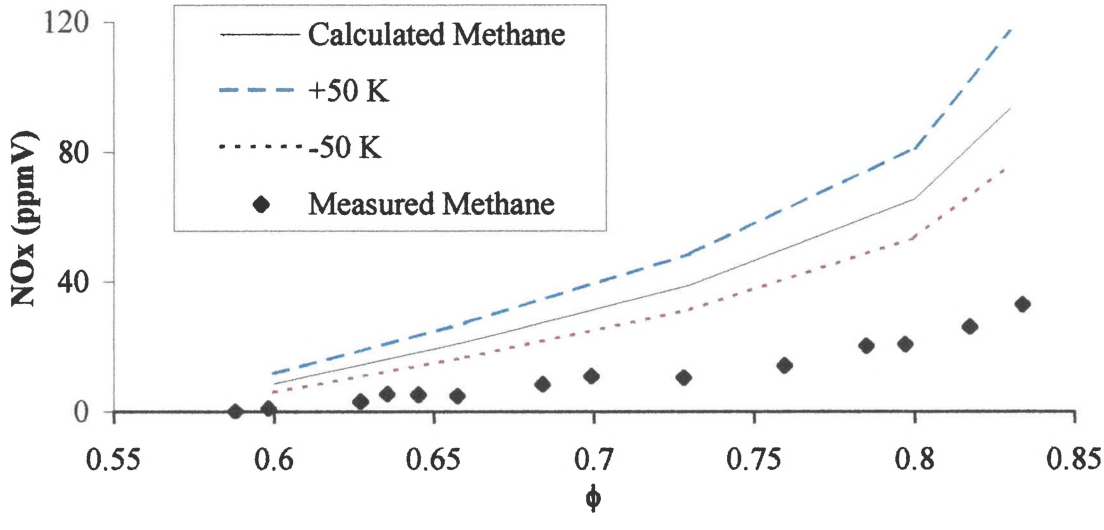

Figure 30. **Computed and measured NO_x emissions for methane at $\tau \sim 6.3$ msec versus ϕ. The temperature is varied ± 50 K at each computed point to illustrate the sensitivity of emissions to temperature uncertainty.**

Uncertainties in T_f result in a maximum variation in computed CO of 25% at ϕ = 0.6 (Figure 27 and 28). The sensitivity of CO predictions to T_f decreases as ϕ increases. Carbon monoxide emissions decrease for the +50 K condition at low T_f, but increase at higher T_f. This is not surprising, as the primary effect of temperature changes is to shift operating points on the U-shaped CO curve. Thus, when T_f is low, increasing temperature shifts emissions towards the minimum. By contrast, when T_f is high, a further increase in temperature shifts emissions away from the minimum. However, the curves in Figures 27 and 28 do not overlap exactly, indicating that T_f is not the only factor determining emissions. Reactant concentrations show a modest effect on CO formation, which appears independent of temperature.

Predictions of NO_x are generally more sensitive to T_f than observed for CO emissions (Figures 29 and 30). Uncertainties in T_f result in variations in computed NO_x emissions between 20 - 40% over the full range of ϕ considered. Figures 29 and 30 show that uncertainties in T_f result in nearly constant variations in predicted NO_x, indicating that temperature is the major factor determining emissions. Therefore, reactant concentrations play only a secondary role in NO_x formation. Similar results are obtained for all fuels.

Probe Effects

Another possible explanation for the discrepancies between the measured and calculated emissions is the effect of the probe and sampling system on the various reactions. In order to provide realistic data, a probe must be able to terminate the

combustion reactions in the sample it is withdrawing from the combustor. If a probe cannot adequate quench the reactions, this "probe effect" can lead to an incorrect analysis of the combustion processes. Despite the extensive efforts of Blust et al. (1997b) to develop a probe with minimal probe effect, it is recognized that some probe effect will always exist. Consequently, a modeling study was done to determine how the probe effect could influence the reported emissions from the WSR.

This study considered methane at τ's of approximately 7.3 and 6.4 milliseconds. The data that was collected on the temperature and residence time profiles for the probe during the study by Blust et al. (1997b), was used for this evaluation (Tables 5 and 6). This data was used to run a series of simulations for each of the desired reactor temperatures and residence times. The probe is modeled as a series of perfectly stirred reactors. The procedure involved using the results from computations that simulated the interior of the reactor as the rstart.dat file for the next simulation. The results from the original modeling runs were used when possible. The remaining simulations used the temperature and residence time from the appropriate profiles as the temperature and residence time of a reactor. This was repeated down the entire length of the probe with the results of one simulation used as the starting point for the next.

The CO emissions with probe effect from the combustion of methane are shown in Figures 31 ($\tau \sim 7$ msec) and 32 ($\tau \sim 6$ msec). The calculations including probe effect produce slightly less CO than those that do not. Thus, consideration of probe effect improves the model's prediction of CO emissions. A greater improvement is seen at low T_f and at high T_f, while only slight improvement is observed near the CO minimum.

Table 5. Sample temperature and residence time profiles used to model the probe for $\tau \sim 7.3$ msec

T_f (K)	ϕ	τ (msec)
1507	0.55	7.27
x (m)	T (K)	τ (msec)
0	1507	7.27
0.001	1456.7	0.0028
0.002	1411.2	0.0029
0.004	1329.8	0.0061
0.008	1197.2	0.0132
0.016	1011.1	0.0302
0.032	796.7	0.0739
0.064	596.1	0.1918
0.128	438.3	0.5166

T_f (K)	ϕ	τ (msec)
1596	0.60	7.24
x (m)	T (K)	τ (msec)
0	1596	7.24
0.001	1536.6	0.0027
0.002	1483.4	0.0028
0.004	1389.4	0.0058
0.008	1239.3	0.0127
0.016	1034.6	0.0294
0.032	806.6	0.0726
0.064	599.4	0.1900
0.128	439.4	0.5144

T_f (K)	ϕ	τ (msec)
1696	0.66	7.21
x (m)	T (K)	τ (msec)
0	1696	7.21
0.001	1625	0.0025
0.002	1562.4	0.0026
0.004	1453.2	0.0055
0.008	1282.8	0.0122
0.016	1057.7	0.0285
0.032	815.9	0.0713
0.064	602.5	0.1884
0.128	440.3	0.5124

T_f (K)	ϕ	τ (msec)
1754	0.70	7.42
x (m)	T (K)	τ (msec)
0	1754	7.42
0.001	1675.7	0.0024
0.002	1607.2	0.0025
0.004	1488.7	0.0054
0.008	1306.3	0.0119
0.016	1069.7	0.0281
0.032	820.5	0.0707
0.064	603.9	0.1876
0.128	440.7	0.5116

T_f (K)	ϕ	τ (msec)
1893	0.81	7.29
x (m)	T (K)	τ (msec)
0	1893	7.29
0.001	1795.2	0.0023
0.002	1711.4	0.0024
0.004	1569.5	0.0051
0.008	1357.8	0.0114
0.016	1094.7	0.0272
0.032	829.7	0.0694
0.064	606.8	0.1860
0.128	441.6	0.5097

T_f (K)	ϕ	τ (msec)
1967	0.88	7.42
x (m)	T (K)	τ (msec)
0	1967	7.42
0.001	1857.7	0.0022
0.002	1765.2	0.0023
0.004	1610.1	0.0049
0.008	1382.6	0.0112
0.016	1106.2	0.0268
0.032	833.8	0.0689
0.064	608	0.1853
0.128	441.9	0.5090

Table 6. Sample temperature and residence time profiles used to model the probe for $\tau \sim 6.3$ msec

T_f (K)	ϕ	τ (msec)
1550	0.60	6.07
x (m)	T (K)	τ (msec)
0	1550	6.07
0.001	1495.4	0.0027
0.002	1446.3	0.0028
0.004	1358.9	0.0060
0.008	1217.9	0.0130
0.016	1022.8	0.0298
0.032	801.7	0.0732
0.064	597.8	0.1909
0.128	438.9	0.5155

T_f (K)	ϕ	τ (msec)
1665	0.65	6.27
x (m)	T (K)	τ (msec)
0	1665	6.27
0.001	1597.8	0.0026
0.002	1538.2	0.0027
0.004	1433.8	0.0056
0.008	1269.7	0.0124
0.016	1050.8	0.0288
0.032	813.2	0.0717
0.064	601.6	0.1889
0.128	440	0.5130

T_f (K)	ϕ	τ (msec)
1737	0.70	6.42
x (m)	T (K)	τ (msec)
0	1737	6.42
0.001	1660.9	0.0025
0.002	1594.1	0.0026
0.004	1478.4	0.0054
0.008	1299.5	0.0120
0.016	1066.2	0.0282
0.032	819.2	0.0709
0.064	603.5	0.1878
0.128	440.6	0.5118

T_f (K)	ϕ	τ (msec)
1851	0.80	6.62
x (m)	T (K)	τ (msec)
0	1851	6.62
0.001	1759.4	0.0023
0.002	1680.4	0.0024
0.004	1545.7	0.0052
0.008	1342.9	0.0116
0.016	1087.6	0.0275
0.032	827.2	0.0698
0.064	606	0.1864
0.128	441.3	0.5102

T_f (K)	ϕ	τ (msec)
1918	0.83	6.40
x (m)	T (K)	τ (msec)
0	1918	6.40
0.001	1816.4	0.0022
0.002	1729.7	0.0024
0.004	1583.4	0.0050
0.008	1366.4	0.0113
0.016	1098.7	0.0271
0.032	831.1	0.0692
0.064	607.2	0.1858
0.128	441.7	0.5095

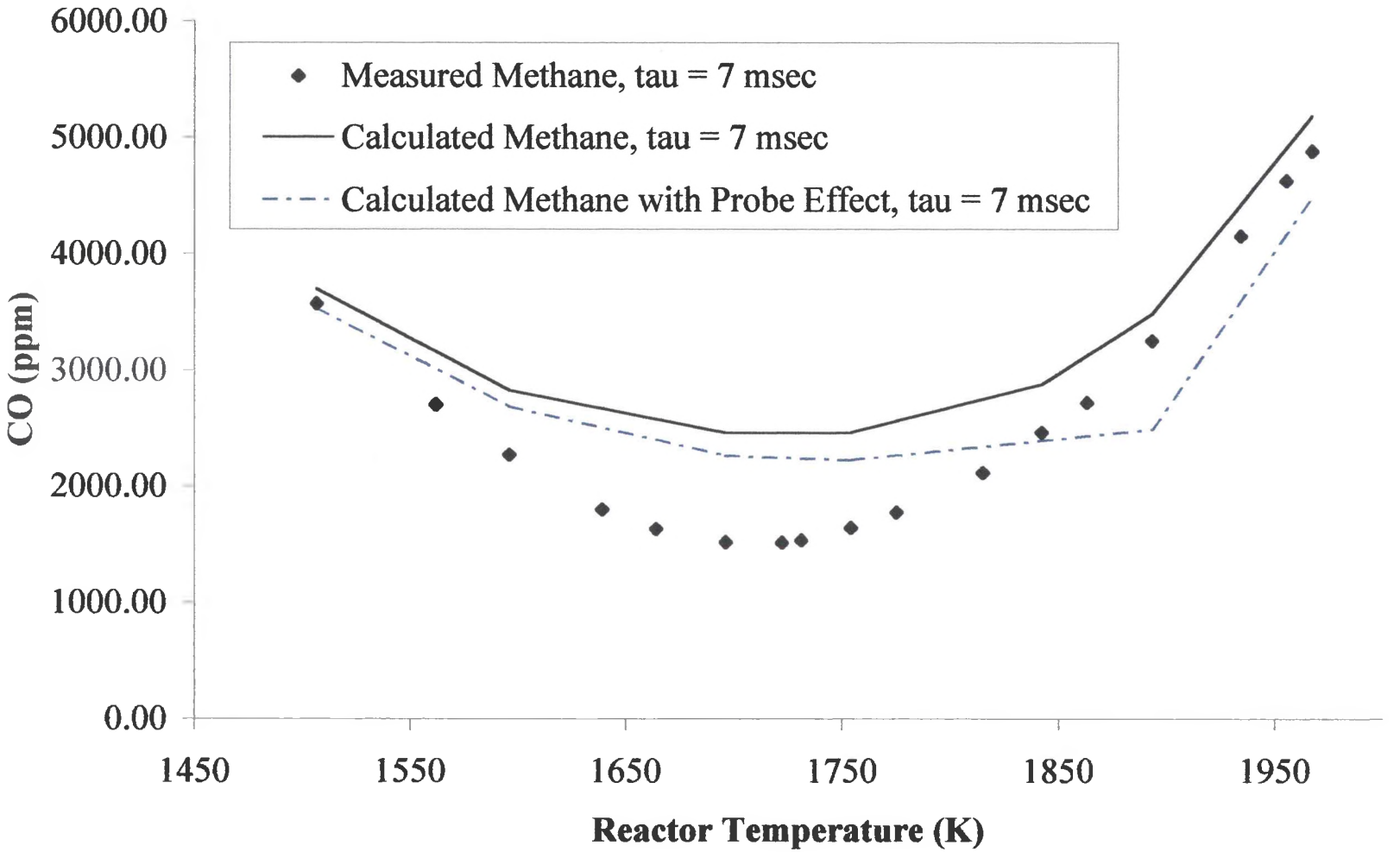

Figure 31. Computed and measured CO emissions including computed probe effect data for methane at $\tau = 7$ msec.

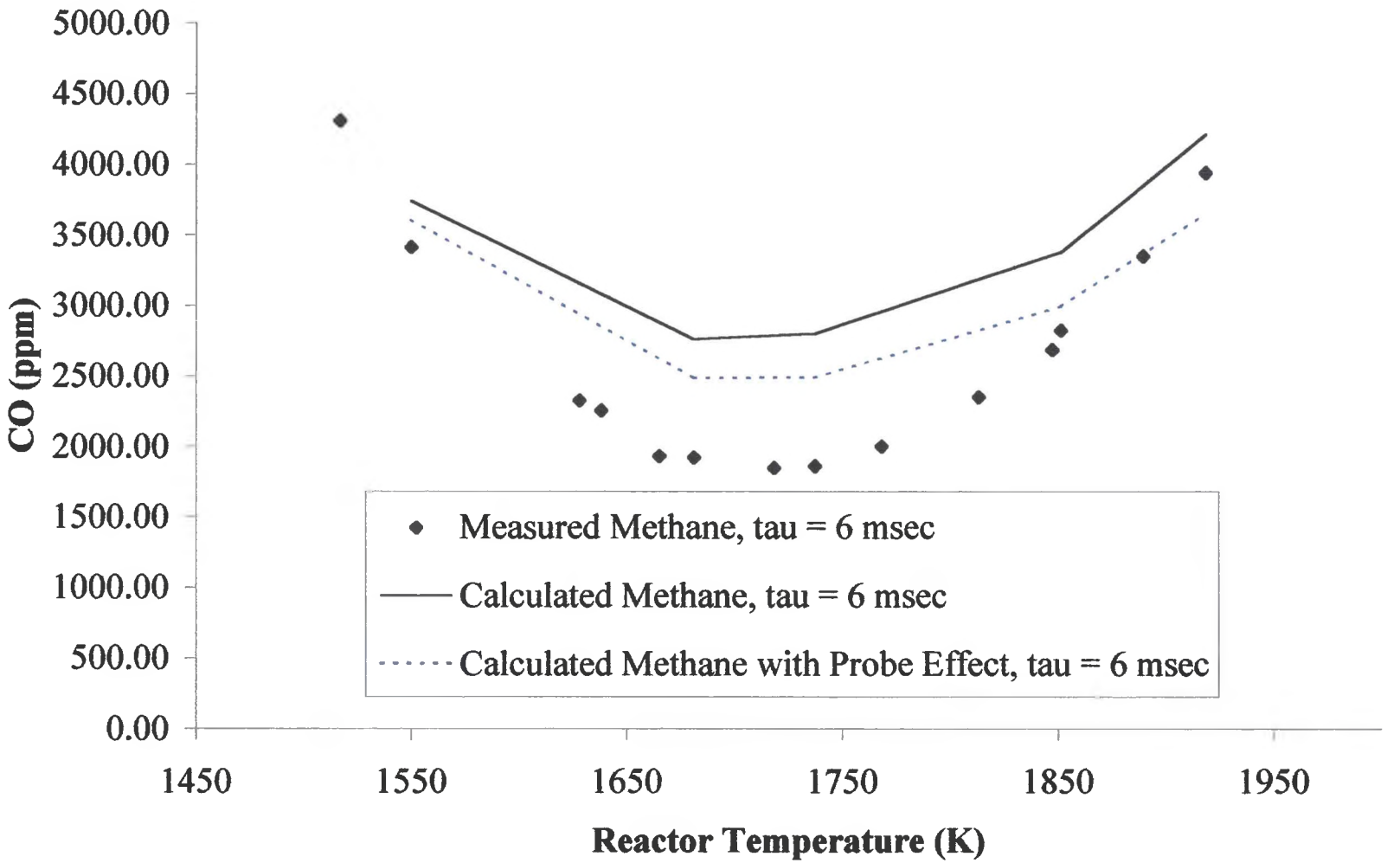

Figure 32. Computed and measured CO emissions including computed probe effect data for methane at τ = 6 msec.

Turbulent Diffusion

The results shown above (Figures 27 through 30) clearly show that potential inaccuracies in measured T_f do not fully explain the observed disagreement between measured and calculated emissions. Also, the effect of the probe on the reactions (Figures 31 and 32) cannot completely explain the discrepancies. Turbulence-chemistry interactions are ignored in the present computations due to the complexity of the detailed chemistry considered. However, it is well known that the latter are important, particularly for reactions featuring high activation energies that are nonlinear in temperature (Correa, 1992). Longwell and Bar-Ziv (1989) estimated that the eddy diffusivity, D, in the WSR is approximately 195 cm^2/sec, which causes a deviation in reactor residence time distribution from that of a perfectly stirred reactor. Their work demonstrated that predictions could be improved by computationally simulating the flow to the combustor exit via turbulent diffusion-convection as two stirred reactors in series, where the volume of the first reactor is 5% of the total reactor volume. This method was tested using the current kinetic mechanism to determine if accounting for turbulent mixing would explain some of the disagreement between measured and calculated emissions.

The simulations of the effect of turbulent diffusion in the WSR on emissions are shown in Figures 33 and 34. The calculated CO and NO_x are reduced by factors of two and ten respectively, resulting in significant under-prediction of emissions. This is indicative both of the excellent mixing provided by the WSR, as well as the ability of the model to investigate mixing phenomena. Thus, the two stirred reactors in series model of

Longwell and Bar-Ziv (1989) does *not* represent an improvement in the predictions of emissions from the WSR studied by Blust (1998).

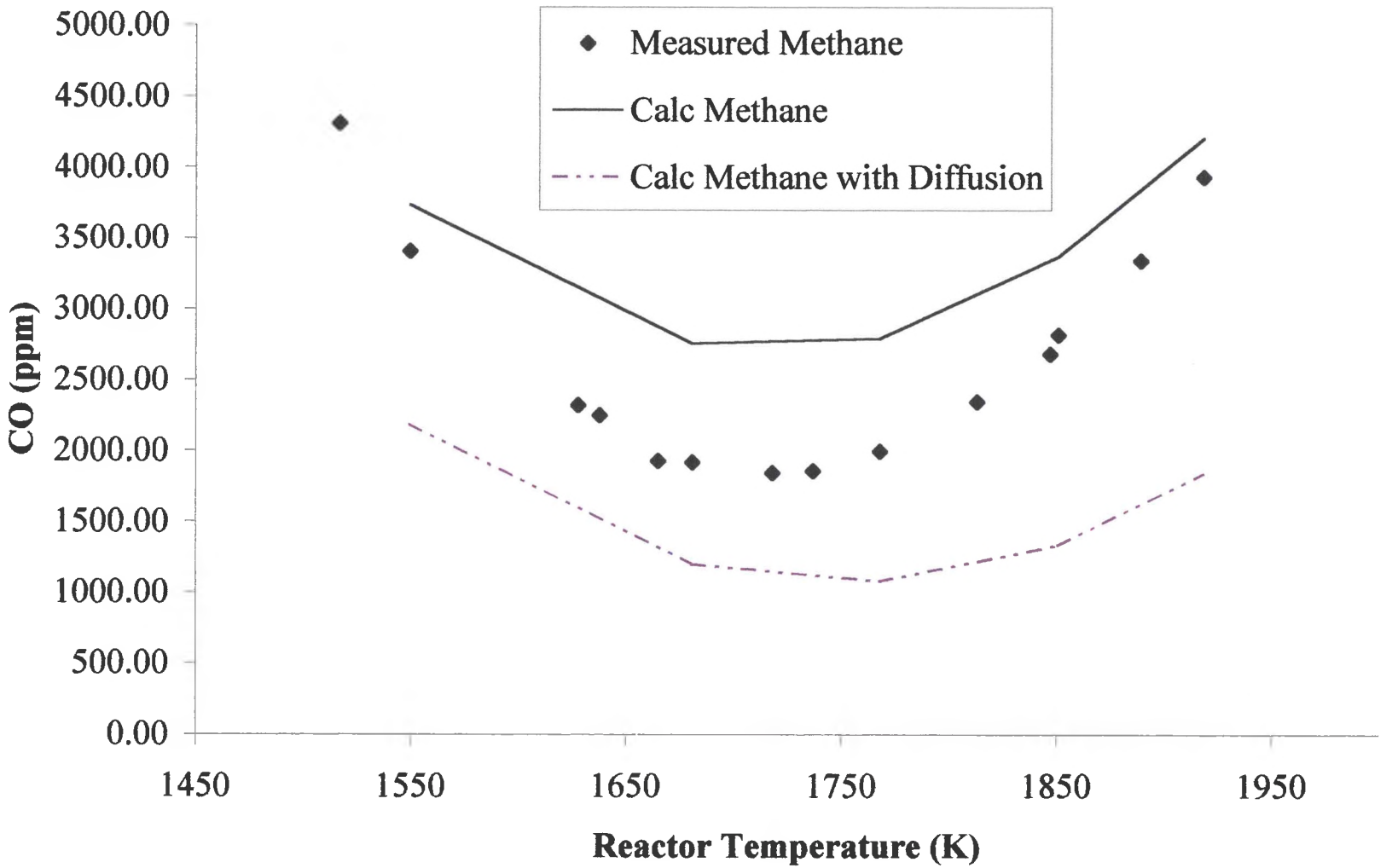

Figure 33. Computed and measured CO emissions including computed turbulent diffusion data for methane at $\tau \sim 6$ msec.

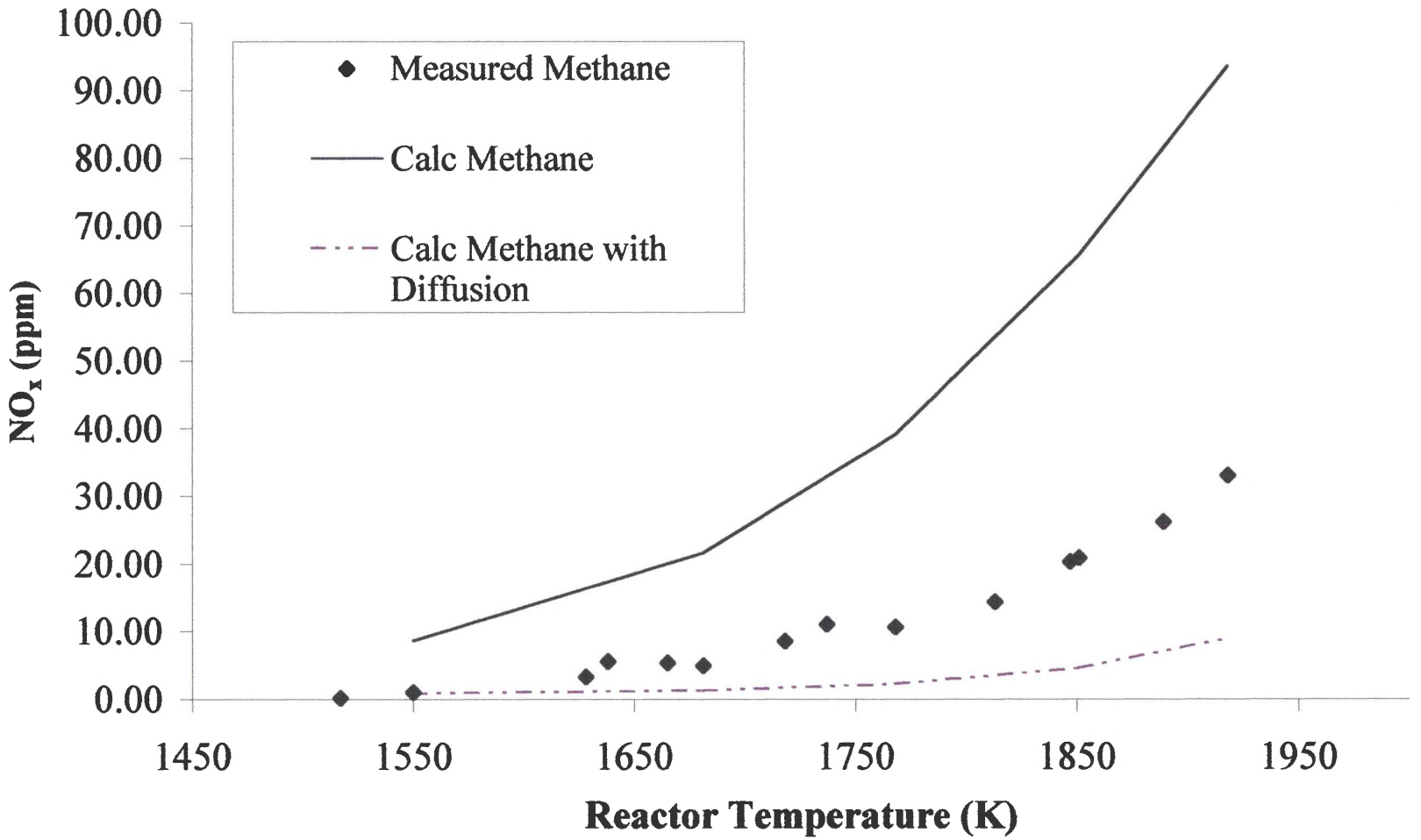

Figure 34. Computed and measured NO_x emissions including computed turbulent diffusion data for methane at $\tau \sim 6$ msec..

CHAPTER VI

CONCLUSIONS AND RECOMMENDATIONS

Experimental measurements of CO_2, O_2, CO, and NO_x emissions for a variety of hydrocarbons, including Jet A and an endothermic fuel simulant at combustion temperatures (> 1400 K) and lean conditions (ϕ = 0.43 - 0.88) are shown. The data sets are useful toward the evaluation of computational tools, and are modeled using a detailed kinetic scheme that addresses higher order hydrocarbons and nitrogen oxides chemistry in order to study the effects of fuel type on emission characteristics. The relative contributions of NO_x formation and destruction paths are shown to be primarily affected by temperature, while fuel effects are secondary. However, the need to consider the multi-component nature of complex hydrocarbon fuels is evident given that variations in intermediate and radical species affect the net emissions. Carbon monoxide predictions as a function of fuel type are generally in very good qualitative agreement with experimental observation. Moreover, predictions for Jet A are within 10% of experimental observations. Predictions of CO emissions for other fuels are within a factor of two or better, and are significantly improved with increasing temperature. Qualitative predictions of NO_x are also in generally good agreement with experimental observations. Quantitative predictions of NO_x are reasonably good for Jet A, aromatics

and endothermic simulant; however, the agreement is diminished for alkanes. Predictions of CO_2 and O_2 also agree well with experimental observations.

New reactions are added to the current Lindstedt-Maurice detailed kinetic mechanism. These reactions allow modeling of the combustion of *n*-dodecane. Predictions of emissions using the new mechanism are generally accurate, both qualitatively and quantitatively. This comparison provides the new mechanism some of the necessary verification before it can be used to predict emissions for which there is not experimental data.

Emissions predictions are shown to be modestly sensitive to uncertainties in the experimental temperature profile and the effects of the probe on quenching reactions. However, turbulent diffusion appears to cause significant underprediction of emissions in the present computations. Also, mechanistic uncertainties that affect global predictions as well as the relative concentrations of intermediate radicals remain. It is recognized that the experimental and mechanistic uncertainties merit further attention. Nevertheless, the present computations show reasonable predictions of emissions for a variety of fuels *without ad hoc* modifications to the kinetic rate parameters. Thus, the applied detailed kinetic mechanism appears to be a sound basis for future simplifications aimed at addressing the complex flowfields of practical devices.

Recommendations for future work include incorporating additional reactions into the current detailed kinetic mechanism. WSR data also exists for cyclohexane (Blust, 1998), but the existing model does not include the appropriate reactions for modeling such a fuel. It would also be useful to further study both mechanistic and experimental uncertainties so that the present kinetic model can be improved. Further experimental

and computational studies would also improve the current model. Recommended fuels include additional cyclic alkanes as well as complex fuels. For instance, it would be interesting to compare data for jet fuels with additives that are currently undergoing testing (e.g. JP-8 + 100). The most important work, however, would be to use the current chemical kinetic model as a basis for creating simplified, or reduced, mechanisms. Simplified mechanisms would make simulation of multi-dimensional turbulent reacting flows possible with available numerical methods and computers. Such mechanisms would be able to accurately predict emissions from practical combustors. With these computational tools, fuels and operating conditions that meet the required environmental restrictions could be found without extensive, and expensive, experimental trial-and-error methods.

REFERENCES

Ballal, D. R. and A. H. Lefebvre. "Ignition and Flame Quenching of Flowing Heterogeneous Fuel-Air Mixtures." *Combustion and Flame* 35 (1979): 155-168.

Baulch, D. L, et al. *Journal of Physical Chemistry*, Ref. Data, 21, 451. 1992.

Baulch, D. L, et al. *Journal of Physical Chemistry*, Ref. Data, 23, 847, 1994.

Benson, Sidney W. The Foundations of Chemical Kinetics. New York: McGraw-Hill, 1960.

Blust, J. W. Ph.D. thesis. Mechanical Engineering Department, University of Dayton, 1998.

Blust, J. W., D. R. Ballal, and G. J. Sturgess. "Emissions Characteristics of Liquid Hydrocarbons in a Well Stirred Reactor." *AIAA Paper 97-2710.* 33rd AIAA/ASME/SAE/ASEE Joint Propulsion Conference & Exhibit. Seattle, 1997a.

Blust, J. W., M. G. Getz, and S. Zabarnick. "Probe Design Optimization for the Well Stirred Reactor." *AIAA Paper No. 97-0907.* 35th Aerospace Sciences Meeting & Exhibit. Reno, 1997b.

Bray, K. N. C. "Turbulent Flows with Premixed Reactants." Turbulent Reacting Flows. Eds. P. A. Libby and F. A. Williams. Berlin: Springer-Verlag, 1980. 39.

Burcat, A. and B. J. McBride. *1994 Ideal Gas Thermodynamic Data for Combustion and Air Pollution Use.* TAE697. 1994.

Castaldi, M. J., et al. "Experimental and Modeling Investigation of Aromatic and Polycyclic Aromatic Hydrocarbon Formation in a Premixed Ethylene Flame." *Twenty-sixth Symposium (International) on Combustion.* The Combustion Institute, 1996. 693-702.

Chevalier, C., et al. "Hydrocarbon Ignition: Automatic Generation of Reaction Mechanisms and Application to Modeling of Engine Knock." *Twenty-Fourth Symposium (International) on Combustion.* The Combustion Institute, 1992. 93 - 101.

Correa, S. M. "Carbon Monoxide Emissions in Lean Premixed Combustion." *Journal of Propulsion and Power,* 8.6 (1992): 1144-1151.

Curran, H. J., et al. "Autoignition Chemistry in a Motored Engine: An Experimental and Kinetic Modelling Study." *Twenty-sixth Symposium (International) on Combustion.* The Combustion Institute, 2 (1996): 2669-2677.

Dagaut, Philippe, et al. "Kerosene Combustion at Pressures up to 40 atm: Experimental Study and Detailed Chemical Kinetic Modeling." *Twenty-Fifth Symposium (International) on Combustion.* The Combustion Institute, 1994a. 919-926.

Dagaut, P., M. Reuillon, and M. Cathonnet. "High Pressure Oxidation of Liquid Fuels from Low to High Temperature. 3. *n*-Decane." *Combustion, Science, and Technology* 103 (1994b): 349.

Douté, C., et al. "Chemical Structure of Atmospheric Pressure Premixed *n*-Decane and Kerosene Flames." *Combustion, Science, and Technology.* 106 (1995): 327-344.

Dryer, F. "The Phenomenology of Modeling Combustion Chemistry." Fossil Fuel Combustion. Eds. Bartok, W. and Sarofin, A. F. New York, 1989. 121.

Gordon, S. and B. J. McBride. NASA. "Computer Program for Calculation of Complex Chemical Equilibrium Compositions, Rocket Performance, Incident and Reflected Shocks, and Chapman-Jouget Detonations." *SP-273 Interim Revision.* Washington, D. C., 1976.

Griffiths, J. F. and J. A. Barnard. Flame and Combustion. Glasgow: Chapman & Hall, 1995.

Guéret, Corinne, et al. "Experimental Study and Modeling of Kerosene Oxidation in a Jet-Stirred Flow Reactor." *Twenty-Third Symposium (International) on Combustion.* The Combustion Institute, 1990. 211-216.

Jones, W. P. and R. P. Lindstedt. "Global Reaction Schemes for Hydrocarbon Combustion." *Combustion and Flame* 73 (1988a): 233-249.

Jones, W. P. and R. P. Lindstedt. "The Calculation of the Structure of Laminar Counterflow Diffusion Flames Using a Global Reaction Mechanism." *Combustion, Science, and Technology* 61 (1988b): 31-49.

Jones, W. P. and W. H. Whitelaw. "Modelling and Measurements in Turbulent Combustion." *Twentieth Symposium (International) on Combustion.* The Combustion Institute, 1984. 233 - 249.

Lefebvre, A. H. Gas Turbine Combustion. New York: Hemisphere Publishing, 1983.

Leung, K. M. Ph. D. Thesis. University of London, 1995.

Leung, K. M. and R. P. Lindstedt. "Detailed Kinetic Modeling of C_1-C_3 Alkane Diffusion Flames." *Combustion and Flame* 102 (1995): 129-160.

Levenspiel, Octave. The Chemical Reactor Omnibook. Corvallis, Oregon: Oregon State University, 1996.

Lias, Sharon G., et al. NIST Standard Reference Database 25 Structures and Properties. Computer software. U. S. Secretary of Commerce, 1994.

Libby, P. A. and F. A. Williams. "Fundamental Aspects." Turbulent Reacting Flows. Eds. P. A. Libby and F. A. Williams. Berlin: Springer-Verlag, 1980. 39.

Lindstedt, R. P. and L. Q. Maurice. "A Detailed Chemical Kinetic Model for Practical Aviation Fuels." *AIAA Paper No. 97-2836.* 33rd AIAA/ASME/SAE/ASEE Joint Propulsion Conference & Exhibit. Seattle, 1997.

Lindstedt, R. P. and L. Q. Maurice. "Detailed Kinetic Modelling of Toluene Combustion." *Combustion, Science, and Technology* 120 (1996): 119-167.

Lindstedt, R. P. and M. A. Selim. "Reduced Reaction Mechanisms for Ammonia Oxidation in Premixed Laminar Flames." *Combustion, Science, and Technology* 99 (1994): 277-298.

Lindstedt, R. P., F. C. Lockwood, and M. A. Selim. "Detailed Kinetic Modelling of Chemistry and Temperature Effects on Ammonia Oxidation." *Combustion, Science, and Technology* 99 (1994): 253-276.

Lindstedt, R. P. and G. Skevis. "Benzene Formation Chemistry in Premixed 1,3-Butadiene Flames." *Twenty-Sixth Symposium (International) on Combustion.* The Combustion Institute, 1996. 703-709.

Lindstedt, R. P. and G. Skevis. "Chemistry of Acetylene Flames." *Combustion Science and Technology* 125 (1997): 73-137.

Longwell, John P. and Ezra Bar-Ziv. "Modeling of Inhomogeneities in the Toroidal Jet-Stirred Reactor." *Combustion and Flame* 78 (1989): 99-119.

Longwell, J. P. and M. A. Weiss. "High Temperature Reaction Rates in Hydrocarbon Combustion." *Industrial and Engineering Chemistry.* 47: 1955.

Maurice, L.Q. Ph.D. thesis. University of London, 1996.

Mellor, A. M. and C. R. Ferguson. "Practical Problems in Turbulent Reacting Flows." Turbulent Reacting Flows. Eds. P. A. Libby and F. A. Williams. Berlin: Springer-Verlag, 1980. 53.

Miller, J. A. and R. J. Kee. "Chemical Kinetics and Combustion Modeling." *Annual Review of Phsical Chemistry.* 41 (1990): 345-387.

Miller, James A. "Theory and Modeling in Combustion Chemistry." *Twenty-Sixth Symposium (International) on Combustion.* The Combustion Institute, 1996. 461-480.

Muller, C., G. Scacchi, and G. M. Come. "THERGAS: a computer program for the evaluation of thermochemical data of molecules and free radicals in the gas phase." *Journal of Chemistry and Physics.* 92 (1995): 1154-1178.

Nenniger, J. E., et al. "Characterization of a Toroidal Well Stirred Reactor." *Twentieth Symposium (International) on Combustion.* The Combustion Institute, 1984. 473-479.

Pop, G., et al. "Kinetics of the thermal decomposition of *n*-dodecane-decalin binary mixture in the presence of water vapor." Neftekhim, 1979, 19, 535.

Ranzi, E., et al. "A New Comprehensive Reaction Mechanism for Combustion of Hydrocarbon Fuels." *Combustion and Flame* 99 (1994): 201-211.

Ritter, E. R. "THERM: Thermodynamic Property Estimation for Gas Phase Radicals and Molecules." NJIT, Newark, 1989.

Rumyanstev, A. N., et al. "Dependence of the Decomposition Rate Constant of Higher *n*-Paraffin Hydrocarbons on their Molecular Weight." Neftkhim, 1980, 20, 212.

Seaton, W. H., E. Freedman, and D. N. Treweek. "CHEETAH: the ASTM Chemical Thermodynamic and Energy Release Evaluation Program." ASTM DS 51, American Society for Testing Materials, 1974.

Selim, M. A. Ph.D. Thesis. Mechanical Engineering Department, Imperial College, University of London, 1995.

Skevis, G. Ph. D. Thesis. University of London, 1996.

Sobel, D. R. and L. J. Spadaccini. "Hydrocarbon Fuel Cooling Technologies for Advanced Propulsion." *Journal of Engineering for Gas Turbines and Power,* 119 (1997): 345.

Stein, S. E., et al. NIST Structures and Properties. Computer software. NIST Standard Reference Database 25, Version 2.0. National Institute of Standards and Technology, 1994.

Stoffel, B. and L. Reh. "Conversion of Liquid to Gaseous Fuels for Lean Premixed Combustion." *ASME Paper No. 95-GT-412.* International Gas Turbine and Aeroengine Congress and Exposition. Houston, 1995.

Sturgess, G. J. "Assessment of an Abbreviated Jet-A/JP-5/JP-8 Reaction Mechanism for Modeling Gas Turbine Engine Gaseous Emissions." *AIAA Paper No. 97-2709,* 1997.

Tsang, W. *Journal of Physical Chemistry*, Ref. Data, 16, 471, 1987.

Tsang, W. *Journal of Physical Chemistry*, Data, 17, 887, 1988.

Tsang, W. *Journal of Physical Chemistry*, Ref. Data, 19, 1, 1990.

Tsang, W. *Journal of Physical Chemistry*, Ref. Data, 20, 221, 1991.

Tsang, W., V. Bedanov, and M. R. Zachariah. "Master Equation Analysis of Thermal Activation Reactions: Energy-Transfer Constraints on Falloff Behavior in the Decomposition of Reactive Intermediates with Low Thresholds." *Journal of Physical Chemistry*, 100 (1996): 4011-4018.

Vovelle, Christian, Jean-Louis Delfau, and Marcelline Reuillon. "Formation of Aromatic Hydrocarbons in Decane and Kerosene Flames at Reduced Pressure."

Mechanisms and Models of Soot Formation. Ed. H. Bockhorn. Springer-Verlag, Berlin, 1994. 50-65.

Walker, R. W. "Position Paper on Chemical Kinetics of Combustion Processes." Major Research Topics in Combustion. Eds. M. Y. Hussaini, A. Kumar, and R. G. Voigt. New York: Springer-Verlag, 1992. 277.

Walker, R. W. and C. Morley. "Chapter 1, Basic Chemistry of Combustion", in Comprehensive Chemical Kinetics Volume 35, Low-Temperature Combustion and Ignition. M.J. Pilling, ed. Elsevier, Amsterdam, 1997. 1 - 120.

Warnatz J. *Twentieth Symposium (International) on Combustion.* The Combustion Institute, 1984.

Weinberg, Felix A. "The First Half-Million Years of Combustion Research and Today's Burning Problems." *Fifteenth Symposium (International) on Combustion.* The Combustion Institute, 1974. 1-17.

Westbrook, C. K. and Dryer, F. L. "Chemical Kinetic Modeling of Hydrocarbon Combustion." *Progress in Energy and Combustion Science.* 10 (1984): 1-57.

Williams, Bradley A. and Louise Pasternack. "The Effect of Nitric Oxide on Premixed Flames of CH_4, C_2H_6, C_2H_4, and C_2H_2." *Combustion and Flame* 111 (1997): 87-110.

Zelina, J. and D. R. Ballal. "Combustion Studies in a Well Stirred Reactor." *AIAA Paper No. 94-0114.* 32nd Aerospace Sciences Meeting & Exhibit. Reno, 1994.

APPENDIX

THE *n*-DODECANE MECHANISM

Table A1. Reactions and their rates added to the Lindstedt-Maurice mechanism to create the mechanism for *n*-dodecane

No.	Reaction			A	n	E (kJ/mole)	Reference
1	$C_{12}H_{26}$	⇔	1-$C_{12}H_{25}$ + H	7.3040E+13	0.00	424.099	est. from Maurice (1996), ΔH_f data
2	$C_{12}H_{26}$	⇔	2-$C_{12}H_{25}$ + H	7.3040E+13	0.00	409.799	est. from Maurice (1996), ΔH_f data
3	$C_{12}H_{26}$	⇔	3-$C_{12}H_{25}$ + H	7.3040E+13	0.00	409.699	est. from Maurice (1996), ΔH_f data
4	$C_{12}H_{26}$	⇔	4-$C_{12}H_{25}$ + H	7.3040E+13	0.00	409.699	est. from Maurice (1996), ΔH_f data
5	$C_{12}H_{26}$	⇔	5-$C_{12}H_{25}$ + H	7.3040E+13	0.00	409.699	est. from Maurice (1996), ΔH_f data
6	$C_{12}H_{26}$	⇔	6-$C_{12}H_{25}$ + H	7.3040E+13	0.00	409.699	est. from Maurice (1996), ΔH_f data
7	$C_{12}H_{26}$	⇔	1-C_8H_{17} + p-C_4H_9	1.5450E+12	0.00	265.800	Pop et al. and Rumyantsev et al.
8	$C_{12}H_{26}$	⇔	1-C_7H_{15} + 1-C_5H_{11}	1.5450E+12	0.00	265.810	Pop et al. and Rumyantsev et al.
9	$C_{12}H_{26}$	⇔	1-C_6H_{13} + 1-C6H13	1.5450E+12	0.00	265.820	Pop et al. and Rumyantsev et al.
10	$C_{12}H_{26}$ + H	⇔	1-$C_{12}H_{25}$ + H_2	4.2911E+04	2.00	11.899	est. from Maurice (1996), ΔH_f data
11	$C_{12}H_{26}$ + H	⇔	2-$C_{12}H_{25}$ + H_2	1.3695E+04	2.00	26.199	est. from Maurice (1996), ΔH_f data
12	$C_{12}H_{26}$ + H	⇔	3-$C_{12}H_{25}$ + H_2	1.3695E+04	2.00	26.299	est. from Maurice (1996), ΔH_f data
13	$C_{12}H_{26}$ + H	⇔	4-$C_{12}H_{25}$ + H_2	1.3695E+04	2.00	26.299	est. from Maurice (1996), ΔH_f data
14	$C_{12}H_{26}$ + H	⇔	5-$C_{12}H_{25}$ + H_2	1.3695E+04	2.00	26.299	est. from Maurice (1996), ΔH_f data
15	$C_{12}H_{26}$ + H	⇔	6-$C_{12}H_{25}$ + H_2	1.3695E+04	2.00	26.299	est. from Maurice (1996), ΔH_f data
16	$C_{12}H_{26}$ + OH	⇔	1-$C_{12}H_{25}$ + H_2O	4.0172E+06	0.97	75.069	est. from Maurice (1996), ΔH_f data
17	$C_{12}H_{26}$ + OH	⇔	2-$C_{12}H_{25}$ + H_2O	1.7895E+04	1.61	89.369	est. from Maurice (1996), ΔH_f data
18	$C_{12}H_{26}$ + OH	⇔	3-$C_{12}H_{25}$ + H_2O	1.7895E+04	1.61	89.469	est. from Maurice (1996), ΔH_f data
19	$C_{12}H_{26}$ + OH	⇔	4-$C_{12}H_{25}$ + H_2O	1.7895E+04	1.61	89.469	est. from Maurice (1996), ΔH_f data
20	$C_{12}H_{26}$ + OH	⇔	5-$C_{12}H_{25}$ + H_2O	1.7895E+04	1.61	89.469	est. from Maurice (1996), ΔH_f data
21	$C_{12}H_{26}$ + OH	⇔	6-$C_{12}H_{25}$ + H_2O	1.7895E+04	1.61	89.469	est. from Maurice (1996), ΔH_f data
22	$C_{12}H_{26}$ + O	⇔	1-$C_{12}H_{25}$ + OH	1.7530E+03	2.40	3.727	est. from Maurice (1996), ΔH_f data
23	$C_{12}H_{26}$ + O	⇔	2-$C_{12}H_{25}$ + OH	4.8663E+02	2.50	18.027	est. from Maurice (1996), ΔH_f data
24	$C_{12}H_{26}$ + O	⇔	3-$C_{12}H_{25}$ + OH	4.8663E+02	2.50	18.127	est. from Maurice (1996), ΔH_f data
25	$C_{12}H_{26}$ + O	⇔	4-$C_{12}H_{25}$ + OH	4.8663E+02	2.50	18.127	est. from Maurice (1996), ΔH_f data

Table A1. Continued.

26	$C_{12}H_{26} + O$	$\Leftrightarrow$ $5\text{-}C_{12}H_{25} + OH$	4.8663E+02	2.50	18.127	est. from Maurice (1996), ΔH_f data
27	$C_{12}H_{26} + O$	$\Leftrightarrow$ $6\text{-}C_{12}H_{25} + OH$	4.8663E+02	2.50	18.127	est. from Maurice (1996), ΔH_f data
28	$C_{12}H_{26} + CH_3$	$\Leftrightarrow$ $1\text{-}C_{12}H_{25} + CH_4$	2.2825E+09	0.00	15.358	est. from Maurice (1996), ΔH_f data
29	$C_{12}H_{26} + CH_3$	$\Leftrightarrow$ $2\text{-}C_{12}H_{25} + CH_4$	1.2143E+09	0.00	29.658	est. from Maurice (1996), ΔH_f data
30	$C_{12}H_{26} + CH_3$	$\Leftrightarrow$ $3\text{-}C_{12}H_{25} + CH_4$	1.2143E+09	0.00	29.758	est. from Maurice (1996), ΔH_f data
31	$C_{12}H_{26} + CH_3$	$\Leftrightarrow$ $4\text{-}C_{12}H_{25} + CH_4$	1.2143E+09	0.00	29.758	est. from Maurice (1996), ΔH_f data
32	$C_{12}H_{26} + CH_3$	$\Leftrightarrow$ $5\text{-}C_{12}H_{25} + CH_4$	1.2143E+09	0.00	29.758	est. from Maurice (1996), ΔH_f data
33	$C_{12}H_{26} + CH_3$	$\Leftrightarrow$ $6\text{-}C_{12}H_{25} + CH_4$	1.2143E+09	0.00	29.758	est. from Maurice (1996), ΔH_f data
34	$C_{12}H_{26} + HO_2$	$\Leftrightarrow$ $1\text{-}C_{12}H_{25} + H_2O_2$	8.5270E+09	0.00	57.238	est. from Maurice (1996), ΔH_f data
35	$C_{12}H_{26} + HO_2$	$\Leftrightarrow$ $2\text{-}C_{12}H_{25} + H_2O_2$	5.1820E+09	0.00	42.938	est. from Maurice (1996), ΔH_f data
36	$C_{12}H_{26} + HO_2$	$\Leftrightarrow$ $3\text{-}C_{12}H_{25} + H_2O_2$	5.1820E+09	0.00	42.838	est. from Maurice (1996), ΔH_f data
37	$C_{12}H_{26} + HO_2$	$\Leftrightarrow$ $4\text{-}C_{12}H_{25} + H_2O_2$	5.1820E+09	0.00	42.838	est. from Maurice (1996), ΔH_f data
38	$C_{12}H_{26} + HO_2$	$\Leftrightarrow$ $5\text{-}C_{12}H_{25} + H_2O_2$	5.1820E+09	0.00	42.838	est. from Maurice (1996), ΔH_f data
39	$C_{12}H_{26} + HO_2$	$\Leftrightarrow$ $6\text{-}C_{12}H_{25} + H_2O_2$	5.1820E+09	0.00	42.838	est. from Maurice (1996), ΔH_f data
40	$C_{12}H_{26} + O_2$	$\Leftrightarrow$ $1\text{-}C_{12}H_{25} + HO_2$	1.9082E+10	0.00	218.652	est. from Maurice (1996), ΔH_f data
41	$C_{12}H_{26} + O_2$	$\Leftrightarrow$ $2\text{-}C_{12}H_{25} + HO_2$	3.0129E+10	0.00	204.352	est. from Maurice (1996), ΔH_f data
42	$C_{12}H_{26} + O_2$	$\Leftrightarrow$ $3\text{-}C_{12}H_{25} + HO_2$	3.0129E+10	0.00	204.252	est. from Maurice (1996), ΔH_f data
43	$C_{12}H_{26} + O_2$	$\Leftrightarrow$ $4\text{-}C_{12}H_{25} + HO_2$	3.0129E+10	0.00	204.252	est. from Maurice (1996), ΔH_f data
44	$C_{12}H_{26} + O_2$	$\Leftrightarrow$ $5\text{-}C_{12}H_{25} + HO_2$	3.0129E+10	0.00	204.252	est. from Maurice (1996), ΔH_f data
45	$C_{12}H_{26} + O_2$	$\Leftrightarrow$ $6\text{-}C_{12}H_{25} + HO_2$	3.0129E+10	0.00	204.252	est. from Maurice (1996), ΔH_f data
46	$1\text{-}C_{12}H_{25}$	$\Leftrightarrow$ $1\text{-}C_8H_{17} + 1\text{-}C_4H_8$	1.9173E+13	0.00	68.277	est. from Maurice (1996), ΔH_f data
47	$1\text{-}C_{12}H_{25}$	$\Leftrightarrow$ $1\text{-}C_7H_{15} + 1\text{-}C_5H_{10}$	1.9173E+13	0.00	68.117	est. from Maurice (1996), ΔH_f data
48	$1\text{-}C_{12}H_{25}$	$\Leftrightarrow$ $1\text{-}C_6H_{13} + 1\text{-}C_6H_{12}$	1.9173E+13	0.00	68.414	est. from Maurice (1996), ΔH_f data
49	$1\text{-}C_{12}H_{25}$	$\Leftrightarrow$ $1\text{-}C_5H_{11} + 1\text{-}C_7H_{14}$	1.9173E+13	0.00	68.516	est. from Maurice (1996), ΔH_f data
50	$1\text{-}C_{12}H_{25}$	$\Leftrightarrow$ $p\text{-}C_4H_9 + 1\text{-}C_8H_{16}$	1.9173E+13	0.00	68.831	est. from Maurice (1996), ΔH_f data
51	$1\text{-}C_{12}H_{25}$	$\Leftrightarrow$ $n\text{-}C_3H_7 + 1\text{-}C_9H_{18}$	1.9173E+13	0.00	82.200	est. from Maurice (1996), ΔH_f data
52	$1\text{-}C_{12}H_{25}$	$\Leftrightarrow$ $C_2H_5 + 1\text{-}C_{10}H_{20}$	1.9173E+13	0.00	79.758	est. from Maurice (1996), ΔH_f data
53	$1\text{-}C_{12}H_{25}$	$\Leftrightarrow$ $CH_3 + 1\text{-}C_{11}H_{22}$	1.9173E+13	0.00	87.358	est. from Maurice (1996), ΔH_f data
54	$1\text{-}C_{12}H_{25}$	$\Leftrightarrow$ $2\text{-}C_{12}H_{25}$	1.8260E+11	0.00	14.300	est. from Maurice (1996), ΔH_f data
55	$1\text{-}C_{12}H_{25}$	$\Leftrightarrow$ $3\text{-}C_{12}H_{25}$	1.8260E+11	0.00	14.400	est. from Maurice (1996), ΔH_f data
56	$2\text{-}C_{12}H_{25}$	$\Leftrightarrow$ $1\text{-}C_8H_{17} + 1\text{-}C_4H_8$	1.9173E+13	0.00	82.577	est. from Maurice (1996), ΔH_f data
57	$2\text{-}C_{12}H_{25}$	$\Leftrightarrow$ $1\text{-}C_7H_{15} + 1\text{-}C_5H_{10}$	1.9173E+13	0.00	82.417	est. from Maurice (1996), ΔH_f data
58	$2\text{-}C_{12}H_{25}$	$\Leftrightarrow$ $1\text{-}C_6H_{13} + 1\text{-}C_6H_{12}$	1.9173E+13	0.00	82.714	est. from Maurice (1996), ΔH_f data
59	$2\text{-}C_{12}H_{25}$	$\Leftrightarrow$ $1\text{-}C_5H_{11} + 1\text{-}C_7H_{14}$	1.9173E+13	0.00	82.816	est. from Maurice (1996), ΔH_f data
60	$2\text{-}C_{12}H_{25}$	$\Leftrightarrow$ $p\text{-}C_4H_9 + 1\text{-}C_8H_{16}$	1.9173E+13	0.00	83.131	est. from Maurice (1996), ΔH_f data
61	$2\text{-}C_{12}H_{25}$	$\Leftrightarrow$ $n\text{-}C_3H_7 + 1\text{-}C_9H_{18}$	1.9173E+13	0.00	96.500	est. from Maurice (1996), ΔH_f data
62	$2\text{-}C_{12}H_{25}$	$\Leftrightarrow$ $C_2H_5 + 1\text{-}C_{10}H_{20}$	1.9173E+13	0.00	94.058	est. from Maurice (1996), ΔH_f data
63	$2\text{-}C_{12}H_{25}$	$\Leftrightarrow$ $CH_3 + 1\text{-}C_{11}H_{22}$	1.9173E+13	0.00	101.658	est. from Maurice (1996), ΔH_f data

Table A1. Continued.

64	2-$C_{12}H_{25}$	⇔ 1-$C_{12}H_{25}$	1.8260E+11	0.00	14.300	est. from Maurice (1996), ΔH_f data
65	2-$C_{12}H_{25}$	⇔ 3-$C_{12}H_{25}$	1.8260E+11	0.00	0.100	est. from Maurice (1996), ΔH_f data
66	2-$C_{12}H_{25}$	⇔ 4-$C_{12}H_{25}$	1.8260E+11	0.00	0.100	est. from Maurice (1996), ΔH_f data
67	3-$C_{12}H_{25}$	⇔ 1-C_8H_{17} + 1-C_4H_8	1.9173E+13	0.00	82.677	est. from Maurice (1996), ΔH_f data
68	3-$C_{12}H_{25}$	⇔ 1-C_7H_{15} + 1-C_5H_{10}	1.9173E+13	0.00	82.517	est. from Maurice (1996), ΔH_f data
69	3-$C_{12}H_{25}$	⇔ 1-C_6H_{13} + 1-C_6H_{12}	1.9173E+13	0.00	82.814	est. from Maurice (1996), ΔH_f data
70	3-$C_{12}H_{25}$	⇔ 1-C_5H_{11} + 1-C_7H_{14}	1.9173E+13	0.00	82.916	est. from Maurice (1996), ΔH_f data
71	3-$C_{12}H_{25}$	⇔ p-C_4H_9 + 1-C_8H_{16}	1.9173E+13	0.00	83.231	est. from Maurice (1996), ΔH_f data
72	3-$C_{12}H_{25}$	⇔ n-C_3H_7 + 1-C_9H_{18}	1.9173E+13	0.00	96.600	est. from Maurice (1996), ΔH_f data
73	3-$C_{12}H_{25}$	⇔ C_2H_5 + 1-$C_{10}H_{20}$	1.9173E+13	0.00	94.158	est. from Maurice (1996), ΔH_f data
74	3-$C_{12}H_{25}$	⇔ CH_3 + 1-$C_{11}H_{22}$	1.9173E+13	0.00	101.758	est. from Maurice (1996), ΔH_f data
75	3-$C_{12}H_{25}$	⇔ 1-$C_{12}H_{25}$	1.8260E+11	0.00	14.400	est. from Maurice (1996), ΔH_f data
76	3-$C_{12}H_{25}$	⇔ 2-$C_{12}H_{25}$	1.8260E+11	0.00	0.100	est. from Maurice (1996), ΔH_f data
77	3-$C_{12}H_{25}$	⇔ 4-$C_{12}H_{25}$	1.8260E+11	0.00	0.000	est. from Maurice (1996), ΔH_f data
78	3-$C_{12}H_{25}$	⇔ 5-$C_{12}H_{25}$	1.8260E+11	0.00	0.000	est. from Maurice (1996), ΔH_f data
79	4-$C_{12}H_{25}$	⇔ 1-C_8H_{17} + 1-C_4H_8	1.9173E+13	0.00	82.677	est. from Maurice (1996), ΔH_f data
80	4-$C_{12}H_{25}$	⇔ 1-C_7H_{15} + 1-C_5H_{10}	1.9173E+13	0.00	82.517	est. from Maurice (1996), ΔH_f data
81	4-$C_{12}H_{25}$	⇔ 1-C_6H_{13} + 1-C_6H_{12}	1.9173E+13	0.00	82.814	est. from Maurice (1996), ΔH_f data
82	4-$C_{12}H_{25}$	⇔ 1-C_5H_{11} + 1-C_7H_{14}	1.9173E+13	0.00	82.916	est. from Maurice (1996), ΔH_f data
83	4-$C_{12}H_{25}$	⇔ p-C_4H_9 + 1-C_8H_{16}	1.9173E+13	0.00	83.231	est. from Maurice (1996), ΔH_f data
84	4-$C_{12}H_{25}$	⇔ n-C_3H_7 + 1-C_9H_{18}	1.9173E+13	0.00	96.600	est. from Maurice (1996), ΔH_f data
85	4-$C_{12}H_{25}$	⇔ C_2H_5 + 1-$C_{10}H_{20}$	1.9173E+13	0.00	94.158	est. from Maurice (1996), ΔH_f data
86	4-$C_{12}H_{25}$	⇔ CH_3 + 1-$C_{11}H_{22}$	1.9173E+13	0.00	101.758	est. from Maurice (1996), ΔH_f data
87	4-$C_{12}H_{25}$	⇔ 2-$C_{12}H_{25}$	1.8260E+11	0.00	0.100	est. from Maurice (1996), ΔH_f data
88	4-$C_{12}H_{25}$	⇔ 3-$C_{12}H_{25}$	1.8260E+11	0.00	0.000	est. from Maurice (1996), ΔH_f data
89	4-$C_{12}H_{25}$	⇔ 5-$C_{12}H_{25}$	1.8260E+11	0.00	0.000	est. from Maurice (1996), ΔH_f data
90	4-$C_{12}H_{25}$	⇔ 6-$C_{12}H_{25}$	1.8260E+11	0.00	0.000	est. from Maurice (1996), ΔH_f data
91	5-$C_{12}H_{25}$	⇔ 1-C_8H_{16} + p-C_4H_9	1.9173E+13	0.00	83.231	est. from Maurice (1996), ΔH_f data
92	5-$C_{12}H_{25}$	⇔ 1-C_7H_{15} + 1-C_5H_{10}	1.9173E+13	0.00	82.517	est. from Maurice (1996), ΔH_f data
93	5-$C_{12}H_{25}$	⇔ 1-C_6H_{13} + 1-C_6H_{12}	1.9173E+13	0.00	82.814	est. from Maurice (1996), ΔH_f data
94	5-$C_{12}H_{25}$	⇔ 1-C_5H_{11} + 1-C_7H_{14}	1.9173E+13	0.00	82.916	est. from Maurice (1996), ΔH_f data
95	5-$C_{12}H_{25}$	⇔ p-C_4H_9 + 1-C_8H_{16}	1.9173E+13	0.00	83.231	est. from Maurice (1996), ΔH_f data
96	5-$C_{12}H_{25}$	⇔ n-C_3H_7 + 1-C_9H_{18}	1.9173E+13	0.00	96.600	est. from Maurice (1996), ΔH_f data
97	5-$C_{12}H_{25}$	⇔ C_2H_5 + 1-$C_{10}H_{20}$	1.9173E+13	0.00	94.158	est. from Maurice (1996), ΔH_f data
98	5-$C_{12}H_{25}$	⇔ CH_3 + 1-$C_{11}H_{22}$	1.9173E+13	0.00	101.758	est. from Maurice (1996), ΔH_f data
99	5-$C_{12}H_{25}$	⇔ 3-$C_{12}H_{25}$	1.8260E+11	0.00	0.000	est. from Maurice (1996), ΔH_f data
100	5-$C_{12}H_{25}$	⇔ 4-$C_{12}H_{25}$	1.8260E+11	0.00	0.000	est. from Maurice (1996), ΔH_f data
101	5-$C_{12}H_{25}$	⇔ 6-$C_{12}H_{25}$	1.8260E+11	0.00	0.000	est. from Maurice (1996), ΔH_f data

Table A1. Continued.

64	2-$C_{12}H_{25}$	⇔	1-$C_{12}H_{25}$	1.8260E+11	0.00	14.300	est. from Maurice (1996), ΔH_f data
65	2-$C_{12}H_{25}$	⇔	3-$C_{12}H_{25}$	1.8260E+11	0.00	0.100	est. from Maurice (1996), ΔH_f data
66	2-$C_{12}H_{25}$	⇔	4-$C_{12}H_{25}$	1.8260E+11	0.00	0.100	est. from Maurice (1996), ΔH_f data
67	3-$C_{12}H_{25}$	⇔	1-C_8H_{17} + 1-C_4H_8	1.9173E+13	0.00	82.677	est. from Maurice (1996), ΔH_f data
68	3-$C_{12}H_{25}$	⇔	1-C_7H_{15} + 1-C_5H_{10}	1.9173E+13	0.00	82.517	est. from Maurice (1996), ΔH_f data
69	3-$C_{12}H_{25}$	⇔	1-C_6H_{13} + 1-C_6H_{12}	1.9173E+13	0.00	82.814	est. from Maurice (1996), ΔH_f data
70	3-$C_{12}H_{25}$	⇔	1-C_5H_{11} + 1-C_7H_{14}	1.9173E+13	0.00	82.916	est. from Maurice (1996), ΔH_f data
71	3-$C_{12}H_{25}$	⇔	p-C_4H_9 + 1-C_8H_{16}	1.9173E+13	0.00	83.231	est. from Maurice (1996), ΔH_f data
72	3-$C_{12}H_{25}$	⇔	n-C_3H_7 + 1-C_9H_{18}	1.9173E+13	0.00	96.600	est. from Maurice (1996), ΔH_f data
73	3-$C_{12}H_{25}$	⇔	C_2H_5 + 1-$C_{10}H_{20}$	1.9173E+13	0.00	94.158	est. from Maurice (1996), ΔH_f data
74	3-$C_{12}H_{25}$	⇔	CH_3 + 1-$C_{11}H_{22}$	1.9173E+13	0.00	101.758	est. from Maurice (1996), ΔH_f data
75	3-$C_{12}H_{25}$	⇔	1-$C_{12}H_{25}$	1.8260E+11	0.00	14.400	est. from Maurice (1996), ΔH_f data
76	3-$C_{12}H_{25}$	⇔	2-$C_{12}H_{25}$	1.8260E+11	0.00	0.100	est. from Maurice (1996), ΔH_f data
77	3-$C_{12}H_{25}$	⇔	4-$C_{12}H_{25}$	1.8260E+11	0.00	0.000	est. from Maurice (1996), ΔH_f data
78	3-$C_{12}H_{25}$	⇔	5-$C_{12}H_{25}$	1.8260E+11	0.00	0.000	est. from Maurice (1996), ΔH_f data
79	4-$C_{12}H_{25}$	⇔	1-C_8H_{17} + 1-C_4H_8	1.9173E+13	0.00	82.677	est. from Maurice (1996), ΔH_f data
80	4-$C_{12}H_{25}$	⇔	1-C_7H_{15} + 1-C_5H_{10}	1.9173E+13	0.00	82.517	est. from Maurice (1996), ΔH_f data
81	4-$C_{12}H_{25}$	⇔	1-C_6H_{13} + 1-C_6H_{12}	1.9173E+13	0.00	82.814	est. from Maurice (1996), ΔH_f data
82	4-$C_{12}H_{25}$	⇔	1-C_5H_{11} + 1-C_7H_{14}	1.9173E+13	0.00	82.916	est. from Maurice (1996), ΔH_f data
83	4-$C_{12}H_{25}$	⇔	p-C_4H_9 + 1-C_8H_{16}	1.9173E+13	0.00	83.231	est. from Maurice (1996), ΔH_f data
84	4-$C_{12}H_{25}$	⇔	n-C_3H_7 + 1-C_9H_{18}	1.9173E+13	0.00	96.600	est. from Maurice (1996), ΔH_f data
85	4-$C_{12}H_{25}$	⇔	C_2H_5 + 1-$C_{10}H_{20}$	1.9173E+13	0.00	94.158	est. from Maurice (1996), ΔH_f data
86	4-$C_{12}H_{25}$	⇔	CH_3 + 1-$C_{11}H_{22}$	1.9173E+13	0.00	101.758	est. from Maurice (1996), ΔH_f data
87	4-$C_{12}H_{25}$	⇔	2-$C_{12}H_{25}$	1.8260E+11	0.00	0.100	est. from Maurice (1996), ΔH_f data
88	4-$C_{12}H_{25}$	⇔	3-$C_{12}H_{25}$	1.8260E+11	0.00	0.000	est. from Maurice (1996), ΔH_f data
89	4-$C_{12}H_{25}$	⇔	5-$C_{12}H_{25}$	1.8260E+11	0.00	0.000	est. from Maurice (1996), ΔH_f data
90	4-$C_{12}H_{25}$	⇔	6-$C_{12}H_{25}$	1.8260E+11	0.00	0.000	est. from Maurice (1996), ΔH_f data
91	5-$C_{12}H_{25}$	⇔	1-C_8H_{16} + p-C_4H_9	1.9173E+13	0.00	83.231	est. from Maurice (1996), ΔH_f data
92	5-$C_{12}H_{25}$	⇔	1-C_7H_{15} + 1-C_5H_{10}	1.9173E+13	0.00	82.517	est. from Maurice (1996), ΔH_f data
93	5-$C_{12}H_{25}$	⇔	1-C_6H_{13} + 1-C_6H_{12}	1.9173E+13	0.00	82.814	est. from Maurice (1996), ΔH_f data
94	5-$C_{12}H_{25}$	⇔	1-C_5H_{11} + 1-C_7H_{14}	1.9173E+13	0.00	82.916	est. from Maurice (1996), ΔH_f data
95	5-$C_{12}H_{25}$	⇔	p-C_4H_9 + 1-C_8H_{16}	1.9173E+13	0.00	83.231	est. from Maurice (1996), ΔH_f data
96	5-$C_{12}H_{25}$	⇔	n-C_3H_7 + 1-C_9H_{18}	1.9173E+13	0.00	96.600	est. from Maurice (1996), ΔH_f data
97	5-$C_{12}H_{25}$	⇔	C_2H_5 + 1-$C_{10}H_{20}$	1.9173E+13	0.00	94.158	est. from Maurice (1996), ΔH_f data
98	5-$C_{12}H_{25}$	⇔	CH_3 + 1-$C_{11}H_{22}$	1.9173E+13	0.00	101.758	est. from Maurice (1996), ΔH_f data
99	5-$C_{12}H_{25}$	⇔	3-$C_{12}H_{25}$	1.8260E+11	0.00	0.000	est. from Maurice (1996), ΔH_f data
100	5-$C_{12}H_{25}$	⇔	4-$C_{12}H_{25}$	1.8260E+11	0.00	0.000	est. from Maurice (1996), ΔH_f data
101	5-$C_{12}H_{25}$	⇔	6-$C_{12}H_{25}$	1.8260E+11	0.00	0.000	est. from Maurice (1996), ΔH_f data

Table A1. Continued.

102	6-$C_{12}H_{25}$	⇔ 2-C_8H_{16} + p-C_4H_9	1.9173E+13	0.00	83.231	est. from Maurice (1996), ΔH_f data
103	6-$C_{12}H_{25}$	⇔ 1-C_7H_{14} + 1-C_5H_{11}	1.9173E+13	0.00	82.916	est. from Maurice (1996), ΔH_f data
104	6-$C_{12}H_{25}$	⇔ 1-C_6H_{13} + 1-C_6H_{12}	1.9173E+13	0.00	82.814	est. from Maurice (1996), ΔH_f data
105	6-$C_{12}H_{25}$	⇔ 1-C_5H_{11} + 1-C_7H_{14}	1.9173E+13	0.00	82.916	est. from Maurice (1996), ΔH_f data
106	6-$C_{12}H_{25}$	⇔ p-C_4H_9 + 1-C_8H_{16}	1.9173E+13	0.00	83.231	est. from Maurice (1996), ΔH_f data
107	6-$C_{12}H_{25}$	⇔ n-C_3H_7 + 1-C_9H_{18}	1.9173E+13	0.00	96.600	est. from Maurice (1996), ΔH_f data
108	6-$C_{12}H_{25}$	⇔ C_2H_5 + 1-$C_{10}H_{20}$	1.9173E+13	0.00	94.158	est. from Maurice (1996), ΔH_f data
109	6-$C_{12}H_{25}$	⇔ CH_3 + 1-$C_{11}H_{22}$	1.9173E+13	0.00	101.758	est. from Maurice (1996), ΔH_f data
110	6-$C_{12}H_{25}$	⇔ 4-$C_{12}H_{25}$	1.8260E+11	0.00	0.000	est. from Maurice (1996), ΔH_f data
111	6-$C_{12}H_{25}$	⇔ 5-$C_{12}H_{25}$	1.8260E+11	0.00	0.000	est. from Maurice (1996), ΔH_f data
112	1C_9H_{18}	⇔ C_3H_5(A) + 1C_6H_{13}	2.0000E+15	0.00	297480.000	est. from Maurice (1996), ΔH_f data
113	1C_9H_{18}	⇔ PC_4H_9 + C_5H_9	1.0000E+16	0.00	342250.000	est. from Maurice (1996), ΔH_f data
114	1C_9H_{18} + O	⇔ C_2H_3O + 1C_7H_{15}	1.0000E+08	0.00	0.000	est. from Maurice (1996), ΔH_f data
115	1C_9H_{18} + O	⇔ CHO + C_8H_{17}	1.0000E+08	0.00	0.000	est. from Maurice (1996), ΔH_f data
116	1C_9H_{18} + OH	⇔ C_2H_4O + 1C_7H_{14}	1.0000E+08	0.00	0.000	est. from Maurice (1996), ΔH_f data
117	1C_9H_{18} + OH	⇔ CH_2O + C_8H_{16}	1.0000E+08	0.00	0.000	est. from Maurice (1996), ΔH_f data
118	1$C_{10}H_{20}$	⇔ C_3H_5(A) + 1C_7H_{15}	2.0000E+15	0.00	297480.000	est. from Maurice (1996), ΔH_f data
119	1$C_{10}H_{20}$	⇔ PC_4H_9 + C_6H_{11}	1.0000E+16	0.00	342250.000	est. from Maurice (1996), ΔH_f data
120	1$C_{10}H_{20}$ + O	⇔ C_2H_3O + C_8H_{17}	1.0000E+08	0.00	0.000	est. from Maurice (1996), ΔH_f data
121	1$C_{10}H_{20}$ + OH	⇔ C_2H_4O + C_8H_{16}	1.0000E+08	0.00	0.000	est. from Maurice (1996), ΔH_f data
122	1$C_{10}H_{20}$ + OH	⇔ CH_2O + 1C_9H_{18}	1.0000E+08	0.00	0.000	est. from Maurice (1996), ΔH_f data
123	1$C_{11}H_{22}$	⇔ C_3H_5(A) + C_8H_{17}	2.0000E+15	0.00	297480.000	est. from Maurice (1996), ΔH_f data
124	1$C_{11}H_{22}$	⇔ PC_4H_9 + C_7H_{13}	1.0000E+16	0.00	342250.000	est. from Maurice (1996), ΔH_f data
125	1$C_{11}H_{22}$ + O	⇔ CHO + 1$C_{10}H_{21}$	1.0000E+08	0.00	0.000	est. from Maurice (1996), ΔH_f data
126	1$C_{11}H_{22}$ + OH	⇔ C_2H_4O + 1C_9H_{18}	1.0000E+08	0.00	0.000	est. from Maurice (1996), ΔH_f data
127	1$C_{11}H_{22}$ + OH	⇔ CH_2O + 1$C_{10}H_{20}$	1.0000E+08	0.00	0.000	est. from Maurice (1996), ΔH_f data

Table A2. Thermodynamic data for species added to the Lindstedt-Maurice mechanism to create the mechanism for *n*-dodecane

Specie	ΔH_f^0 (kJ/mole)	S^0 (J/mole/K)	Reference
1-C_9H_{18}	-103.300	505.000	Stein et al. (1994)
1-$C_{10}H_{20}$	-123.900	544.500	Stein et al. (1994)
1-$C_{11}H_{22}$	-144.500	583.900	Stein et al. (1994)
1-$C_{12}H_{25}$	-85.000	642.300	Stein et al. (1994)
2-$C_{12}H_{25}$	-99.300	646.100	Stein et al. (1994)
3-$C_{12}H_{25}$	-99.400	646.100	Stein et al. (1994)
4-$C_{12}H_{25}$	-99.400	646.100	Stein et al. (1994)
5-$C_{12}H_{25}$	-99.400	646.100	Stein et al. (1994)
6-$C_{12}H_{25}$	-99.400	646.100	Stein et al. (1994)
$C_{12}H_{26}$	-291.100	624.600	Stein et al. (1994)

Table A3. JANAF-type polynomials for species added to the Lindstedt-Maurice mechanism to create the mechanism for *n*-dodecane

1-C_9H_{18}				
0.57211441E+00	0.11917206E+00	-0.64162879E-04	0.11864003E-07	0.80262424E-12
-0.17123990E+05	0.31142460E+02	-0.57211441E+00	0.11917206E+00	-0.64162879E-04
0.11864003E-07	0.80262424E-12	-0.17123990E+05	0.31142460E+02	
1-$C_{10}H_{22}$				
0.14116570E+02	0.78702390E-01	-0.38137303E-04	0.92046113E-08	-0.89854003E-12
-0.38875109E+05	-0.40076538E+02	0.56013346E-01	0.10784968E+00	-0.48558370E-04
-0.10920577E-08	0.47324675E-11	-0.34466523E+05	0.35138103E+02	
1-$C_{11}H_{22}$				
0.44540837E+00	0.11840130E+00	-0.62584520E-04	0.10555050E-07	0.11772755E-11
-0.22094627E+05	0.40081467E+02	-0.44540837E+00	0.11840130E+00	-0.62584520E-04
0.10555050E-07	0.11772755E-11	-0.22094627E+05	0.40081467E+02	
1-$C_{12}H_{25}$				
0.24171686E+00	0.13217595E+00	-0.68991838E-04	0.10509754E-07	0.16741476E-11
-0.15570696E+05	0.42105419E+02	-0.24171686E+00	0.13217595E+00	-0.68991838E-04
0.10509754E-07	0.16741476E-11	-0.15570696E+05	0.42105419E+02	
2-$C_{12}H_{25}$				
0.86466610E-01	0.13099597E+00	-0.69043148E-04	0.12180277E-07	0.91126510E-12
-0.17286717E+05	0.42021694E+02	-0.86466610E-01	0.13099597E+00	-0.69043148E-04
0.12180277E-07	0.91126510E-12	-0.17286717E+05	0.42021694E+02	
3-$C_{12}H_{25}$				
0.81788898E-01	0.12996107E+00	-0.66891909E-04	0.10359480E-07	0.14474796E-11
-0.17318666E+05	0.41291580E+02	0.81788898E-01	0.12996107E+00	-0.66891909E-04
0.10359480E-07	0.14474796E-11	-0.17318666E+05	0.41291580E+02	
4-$C_{12}H_{25}$				
0.81788898E-01	0.12996107E+00	-0.66891909E-04	0.10359480E-07	0.14474796E-11
-0.17318666E+05	0.41291580E+02	0.81788898E-01	0.12996107E+00	-0.66891909E-04
0.10359480E-07	0.14474796E-11	-0.17318666E+05	0.41291580E+02	
5-$C_{12}H_{25}$				
0.81788898E-01	0.12996107E+00	-0.66891909E-04	0.10359480E-07	0.14474796E-11
-0.17318666E+05	0.41291580E+02	0.81788898E-01	0.12996107E+00	-0.66891909E-04
0.10359480E-07	0.14474796E-11	-0.17318666E+05	0.41291580E+02	
6-$C_{12}H_{25}$				
0.81788898E-01	0.12996107E+00	-0.66891909E-04	0.10359480E-07	0.14474796E-11
-0.17318666E+05	0.41291580E+02	0.81788898E-01	0.12996107E+00	-0.66891909E-04
0.10359480E-07	0.14474796E-11	-0.17318666E+05	0.41291580E+02	
$C_{12}H_{26}$				
0.28822377E+02	0.18479874E-01	0.30092618E-05	-0.21478362E-08	0.21420786E-12
-0.12739461E 05	-0.12572266E+03	0.17747404E+02	0.24605739E+00	-0.10760834E-02
0.15022143E-05	-0.65955779E-09	-0.88918223E 04	-0.91761680E+02	